Politecnico di Torino

Master's Degree in Environmental and Land Engineering
Track: Climate Change

North Atlantic climate variability in observations and model simulations

Supervisors:
Jost von Hardenberg
Javier García-Serrano

Candidate:
Marianna Albanese

Academic Year 2023/2024
March 2024

Acknowledgements

If I was able to get here and reach this achievement, it was not only because of me but also because of the people who were by my side along the way. Thanks to all my companions.

First of all, I deeply thank my supervisor Jost von Hardenberg. Thank you for transmitting me your knowledge and for making me passionate about your subject. Thank you for giving me the opportunity to expand my horizons and discover the direction of my future. Thank you for the guidance and support you have given me.

I would also like to sincerely thank my other supervisor, Javier García-Serrano. Thank you for welcoming me and accompanying me to the end during my research stay at the University of Barcelona. Your experience and knowledge fascinated me and gave me the extra motivation I needed to decide which road to take. I also thank you for your guidance and support.

Special thanks also to the entire meteorology group at the University of Barcelona with whom I had the opportunity to exchange opinions, doubts and knowledge that allowed me to grow academically. But I also thank you, above all, for all the moments of fun we shared together, from lunches at the university to dinners out and walks. Thank you because when I think about it I smile.

Finally, I thank my family and friends with all my heart, because without you I would not be here today.

Abstract

The North Atlantic climate variability is mainly regulated by the North Atlantic Oscillation (NAO), one of the most important patterns of atmospheric circulation variability. It has a strong influence on surface climate over this region with a marked impact on the environment, society and economy. Thus, it is of paramount importance to deepen our understanding of it and its governing mechanisms. In this work I have analysed both observed variability using ERA5 reanalysis (1950-2023) and the simulated variability through a set of twin simulations, provided by the meteorology group of the University of Barcelona, performed with the standard configuration of EC-EARTH3 global climate model (GCM) for CMIP6. In particular, the latter were used to assess the impact of air-sea coupling and radiative forcing on the NAO. As a first step, model biases were evaluated by comparing the climatology of different variables with observational data, and contrasting them with results from previous studies using also EC-EARTH. Although the initial conditions used for the different simulations are different, the model performance is qualitatively similar in terms of position and extent of the biases. Another result obtained from the analysis of model biases is that, in order to get a realistic representation of climate variability in the North Atlantic-European region, variability of sea ice concentration (SIC) throughout the year is required, hence suggesting that it is necessary to consider the effect of the ocean. This evidence is also confirmed by comparing coupled (atmosphere-ocean) and atmosphere-only simulations, performed to assess the effect of air-sea coupling. In fact, to fully explain the variability associated with the winter NAO, the coupled experiment is needed. On the other hand, air-sea coupling has no clear effect on the NAO dynamics in terms of structure and position (e.g. advection of temperature and latitudinal displacements of precipitation/storm-track): thus, it can be argued that the mechanisms involved in the NAO are predominantly dominated by internal atmospheric processes. The effect of radiative forcing has been evaluated by comparing simulations at present (year 2000) and future (year 2050) conditions, assessing also the effect of air-sea coupling. Since the future winter NAO and its impact on precipitation and temperature are similar in the corresponding coupled and atmosphere-only experiments, according to the literature, it has been found that also in this case the ocean does not play a key role in governing the NAO dynamics. However, to fully capture the radiatively-forced changes in climatology and variability of the climate system and to explain the amplitude of the anomalies linked to the NAO it is necessary to consider the effect of the ocean, as it was already the case for present conditions. The fact that the ocean is important in best representing the magnitude of NAO-related anomalies is a result that can help in defining the role of air-sea coupling and in increasing the predictability of NAO related climate variations.

With this analysis, a general framework for the most important mode of climate variability in the North Atlantic-European region has been provided and the impact of air-sea coupling and radiative forcing was explored, also giving insights for further research.

Contents

Abstract 0
List of figures 2
List of abbreviations 3
1. Introduction 5
2. From literature: atmospheric circulation and variability in the Northern Hemisphere 7
2.1 Atmospheric circulation and persistent variability 7
2.2 The North Atlantic Oscillation and its relationship with surface climate 11
2.2.1 Impacts: variations in North Atlantic climate 13
2.2.2 Mechanism and dynamics 16
3. Data and methods 18
3.1 Data from ERA5 18
3.2 Data from EC-Earth 19
3.3 Methodology 21
3.3.1 Field's spatial visualization: climatology and standard deviation 21
3.3.2 Look for teleconnection patterns in NAE region with focus on NAO: EOF analysis 21
3.3.3 Anomaly's spatial visualization related to NAO: linear regression and correlation 23
3.3.4 Statistical significance 23
4. Observed variability 25
4.1 The first 4 EOFs: main teleconnection patterns in NAE regions 25
4.2 NAO's behaviour and its impact throughout the year 30
5. Simulated variability 42
5.1 Model biases: how the model simulates the North Atlantic climate 42
5.2 The impact of air-sea coupling on the NAO 56
5.3 The impact of radiative forcing on NAO 67
6. Conclusions 78
7. References 79
Appendix 86
Appendix A 86
Appendix B 88

List of figures

Figure 1 Essential features of the zonally averaged general circulation 7
Figure 2 Zonal (u), meridional (v) and vertical (w) components of the local vector wind velocity 8
Figure 3 Positive NAO phase 12
Figure 4 Negative NAO phase 12
Figure 5 The positive and negative NAO phase calculated using the EOF analysis 13
Figure 6 Storm track anomalies for 1958-1998 winters 14
Figure 7 The leading four patterns of North Atlantic European region winter (DJF) SLP variability 26
Figure 8 Principal storm-tracks of the extratropical cyclones in the EA winter 27
Figure 9 Principal component time series of the four leading EOFs of the NAE region sea level pressure 29
Figure 10 Climatology of SLP field (hPa) for DJF, MAM, JJA and SON seasons 30
Figure 11 Standard deviation of SLP anomaly (hPa) for DJF, MAM, JJA and SON seasons 32
Figure 12 Climatology of t2m field (°C) for DJF, MAM, JJA and SON seasons 34
Figure 14 Climatology of TP field (mm/d) for DJF, MAM, JJA and SON seasons 35
Figure 15 Standard deviation of t2m anomaly (mm/d) for DJF, MAM, JJA and SON seasons 36
Figure 16 Seasonal SLP anomalies due to NAO in the North Atlantic European sector 37
Figure 17 Seasonal t2m anomalies due to NAO in the North Atlantic European sector 39
Figure 18 Seasonal TP anomalies due to NAO in the North Atlantic European sector 40
Figure 19 Principal component time series of the first leading EOF of the NAE region SLP 41
Figure 20 Difference between the SLP climatologies of the simulations and the reanalysis 44
Figure 21 Comparison between the differences in pressure climatologies 45
Figure 22 Difference between the SLP standard deviations of the simulations and the reanalysis 46
Figure 23 Difference between the t2m climatologies of the simulations and the reanalysis 48
Figure 24 Comparison between the differences in temperature climatologies 49
Figure 25 Difference between the t2m standard deviations of the simulations and the reanalysis 50
Figure 26 Difference between the TP climatologies of the simulations and the reanalysis 52
Figure 27 Comparison between the differences in temperature climatologies 53
Figure 28 Bar plot of the TP standard deviation's weighted average in NAE region 53
Figure 29 Difference between the TP standard deviations of the simulations and the reanalysis 55
Figure 30 Seasonal SLP anomalies due to NAO in the North Atlantic European sector 60
Figure 31 Seasonal t2m anomalies due to NAO in the North Atlantic European sector 64
Figure 32 Seasonal TP anomalies due to NAO in the North Atlantic European sector 66
Figure 33 Difference between the SLP climatologies of the present and future simulations 69
Figure 34 Difference between the t2m climatologies of the present and future simulations 70
Figure 35 Difference between the TP climatologies of the present and future simulations 72
Figure 36 Seasonal present and future SLP anomalies due to NAO in the NAE region 74
Figure 37 Seasonal present and future t2m anomalies due to NAO in the NAE region 75
Figure 38 Seasonal present and future TP anomalies due to NAO in the NAE region 77
Figure 39 The first 4 EOFs in the NAE region 87
Figure 40 Climatology and standard deviation of SLP field in reanalysis and present simulations 89
Figure 41 Climatology and standard deviation of t2m field in reanalysis and present simulations 90
Figure 42 Climatology and standard deviation of TP field in reanalysis and present simulations 92
Figure 43 Climatology and standard deviation of SLP field in future simulations 93
Figure 44 Climatology and standard deviation of t2m field in future simulations 94
Figure 45 Climatology and standard deviation of TP field in future simulations 95

List of abbreviations

AGCM – Atmospheric General Circulation Model
AMO – Atlantic Multidecadal Oscillation
AMV – Atlantic Multidecadal Variability
AO – Atlantic Oscillation
AOGCM – Atmospheric Ocean General Circulation Model
CAM – Community Atmospheric Model
CGCM – Coupled ocean-atmosphere General Circulation Models
CESM – Community Earth System Model
CMIP – Coupled Model Intercomparison Project
CORR – Correlation Map
DJF – December-January-February
DOF – Degree Of Freedom
E – Evaporation
EA – East Atlantic pattern
EA/WR – East Atlantic/West Russia pattern
ECMWF – European Centre Medium Weather Forecast
ENSO – El Niño-Southern Oscillation
EOF – Empirical Orthogonal Function
EOT – Empirical Orthogonal Teleconnection
ESM – Earth System Model
FVAR – Fraction of Explained Variance
GCM – Global Climate Model
GHG – Greenhouse Gas
GIN – Greenland-Icelandic-Norwegian
IPCC – Intergovernmental Panel on Climate Change
ITCZ – Intertropical Convergence Zone
JJA – June-July-August
MAM – March-April-May
MJO – Madden-Julian Oscillation
NAO – North Atlantic Oscillation
NAE – North-Atlantic European
NAM – Northern Annular Mode
NH – Northern Hemisphere
P – Precipitation
PCA – Principal Component Analysis
PNA – Pacific/North American pattern
RCPs – Representative Concentration Pathways
SCA – Scandinavia pattern
SIC – Sea Ice Concentration
SLP – Sea Level Pressure

SON – September-October-November
SSPs – Shared Socioeconomic Pathways
SST – Sea Surface Temperature
SVD – Singular Value Decomposition
T2m – 2 meters Temperature
TP – Total Precipitation
WCRP – World Climate Research Program
Z500 – 500-hPa geopotential height

1. Introduction

The atmospheric circulation regulates the distribution of temperature and humidity gradients, which in turn determine the climate in various Earth regions. The fundamental components of atmospheric circulation are the zonal averages of climate variables and their variability. This has important impacts, often greater than seasonal means, on the environment, society and the economy. The North Atlantic European region is governed by unforced variability, which derives from climate system dynamics and that is defined as circulation anomalies. When they are recurrent, persistent, large-scale and extended over large geographical areas, they are called teleconnection patterns.
In particular, the pattern that governs climate variability in this geographical region is the North Atlantic Oscillation, which determines climate variability from the east seaboard of the United States to Siberia and from the Arctic to the subtropical Atlantic. The impacts it has, affect for example, surface temperatures, storms, and may have consequences for ecology, economy, and so on. Thus, considering the vastness of the area it influences, understanding the processes behind its behaviour is of high priority, particularly in the context of climate change. Depending on the phase in which the NAO is, the Mediterranean can experience cold and dry winters or, conversely, warmer and wetter ones. Additionally, strong variations in climate caused by the NAO exert a strong impact on marine temperatures and nutrients distribution, thus affecting aquatic ecosystems. For these reasons, it is crucial to understand what mechanisms regulate the teleconnection pattern and how its influence varies in the context of climate change and global warming, improving the predictability of its phases and understanding the impact that mechanisms have on the structure and amplitude of NAO-related climate anomalies.
The NAO is a mode of variability internal to the atmosphere and resulting from stochastic interactions between atmospheric storms and both the climatological stationary eddies and the time mean jet stream. However, there were evidence of a possible impact on its behaviour by natural external factors, such as the air-sea coupling, or by anthropological external factors, such as the increase in greenhouse gases, which leads to an increase in the radiative forcing (i.e. atmospheric warming). Even today, these mechanisms and their effects are still being analysed, and any further research in this area may help to increase the predictive abilities of the NAO, due to the greater level of persistence of external forcing interactions in comparison to those related to atmospheric noise only.

This research provides a general overview of climate variability in the North Atlantic region and then focuses on the NAO pattern and the impact that air-sea coupling and increased radiative forcing have on it. To do this, the observed variability was analysed through the ERA5 reanalysis model and that simulated through a series of experiments, provided by the meteorology group of the University of Barcelona, calculated with the standard configuration of the EC-EARTH3 global climate model for CMIP6. To assess the air-sea coupling, simulations in atmosphere-only mode (i.e., where the variables related to the ocean effect were fixed) and those in coupled mode, where the ocean also plays a role, were compared. Instead, to assess the impact of the radiative forcing, simulations forced at present conditions (year 2002) were compared with those forced at future conditions (year 2050).

This thesis firstly provides a detailed analysis of the climatology and climate variability in the North Atlantic European area with a focus on the NAO and the spatial structures of the climate anomalies associated with it, in order to present the mechanisms that regulate them, i.e. advection in the case of temperatures and the latitudinal shift of storms in the case of precipitation. The second objective is to assess the validity of the simulations performed with EC-EARTH by comparing the results obtained using the latter with those obtained with observations. Once the robustness of the experiments has been assessed, the third intention is to analyse the impact of the air-sea coupling on the NAO, in order to identify the degree of importance of the ocean action in the variations in the percentage of variability explained by the NAO and in the structure and position of the anomalies. Finally, given the extreme relevance of the topic of climate change, the last objective is to assess the impact of global warming, intended as an increase in the radiative forcing, on the NAO and simultaneously study how this varies depending on whether ocean action is taken into account or not. The impact is again assessed in terms of changes in the fraction of the variance explained and the shape and magnitude of the NAO-related climate variable anomalies. In this way, this research aims to increase knowledge about the effects of these two external forcings and to assess how relevant their consideration in future research may be.

After Chapter 1 which is the introduction, Chapter 2 provides a guide from the literature to introduce the topic and give a general framework on atmospheric circulation in the Northern Hemisphere and the NAO in particular. Chapter 3 describes data and methodologies used in the analysis. Chapters 4 and 5, on the other hand, provide the results obtained from the reanalysis model and simulations, respectively, introduced and compared with other studies. Finally, Chapter 6 provides conclusions and summarises the key points of the work.

2. From literature: atmospheric circulation and variability in the Northern Hemisphere

2.1 Atmospheric circulation and persistent variability

The atmospheric general circulation refers to the motion of the atmosphere as viewed from a global, long-term perspective and it explains how thermal energy and storm systems move over the Earth's surface. Usually it involves the seasonally-varying, climatological-mean circulation and its statistical properties of variability from day-to-day to year-to-year time scales and long-term variations associated with climate change. The circulation of the atmosphere is a key component of the climate, since it both responds to temperature and humidity gradients and helps to determine them by transporting energy and moisture. Features of interest include the belts of midlatitude westerlies and subtropical trade winds at the Earth's surface, the jet streams aloft and the storm tracks as is shown in **Errore. L'autoriferimento non è valido per un segnalibro.** (Wallace et al. 2015).

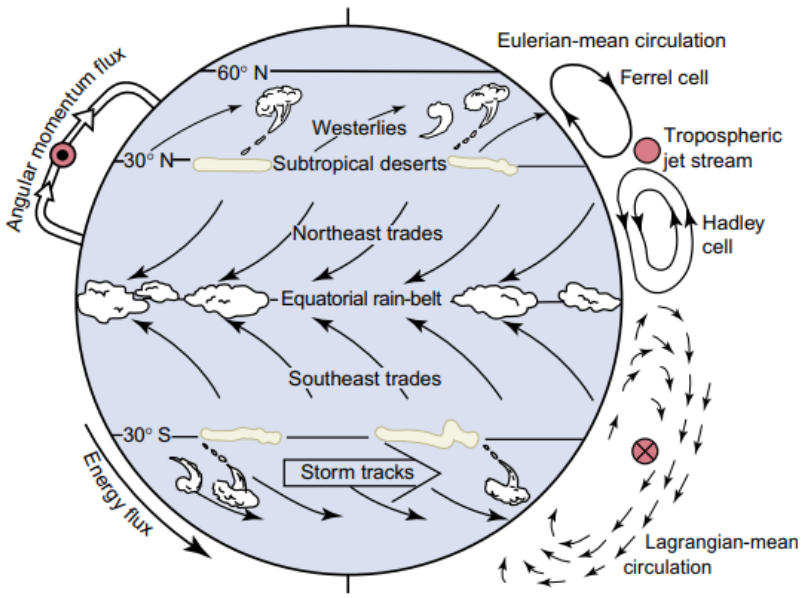

Figure 1 Schematic showing some of the essential features of the zonally averaged general circulation as they would appear on an idealized ocean covered but otherwise 'Earthlike' planet under equinox conditions. The red arrows pointing into the page at right and out of the page at left represent the eastward tropospheric jet streams. (From: Wallace et al. 2015)

The main effect of atmosphere motions is the transport of heat from the tropics to the polar regions in order to reduce the extremes of temperature that would otherwise result. Indeed with the sun directly over the equator, the ground and atmosphere there would heat up more than the rest of the planet because the solar radiation are spread over a small surface area to respect the high latitudes. In addition, there are the tilt of the Earth (which means that the location that receives most of the sun's radiation is constantly changing), the Earth's rotation accompanied by the Coriolis effect, the uneven distribution of water and land and the meridional gradient of insolation and albedo variations that are responsible of geographical variations in heating of the surface. All these factor leads to a complicate pattern of atmospheric circulation (Global Physical Climatology 2016).

Deepening the energy flows associated with atmospheric motions, the local energy balance of an atmospheric column of unit horizontal area includes the effect of radiation, sensible and latent heat exchange with surface, and the horizontal flux of energy in the atmosphere. The annually and zonally averaged net effect of radiative transfer in the atmosphere is a cooling, balanced by heating from latent heat of condensation and sensible heat from the surface. Among these two, the largest contribution is the supply of latent heat of vaporization from the surface that has a latitudinal structure reflected in the latitudinal structure of the atmospheric energy flux divergence: atmospheric motions export energy from the equatorial region to import it into the polar regions.

The physical phenomena associated with this energy transport have a wide variety of spatial and temporal scales. There are small-scale phenomena such as turbulence or mesoscale phenomena that are responsible for the vertical transport of momentum, moisture and energy flows. On the other hand, events that are responsible for the horizontal exchange of atmospheric fluxes between the tropics and the polar regions, are the large-scale phenomena such as extratropical cyclones, planetary-scale waves and the slow meridional circulation (Global Physical Climatology 2016). Underlying all these phenomena is the wind and its speed, which can be defined through three components (Figure 2): *u* is the zonal (or the eastward component), *v* is the meridional (also called northward component) and *w* is the vertical component which can be defined as the rate of change of altitude or pressure following a particle of air (Global Physical Climatology 2016).

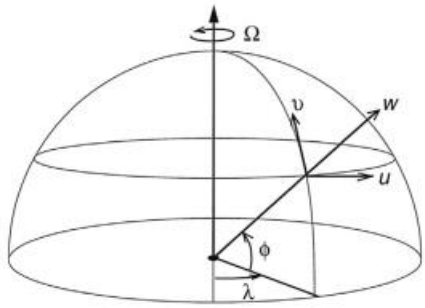

Figure 2 Local Cartesian coordinates on a sphere and the zonal (u), meridional (v) and vertical (w) components of the local vector wind velocity. (From: Global Physocal Climatology 2016)

Atmospheric circulation can be subdivided into zonally symmetric and eddy components, where zonally symmetric denotes longitudinally (zonally) averaged (i.e. averaged over a specific latitude and altitude) and eddy denotes departures from the zonal average (Wallace et al. 2015).

The zonally symmetric component can be divided into the zonal mean wind and the *Meridional Mean Circulation* (MMC). The former is derived from the zonal mean of the eastward component of the wind (*u*) and at the Earth's surface is westerly[1] in most latitudes between 30° and 70° while it becomes easterly, named also *trade wind*, in the tropics. The easterly wind in the middle latitudes strengthens in winter (when the north-south temperature gradient is higher) and with altitude, and peaks in the boundary zone between the troposphere and stratosphere where it is named *tropospheric jet stream*. In contrast, in high latitudes, westerly winter winds increase in intensity with altitude even in the stratosphere and are associated with *polar night jets* (Global Physical Climatology 2016).

The MMC, weaker than the eastward component, is derived from the zonal average of the meridional (*v*) and vertical (*w*) components of wind speed and can be described by a mass stream function. The motion is organized into distinct patterns called meridional cells. Their behaviour

[1] In meteorology, winds are called westerly when they flow from west to east and easterly when they flow from east to west.

results in a flow toward the equator at the Earth's surface in the trade wind belt and a poleward flow in the eastward wind belt at higher latitudes.

The strongest of the cells that dominate the meridional circulation is the tropical *Hadley cell*: it has the rising branch of air in the tropical latitudes in the summer hemisphere, in correspondence of the belt of the heaviest tropical rainfall, and the sinking branch in the colder subtropical latitudes in the winter hemisphere, where the desert regions are located. The circulation that takes place in this cell is called *thermally direct* in that it is characterized by the rise of warmer air and the sinking of cooler air. If the annual average is taken into account, the effect obtained is a weak transport of energy from the northern hemisphere to the southern hemisphere. Then there are the *Ferrels cells*, which are located in the middle latitudes and have a weaker and opposite circulation than the Hadley ones. In fact, the movement of air in this case is *indirect thermally* with the rising located in colder regions and sinking in warmer ones. These types of cells are a by-product of the strong transport of energy and momentum to the pole by the eddy circulations and compensate these flux transfers by preventing the thermal wind balance from being destroyed (Global Physical Climatology 2016; Wallace et al. 2015).

So eddies, which as anticipated are deviations from the time or zonal mean, are critical in transporting flows in the middle latitudes. In fact, the meridional transport in this area is dominated by cyclones and anti-cyclones which are disturbances that result in large variations in wind and temperature with important effects in the zonal mean climate. The fluctuations associated with eddies can be either transient, and thus variations over time, or stationary, i.e. deviations from the zonal mean. The main effect given by eddies is the transport of air particles charged with sensible and latent heat to the pole. Northward eddy fluxes of temperature are produced when northward-flowing air is warmer than southward-flowing air. (Global Physical Climatology 2016; Wallace et al. 2015)

Transient eddy fluxes are related with the rapidly developing and decaying weather disturbances of middle latitudes, which generally move eastward with the prevailing flow and contribute much of the variations of wind and temperature. The energy available in the mean meridional temperature gradient is converted to energy of waves and it give rise to a westward displacement of the temperature wave relative to the pressure wave. At the Earth’s surface these latter are marked by intensifying cyclones (gyres that circulate in the same sense as Earth’s rotation, so counterclockwise in the Northern Hemisphere) that have a large zonal phase shift between their pressure and temperature waves, and thus produce efficient poleward transport of heat and moisture (Global Physical Climatology 2016).

Stationary eddy fluxes, also called *stationary planetary waves*, are departures of the time average from zonal symmetry and they result from east-west variations in surface elevation and surface temperature associated with the continents and oceans (Global Physical Climatology 2016). They make an appreciable contribution to the poleward transport of sensible heat particularly in the Northern Hemisphere in the winter season, when for example the Icelandic and Aleutian lows are prominent stationary wave features (Wallace et al. 2015).

The poleward fluxes of temperature by stationary and transient eddies peak at about 50° of latitude in the winter hemisphere in the lower part of troposphere, where these fluxes have large seasonal

variations, with large values in winter and small values during summer (Global Physical Climatology 2016; Nigam & Baxter 2015).

When discussing atmospheric circulation, therefore, in addition to considering zonal averages, it is important to take climate variability into account. Indeed, weather conditions are always a little different from their average due to instabilities of the state toward which the heating gradients drive it. These fluctuations constitute climate variability and are as important for characterizing climate as their mean: their amplitude is a characteristic of the climate itself (because it's low in the equatorial region and high in the polar regions) and their impacts on ecosystems and societies are much greater than regular seasonal variations (Delaygue Gilles 2019). Studying them and analysing their mechanisms can increase the ability to predict climate, and enhancing knowledge of climate forcing mechanisms, such as greenhouse gas emissions, increases the possibility of understanding how greenhouse gas emissions will continue in the future (Global Physical Climatology 2016). Also, these patterns of variability are linked to numerous phenomena such as sea ice variations, large-scale temperature anomalies, fluctuations in the Atlantic thermohaline circulation and impacts on the biosphere, such as bird migrations or the growth cycle of plants (Feldstein & Franzke 2016). So learning more about them is of great importance.

Variability is distinguished into unforced and forced by natural or anthropological causes. The former derives from internal dynamics, without specific causes, while the latter can be associated with changes in climate boundary conditions that are either natural such as volcanic eruptions or anthropogenic such as increased greenhouse gases (GHGs) emissions.

Unforced variability reflects weather patterns and circulation systems that occur on many time scales, lasting from a few days, to a few weeks, a few months, several years or several centuries. It is usually characterized in terms of anomalies, that are differences between the instantaneous state of the climate system and the climatology (the main state computed over many years representative of the era under consideration) (Climate Prediction Center Internet Team 2008). Recurring and persistent, large-scale pattern of pressure and circulation anomalies that spans vast geographical areas are called *teleconnection pattern*. Teleconnections refer to the climate variability links between non-contiguous geographic regions exhibiting contemporaneous variations of opposite sign. These patterns are also referred to as preferred modes of low-frequency (or long time scale) variability. Indeed they typically last for several weeks to several months, but sometimes they can be prominent for several consecutive years reflecting an important part of both the interannual and interdecadal variability of the atmospheric circulation. The features that cause teleconnections to be long lasting are their long wavelength, their slow growth and decay and their forcing mechanism (Feldstein & Franzke 2016). Teleconnections are especially well-developed in Northern winter, when they influence sub seasonal variability, notably, in surface temperature and precipitation. Many of the teleconnection patterns are also planetary-scale in nature, and span entire ocean basins and continents. For example, some patterns span the entire North Pacific basin, while others extend from eastern North America to central Europe (Climate Prediction Center Internet Team 2008).

The reasons for their origin are not yet very well understood. It is known that the forcing mechanisms for teleconnections include tropical convection, a positive feedback process that involves synoptic-scale eddies and anomalies in the strength of stratospheric polar vortex (Feldstein & Franzke 2016). The large-scale interactions in middle latitude weather systems move energy from the scale at which

baroclinic instability generates waves to both larger and smaller scale. The energy of the middle latitude westerly winds is delivered from the smaller scale eddies that define the weather in middle latitudes. The energetic interactions between middle latitude storm system and zonal jets are thus intense and this translates into mode of variability in which jets and their embedded eddy structures move towards north and south (Global Physical Climatology 2016).

They are all a naturally occurring aspect of the chaotic atmospheric system, and they can arise primarily as a reflection of internal atmospheric dynamics. Additionally, some of these, particularly those over the North Pacific, are sometimes forced by changes in tropical sea-surface temperatures and tropical convection associated with both the El Niño-Southern Oscillation (ENSO) [2] cycle and the Madden-Julian Oscillation (MJO)[3] (Climate Prediction Center Internet Team 2008).

Teleconnection patterns reflect large-scale changes in the atmospheric wave and jet stream patterns, and influence temperature, rainfall, storm tracks, and jet stream location/intensity over vast areas. Thus, they are often responsible for abnormal weather patterns occurring simultaneously over seemingly vast distances. For example, the 1995/1986 winter was very cold and snowy over much of eastern North America, while northern Europe and Scandinavia were cold and southern Europe/northern Africa experienced very wet and stormy conditions. These conditions were all partly related to the same teleconnection pattern: a strong negative phase of the NAO. Ten prominent teleconnection patterns can be identified in the Northern Hemisphere extratropic throughout the year, and all of these patterns have appeared previously in the meteorological literature (Climate Prediction Center Internet Team 2008). The dominant ones are the NAO along with the very similar Northern Annular Mode (NAM or Atlantic Oscillation (AO)) and the Pacific/North American (PNA) pattern (Feldstein & Franzke 2016).

Instead the prominent patterns over North Atlantic European (NAE) region are the NAO accompanied by the East Atlantic pattern (EA), the East Atlantic/West Russia pattern (EA/WR) and the Scandinavia pattern (SCA).

In the following section the structure and behaviour of the NAO will be discussed in more detail, while the other three modes of variability are explained better in Chapter 4.

2.2 The North Atlantic Oscillation and its relationship with surface climate

The North Atlantic Oscillation is one of the most prominent teleconnection patterns throughout the year. It is a simultaneous variation in climate over distant parts of the globe as a consequence of transient behaviour of atmospheric planetary-scale waves and it dictates climate variability from the eastern seaboard of United States to Siberia and from the Arctic to the subtropical Atlantic, in particular during boreal winter. The NAO swings from one phase to another producing large changes in the mean wind speed and direction over the Atlantic, in the heat and moisture transport between the Atlantic and the neighbouring continents and in the intensity and number of storms, their paths

[2] The ENSO is a recurring climate pattern involving changes in the temperature of waters in the central and eastern tropical Pacific Ocean. (https://www.weather.gov/mhx/ensowhat)

[3] The MJO is a mode of sub-seasonal atmospheric variability that influences the location and strength of tropical precipitation. (https://www.weather.gov/mhx/ensowhat)

and weather. Therefore it has a direct impact on numerous natural processes and consequently on human life, e.g. crop growth, energy supply and water management. Improved understanding of the processes that regulate its behaviour and its variability and how it may be influenced by anthropogenic climate change is thus of paramount importance (Hurrell et al. 2003).

The NAO consists of a north-south dipole of anomalies, with one centre located over Iceland and the other centre of opposite sign spanning the central latitudes of the North Atlantic between 35° N and 40° N (Climate Prediction Center Internet Team 2008). It's the only teleconnection pattern evident throughout the year in the Northern Hemisphere (NH) (Hurrell et al. 2003).

Both phases of the NAO are associated with basin-wide changes in the intensity and location of the North Atlantic jet stream and storm track, and in large-scale modulations of the normal patterns of zonal and meridional heat and moisture transport, which in turn results in changes in temperature and precipitation patterns often extending from eastern North America to western and central Europe (Climate Prediction Center Internet Team 2008).

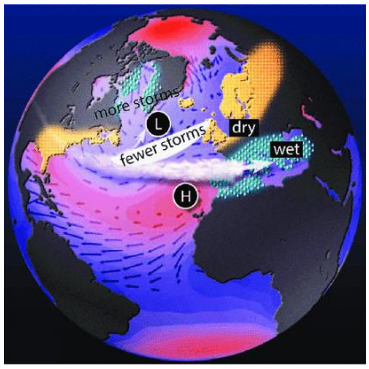

Figure 3 Positive NAO phase. (From: https://www.ldeo.columbia.edu//res/pi/NAO/)

The positive phase of the NAO (Figure 3) reflects higher-than-normal heights and surface pressure south of 55 °N (over the central North Atlantic, the eastern United States and western Europe) combined with a region of anomalously low heights and surface pressure across the high latitudes of the North Atlantic (throughout the Arctic) to enhance the climatological meridional pressure gradient. The largest amplitude anomalies occur in the vicinity of Iceland and across the Iberian Peninsula. This positive phase is associated with stronger-than-average surface westerlies across the middle latitudes of the Atlantic onto Europe, with anomalous northerly flow across the Canadian Arctic and Mediterranean (Hurrell et al. 2003).

These anomalous streams lead to wetter conditions over northern Europe and most of northeastern North America. Also under the positive NAO mode, colder conditions prevail over parts of Quebec, Newfoundland and Labrador, and western Greenland, and additional sea ice develops in Hudson Bay, Baffin Bay, and off western Greenland. The Mediterranean region, meanwhile, experiences cool, dry winter weather (Rafferty J. P. 2023).

The negative phase (Figure 4) reflects an opposite pattern of height and surface pressure anomalies, indeed it's characterized by weaker high and low pressure systems over the regions mentioned above. The reduced pressure gradient over the region slows the pace of westerly winds, which allows cold, dry air to be drawn into northern Europe from northern Russia and the Arctic. During such years a prominent northward-reaching arc in the polar-front jet stream, caused in part by blocking anticyclones that redirect the jet stream northward, allows warmer conditions to prevail from Hudson Bay to western Greenland. The jet stream, after skirting the reduced low-pressure cell over Iceland, arcs south over the North Atlantic carrying moisture and warm air to southern Europe (Rafferty J. P. 2023).

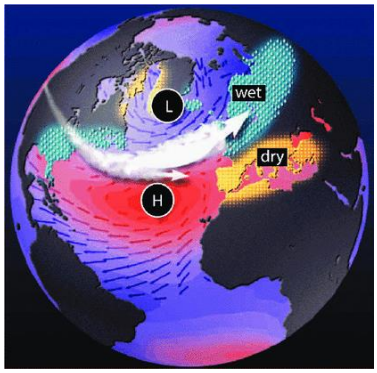

Figure 4 Negative NAO phase. (From: https://www.ldeo.columbia.edu/res/pi/NAO/)

There is not a single way to represent the NAO. One of the most popular techniques is the EOF analysis (which will be explained in detail in Chapter 3 in the methodology section) through which the leading eigenvectors from the monthly Sea Level Pressure anomalies are calculated. In Figure 5 below, the two phases of the variability mode defined using the method just mentioned are shown respectively from top to bottom.

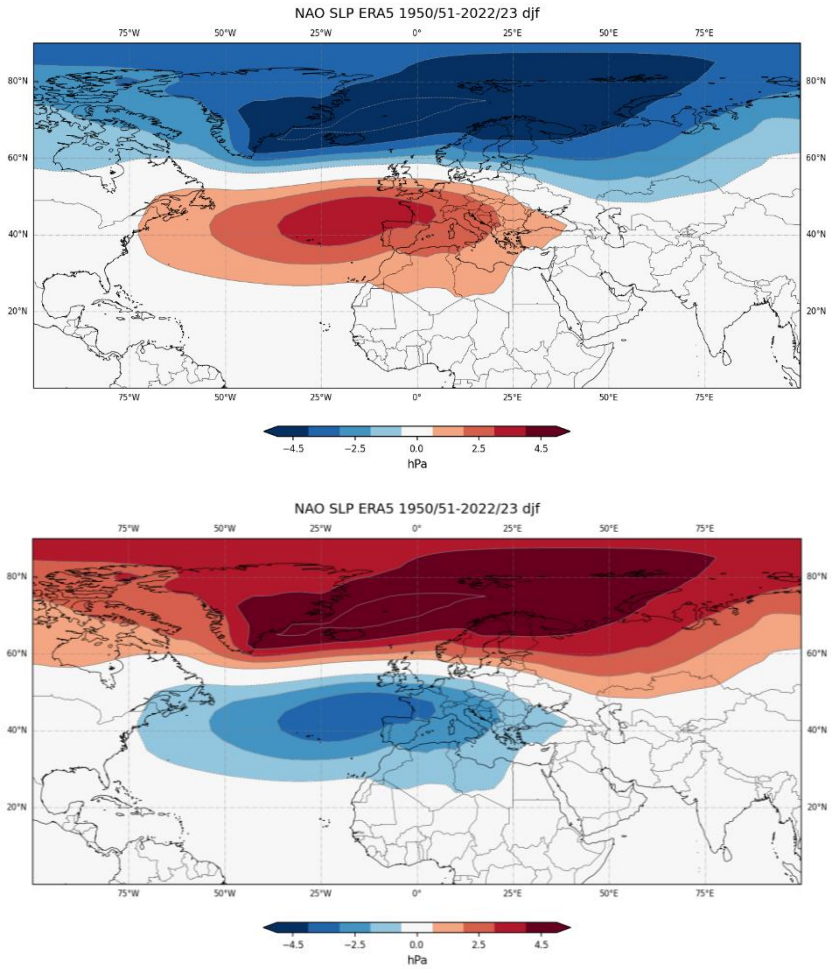

Figure 5 The positive and negative NAO phase calculated from the winter season (DJF) Sea Level Pressure variability in the North Atlantic European region using the EOF analysis. Further details on methods and data are provided in the next chapter.

2.2.1 Impacts: variations in North Atlantic climate

Teleconnection patterns in general and NAO in particular are of considerable interest because of their impacts on surface hydroclimate. Significant climate anomalies on different timescales are often attributable to a dominant phase of one or more teleconnection patterns (Nigam & Baxter 2015). The NAO exerts a dominant influence on wintertime surface air temperature and Sea Surface Temperature (SST) across much of the Northern Hemisphere (NH) and specifically in the North Atlantic European region. Simultaneously with these changes, there are also changes in storminess and precipitation, in the heat content of the ocean and the currents carrying it, and in ice and snow cover: these alterations to the climate obviously have impacts on ecosystems and human activities (Hurrell et al. 2003).

When the NAO mode is positive the enhanced westerly flow across the North Atlantic during winter moves, thanks to advection, relatively warm (and moist) air over much of Europe and downstream, while stronger northerly winds over Greenland and northeastern Canada carry cold air southward and decrease land temperature and SST over the northwest Atlantic. Furthermore cooling of North Africa, eastern Mediterranean and Middle East and warming of south of North America (associated with the stronger clockwise flow around the high pressure centre) are also notable (Hurrell et al. 2003). When the NAO index is well below normal, the tendencies instead are generally opposite: colder conditions are brought to eastern North America and northern Europe mainly by more-frequent intrusions of Arctic air.

It is important to remember that the heat storage of the land is lower than that of the ocean, so changes in continental surface temperature are much larger than over water surface and they tend to dominate average temperature variability. Folland et al. (2001) observed that much of the warming that has contributed to the global temperature increases of recent decades has occurred during winter and spring over the NH. Since 1980s the winter temperatures have been 1-2 °C warmer-than-average over North America, Europe and Asia while temperatures over the northern ocean have been slightly colder-than-average. This pattern is related to changes in atmospheric circulation, which are reflected by Sea Level Pressure (SLP) anomalies and in particular the Atlantic sector SLP changes clearly reflect the predominance of positive NAO index phase over this period. Also Hurrell et al. (2003) showed that much of the local cooling in the northwest Atlantic and warming across Europe and Eurasia resulted directly from decadal changes in the North Atlantic atmospheric circulation in the form of NAO. So the strong impact of this mode of variability on land surface temperature evolution is evident.

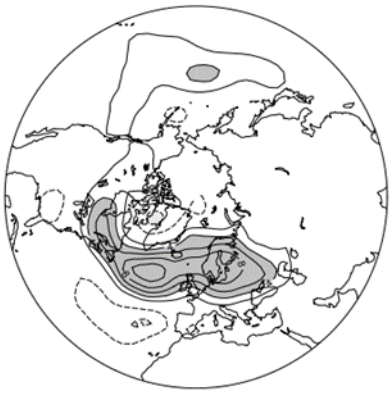

Figure 6 Storm track anomalies for 1958-1998 winters (DJFM) expressed in terms of amplitude (gpm) by regression onto the NAO index. The contour increment is 2 gpm and anomalies greater than 4 gpm in magnitude are shaded. (From: Hurrel et al. 2003)

Also the intensity, number and paths of storms and precipitations are affected by changes in the mean circulation patterns over north Atlantic associated with NAO. During winter a well-defined storm track connects the North Pacific and North Atlantic basins, with maximum storm activity over oceans. Generally positive NAO index winters are associated with a north-eastward shift in the Atlantic storm activity with enhanced activity from Newfoundland into Northern Europe and a modest decrease in activity to the south. Positive NAO index winters are also typified by more intense and frequent storms in the vicinity of Iceland and Norwegian Sea (Figure 6).

The ocean integrates the effects of storms in the form of surface waves, so that it exhibits a marked response to long lasting shifts in the storm climate. The upward trend toward more positive NAO index winters has been associated with increased wave heights over the northeast Atlantic and decreased wave heights south of 40°N, following by consequences for ecology, industries, shipping activities and coastal development (Hurrell et al. 2003).

Changes in the mean flow and storminess associated with swings in the NAO index are reflected in pronounced changes in the transport and convergence of atmospheric moisture and so the distribution of evaporation (E) and precipitation (P): E exceeds P over much of Greenland and the

Canadian Arctic during high NAO index winters where changes between high and low NAO index states are on the order of 1 mm/d. Drier conditions of the same magnitude also occur over much of central and southern Europe, Mediterranean and parts of Middle East, whereas more precipitation than normal falls from Iceland through Scandinavia (Hurrell et al. 2003). Instead during low NAO index winters North America receives additional snow, while Europe receives less precipitation than normal. The drier conditions over northern Europe result from the weak state of the pressure cells over Iceland and the North Atlantic during the NAO's negative mode; the reduced pressure gradient over the region slows the pace of westerly winds, which allows cold, dry air to be drawn into northern Europe from northern Russia and the Arctic (Rafferty J. P. 2023). As was seen for temperature, also in the case of precipitation the changes that were and are observed in the Atlantic basin are correlated with the NAO pattern and its trend. In fact, for example, since 1980 more precipitation than usual has affected the Scandinavian region, which has therefore not been affected by glacier retreat, that was and still is a widespread phenomenon that leads to severe criticality in the Alps (Hurrell et al. 2003).

Also the SST fluctuations are related to the strength of the NAO. The leading pattern of SST variability in winter appear as a tri-polar structure marked, in case of positive mode, by a cold anomaly in the subpolar North Atlantic, a warm anomaly in the middle latitudes centred off Cape Hatteras and a sub-tropical anomaly between the equator and 30°N. This structure suggests that SST anomalies are driven by changes in the surface wind and air-sea heat exchanges associated with NAO variations. This relationship is strongest when the NAO index leads an index of the SST variability by several weeks which confirmed that large scale SST over extratropical oceans responds to atmospheric forcing on monthly/seasonal time-scale. Considering decadal and longer time scale, persistent SST anomalies appear to be related to persistent anomalies patterns of SLP, but also to other different mechanisms like the non-local dynamical processes in the ocean. The oceanic response to NAO variability is also evident in changes in the distribution of winter convective activity in the North Atlantic: the convective renewal of intermediate/deep waters in Labrador Sea and the Greenland-Iceland-Norway (GIN) seas contribute in the production and export of North Atlantic Deep Water and help to drive thermohaline circulation. The intensity of winter convection is characterized by interannual variability and by interdecadal variations that appeared to be synchronized with NAO. Indeed, it has been observed that the generation and termination of salinity propagation modes, which are linked to the thermohaline circulation, are connected to changes in the NAO.

The strong variability in Arctic sea ice in the North Atlantic sector is also associated with variations in SLP that resemble the NAO, which is consistent with the atmosphere directly forcing sea ice anomalies (Hurrell et al. 2003).

The changes just described in temperatures, precipitation, ocean circulations, and sea ice obviously involve effects on ecology and economics. For example Straile et al. (2003) showed an effect of NAO influence in the physics, chemistry and biology of lakes in the winter hemisphere. In fact, the strong variations in climate due to NAO have an important impact in the seasonal distribution and development of temperatures and nutrients. Economic activities are also affected by NAO-related changes in climate: there is, for instance, increased cost to be incurred in order to increase the protection of coasts that are affected by increasingly high waves due to NAO behaviour, or again it

is necessary to re-adapt winter tourism in the Alps due to new conditions given by the lack of snow (Hurrell et al. 2003).

2.2.2 Mechanism and dynamics

The North Atlantic Oscillation is a mode of variability internal to the atmosphere, even if there is some evidence that external factors such as volcanic aerosols, anthropogenic factors as well as interactions between atmosphere and surface or between troposphere and stratosphere may have an influence on it (Hurrell et al., 2003).

In terms of its life cycle, Feldstein & Franzke (2016) showed that both high-frequency and low-frequency eddy momentum fluxes contribute to NAO growth while, during its decay, high-frequency eddies act to maintain the NAO and low-frequency ones contribute to its demise. Benedict et al. (2004) found that the pattern of the NAO results from the breaking of synoptic-scale waves, which according to the way it occurs gives rise to one or the other phase. Rivière (2009) showed that the type of wave breaking depends on both absolute vorticity and the stretching contribution of quasi-geostrophic potential vorticity: when the former term is dominant the positive phase appears from the residual of anticyclonic wave breaking on the anticyclonically sheared equatorward side of the mid-latitude jet; and vice versa when the latter term is larger its negative phase emerge from cyclonic wave breaking on the cyclonically sheared poleward side of the jet.

It is clear that the NAO pattern is a large-scale atmospheric phenomenon primarily arising from stochastic interactions between atmospheric storms and both the climatological stationary eddies and the time mean jet stream. So month-to-month and year-to-year changes are largely unpredictable. But it is not yet clear on what extent the external processes mentioned before play a role in NAO variability, especially where long time scales are concerned. Considering the significant impact of the mode under analysis on the climate of the NH, that external forces might nudge the atmosphere to assume a high or low NAO index value over a particular month or season is important. Even a small amount of predictability could be useful and a better understanding of how the NAO responds to external forcings is crucial to the current debate on climate variability and change (Hurrell et al. 2003). From here on are explained some external physical processes that affect the NAO.

Starting from the atmosphere, Atmospheric General Circulation Models (AGCM) provide evidence that the basic structure of the NAO arises from internal, nonlinear dynamics of the atmosphere. Indeed the observed spatial pattern and amplitude of NAO anomalies are well simulated by AGCMs forced with climatological annual cycles of all forcing external to the atmosphere (insolation, SST, sea ice, snow cover). Thompson et al. (2003) stated that the interactions between the time-mean flow and the transient eddies are central and give rise to a fundamental time scale for NAO fluctuation about 10 days. This intrinsic atmospheric variability exhibits little temporal coherence, mostly consistent with the time scale of observed NAO variability and the climate noise paradigm. One possible exception to this reference is the enhanced NAO variability over the latter half of the 20th century and the apparent upward trend in the boreal winter NAO index. Numerous studies have concluded that the observed trend in the winter NAO index is not explained by the internal variability

of the various coupled climate models (atmosphere-ocean) used. This leads to the conclusion that this trend could result from external processes that have an effect on atmospheric circulation in the lower stratosphere over long time scales, such as an increase in GHG concentration. In fact, in the lower stratosphere it happens that if the variability of geopotential height is less than usual in the polar region, the polar vortex is enhanced and anomalously cold. This causes the NAO tends to assume its positive phase (Hurrell et al. 2003). This result seems to suggest that some stratospheric control of troposphere can occur. Thompson et al. (2003) review the evidence for this downward control and evaluate the possible mechanisms which involve both the effect of stratospheric flow on the refraction of planetary waves dispersing upwards from the troposphere and the direct momentum forcing. Other factors provide evidence for a stratospheric influence on the surface climate are the atmospheric response to tropical volcanic eruptions and reduction in stratospheric ozone and increasing in GHG concentration. Shindell et al. (1999) also find that the latter can lead to a trend toward the positive index phase of the NAO in surface circulation.

So interactions with lower stratosphere are a possibility to enhanced the predictability of the NAO phenomenon: this mechanism may explain how change in atmospheric composition influence the NAO. Knowing the long time scale of stratospheric circulation variability, the coupling between stratosphere and troposphere via wave mean flow interactions could raise the level of predictive skill for winter NAO (Hurrell et al. 2003).

Although the feedback of the SST on the atmosphere has a weak effect when compared with the internal variability of the atmosphere, it is important to study the interactions between the ocean and the atmosphere in order to gain a deeper understanding of the NAO amplitude details and its long-term evolution and consequently to try to increase its predictability. There are a number of studies that have delved into the possible influence by the ocean on the NAO. For example, it has been shown that the time scale imposed by ocean surface heat capacity results in low-frequency variability of both SST and air temperature in the lower troposphere, highlighting the persistence of the ocean. The studies are supported by observations that winter SST anomalies, born in the western subtropical gyre, spread eastward along the path of the Gulf Stream and North Atlantic Current with a transit time of roughly a decade (Hurrell et al. 2003).

An important line of research is to understand the influence of changes in SST (and other factors such as sea ice) on the atmosphere of mid-latitudes. This issue has been addressed in numerous studies based on AGCM experiments with specified SST anomalies. Visbeck et al. (2003) prescribe a realistic reproduction of the entire basin SST response to NAO variability and they obtain a realistic atmospheric NAO pattern as response, but whether the forcing comes from tropical or extra-tropical part of the ocean has not been resolved.

In most of the studies conducted, a weak response of AGCM to SST anomaly changes was noted, and therefore doubt arose regarding the actual importance of oceanic forcing for climate anomalies in general and NAO specifically. It is possible that AGCM experiments with prescribed SST don't correctly represent the process in nature, where atmospheric fluctuations cause SST variability, and it's the "back interaction" of feedback of the SST anomalies that is sought. However, some evidence has been found. For example, Barsugli & Battisti (1998) states that the thermal damping on the atmosphere is reduced when the ocean responds to changes in the atmosphere, resulting in the emergence of stronger and more persistent anomalies in the two systems. Or Kushnir et al. (2002)

explains the fact that the NAO is stronger and more persistent during winter by stating that changes in the SST due to large circulation anomalies alter the thermal gradient at the Earth's surface and consequently the transient baroclinic activity which in turn have an effect on the same large-scale anomalies. Thus this process together with thermal damping may be the causes of the persistence of the NAO in winter and the correlation between the late spring SST anomalies and the condition of the NAO during autumn and early winter.

Another source of ocean-atmosphere interaction is the possible remote forcing by the tropical oceans on the NAO. Indeed, several studies have found that SST variability in the tropical North and South Atlantic can have an effect on tropical Atlantic rainfall and consequently on the North Atlantic circulation at middle latitudes. However, in other studies, this forcing mechanism by the tropical oceans has been considered as a secondary effect, so it is not yet possible to clearly distinguish the effect of atmospheric interactions with the tropical or extra tropical ocean. Similarly, it remains to be determined whether ENSO has a significant effect on the North Atlantic climate and on large-scale anomalies in this region (Hurrell et al., 2003).

The role of sea ice and land snow cover can also be studied as predictors of the NAO. Indeed, studies have shown that changes in sea ice cover in the Labrador and Greenland Seas as well as in the Arctic Sea correlate well with changes in NAO. The possibility of subsequent feedback on atmospheric circulation anomalies is of considerable interest. The latter is still under analysis, and recent studies have found that decreasing (or increasing) ice concentration and snow cover in some areas in the North Atlantic may have an influence on NAO phases (García-Serrano et al. 2015; Hurrell et al. 2003; Santolaria-Otín et al. 2020).

Thus, it has been shown that changes in the amount and location of tropical warming, which is more persistent than that in mid-latitudes, may have an influence on the behaviour of the North Atlantic Oscillation, as well as variations in heat exchange between the atmosphere and other elements such as ocean, sea ice or land systems. All of these possible interactions have greater levels of persistence than atmospheric noise alone and therefore could provide an enhancement to the NAO's predictive abilities.

3. Data and methods

3.1 Data from ERA5

For analysing the state of the climate, monthly Sea Level Pressure (SLP), 2 metres temperature (T2m) and total precipitation (TP) data from 1950 to 2023 from ERA5 have been used. ERA5 is the latest European Centre Medium Weather Forecast (ECMWF) reanalysis. A climate reanalysis gives a numerical description of the recent climate, produced by combining models with observations using the principle of data assimilation. It contains estimates of atmospheric parameters such as air temperature, pressure and wind at different altitudes, and surface parameters such as rainfall, soil moisture content, ocean-wave height and sea-surface temperature. The estimates are produced for all locations on earth, and they span a long time period that can extend back several decades.

ERA5 provides a snapshot of the atmosphere, land surface and ocean waves for each hour from 1940. It continues to be extended forward in time, with daily updates being made available 5 days

behind real time and it includes an uncertainty estimate which highlights the considerable evolution of the observing system, on which reanalysis products rely. Data are available on regular latitude-longitude grids at 0.25° x 0.25° resolution, with atmospheric parameters on 37 pressure levels (Copernicus Climate Change Service; European Centre for Medium-Range Weather Forecasts).

3.2 Data from EC-Earth

To assess the impact of the air-sea coupling on the NAO, the EC-EARTH climate model version 3.3 was used.

EC-EARTH is a modular Earth System Model (ESM), that is a numerical models of the Earth's climate system and it is used to understand how the Earth's various components, including the atmosphere, oceans, land surface, biosphere, and cryosphere, interact with each other and how they respond to natural and human-induced changes. These models simulate the physical, chemical, and biological processes that govern the Earth system, at different levels of complexity. As such, they are essential tools for understanding and predicting climate variability and climate change.

Specifically EC-EARTH is developed by the European consortium of national meteorological services and research institutes and it’s representative of many models. EC-EARTH3 comprises model components for various physical domains and systems components: the atmosphere and land domains are covered by ECMWF's IFS cycle 36r4 (based on Integrated Forecast System 4, https://www.ecmwf.int/sites/default/files/elibrary/2011/11209-new-ecmwf- seasonal-forecast-system-system-4.pdf), which is supplemented with a coupling interface to allow boundary data exchange with other components; NEMO3.6 (Nucleus for European Modelling of the Ocean, Madec 2008, 2015) and LIM3 (Louvain-la-Neuve Sea Ice Model, Rousset et al. 2015; Vancoppenolle et al. 2009) models are the ocean and sea ice components, respectively; HTESSEL (Hydrology Tiled Scheme for Surface Exchanges over Land, Balsamo et al. 2008; Boussetta et al. 2013; Dutra et al. 2010; van den Hurk et al. 2000) is the land surface model interfacing with the atmospheric boundary layer and solving the energy and water balance at the land surface; biogeochemical processes in the ocean are simulated by the PISCES model (Pelagic Interactions Scheme for Carbon and Ecosystem Studies, Aumont et al. 2015); dynamical vegetation, land use, and terrestrial biogeochemistry are provided by LPJ-GUESS (Lund–Potsdam–Jena General Ecosystem Simulator, Lindeskog et al. 2013; Smith et al. 2014); aerosols and chemical processes in the atmosphere are described by TM5 (Tracer Model version 5, van Noije et al. 2014); the ice sheet model PISM (Parallel Ice Sheet Model, Bueler & Brown 2009; The PISM Team: PISM 2019; Winkelmann et al. 2011) could be optionally utilized to model the Greenland Ice Sheet. In this work was used the version Atmosphere-Ocean General Circulation Model (AOGCM), without other components.

The components run separately but they are connected by fluxes of heat and water and the exchange of that fluxes are regulated by a coupler: a piece of software that takes variables from one model and pass them to another and vice versa.

In that case, most of the model components are coupled through the OASIS3-MCT coupling library (Ocean Atmosphere Sea Ice Soil, Craig et al. 2017), while some software components include more than one model component, e.g., the sea ice model being a part of the ocean model. The OASIS3-MCT coupler provides a technical means of exchanging (sending and receiving) two- and three-

dimensional coupling fields between different model components on their different grids (Döscher et al. 2022).
Furthermore EC-EARTH has contributed to the Coupled Model Intercomparison Project (CMIP). CMIP is a coordinate climate modelling experiment adopt by the World Climate Research Program (WCRP), where it has been used a common set of forcing and boundary conditions. In this experiment the models which are been compared, are mainly coupled models that are among the most important tools for the prediction of future climate. Indeed the aim of this project is to evaluate and improve GCM in order to advance the scientific credibility of climate model predictions. The project has been ongoing since 1995 and has led to a better understanding of past, present, and future climates. The current version of EC-EARTH3 for CMIP6 (that is the EC-EARTH v3.3 used for the following analysis) still leans on the original idea of a climate model system based on the seasonal prediction system of ECMWF (Zhang et al. 2020). In order to achieve the goal of improving future climate predictions, CMIP6 commissioned two groups to develop new scenarios to explore how the world might change over the rest of the 21st century (Zeke Hausfather, 2018). One group developed the “Representative Concentration Pathways” (RCPs), describing different levels of greenhouse gases and other radiative forcings that might occur in the future. Researchers have designed four pathways, spanning a broad range of forcing in 2100 (2.6, 4.5, 6.0, and 8.5 watts per meter squared), but purposefully did not include any socioeconomic “narratives” to go alongside them (Zeke Hausfather, 2018). The second group indeed has built a range of "pathways" that examine how global society, demographics and economics might change over the next century. They are collectively known as the "Shared Socioeconomic Pathways" (SSPs) (World Climate Research Programme CMIP6, 2021). These SSPs look at five different ways in which the world might evolve in the absence of climate policy and how different levels of climate change mitigation could be achieved when the mitigation targets of RCPs are combined with the SSPs. The two efforts were designed to be complementary. The RCPs set pathways for greenhouse gas concentrations and, effectively, the amount of warming that could occur by the end of the century. Whereas the SSPs set the stage on which reductions in emissions will – or will not – be achieved. The SSPs are based on five narratives describing broad socioeconomic trends that could shape future society. These are intended to span the range of plausible futures and they include: a world of sustainability-focused growth and equality (SSP1); a “middle of the road” world where trends broadly follow their historical patterns (SSP2); a fragmented world of “resurgent nationalism” (SSP3); a world of ever-increasing inequality (SSP4); and a world of rapid and unconstrained growth in economic output and energy use (SSP5) (Zeke Hausfather, 2018).

A set of twin simulations called “Experiment 2” performed with the standard configuration of EC-EARTH3.3 for CMIP6 have been used and compared. They are characterized by a standard horizontal T255 spectral resolution[4] corresponding approximately to 0.7° in longitude-latitude (~ 80 km), with 91 vertical level up to 0.01 hPa (L91). They are two 250 years long simulations in coupled mode and atmosphere-only mode. The first one has fixed (time-invariant) radiative forcing, aerosols and chemical constituents (including ozone) at year 2002, which is well removed from any explosive

[4] The spectral resolution refers to the highest retained number in linear triangular truncation (Haarsma et al. 2020).

volcanic eruption and ENSO was in a neutral phase; hence, there is no interannual variability or secular change in the applied forcings (Palmeiro et al. 2023). The atmosphere-only simulation, in addition to the radiative forcing fixed at the year 2002, has prescribed, repeated seasonal cycle for SST/SIC (Sea Surface Temperature/Sea Ice Concentration) whose climatology is computed over 1988-2007. Each control integration is initialized in 2002 after a spin-up of 30 years.
To assess the impact of the radiative forcing on NAO together with these two 250-year long simulations at present condition also two 250-year long simulations at near future conditions (fixed radiative forcing at year 2050) both in coupled and atmosphere-only mode have been used. In the latter, initial conditions for the system (ocean, atmosphere, ice) are coming from a long transient run performed forced with SSP2-4.5 scenario[5]. The future atmosphere-only simulation is forced with the same SST as the present one, what varies is the atmospheric composition due to the scenario chosen. The radiative forcing SSP2-4.5 have been kept fixed at 2050 and run 260 years, of which the last 250 are used for analysis.
The climate variables chosen for the analysis were the same used in ERA5.

3.3 Methodology

3.3.1 Field's spatial visualization: climatology and standard deviation

To show the basic state of the geographic distribution of climate variable's monthly average values, climatology maps were computed for both reanalysis and simulation dataset, together with the difference between them to visualize the uncertainty. The data were averaged over all the available time series to reduce the biases. Also the values of the standard deviation of the anomalies without the trend were extracted, to assess how the anomaly oscillates considering only the internal variability for both reanalysis and simulation. The fields taken into consideration have been SLP, T2m and TP. They are respectively: the atmospheric pressure at mean sea level (expressed as hPa); the air temperature 2 meters above the ground (expressed as °C); the accumulated liquid and frozen water, comprising rain and snow, that falls to the Earth's surface (expressed as mm/d).

3.3.2 Look for teleconnection patterns in NAE region with focus on NAO: EOF analysis

There are different approaches to identify and represent the NAO. One diffused technique is the Empirical Orthogonal Function (EOF) analysis: the NAO is usually identified by analysing the eigenvectors derived from the cross-covariance (or cross-correlation) matrix which is calculated based on the temporal changes in grid point values of SLP or some other climate variable. The eigenvectors, each constrained to be spatially and temporally orthogonal to the others, are then scaled on the extent to which they account for the overall variance in the data. This linear approach assumes that the preferred states of atmospheric circulation occur in pairs, where anomalies of

[5]SSP2-4.5 is an intermediate greenhouse gas emissions scenario where carbon dioxide emissions continue around current levels until 2050, then decrease but do not reach net zero by 2100(World Climate Research Programme CMIP6, 2021). 4.5 radiative forces are those used for decadal predictions

opposing polarity exhibit identical spatial structures (Hurrell et al. 2003). In the following, the above mentioned approach has been used.

The method applied is the EOF analysis (or principal component Analysis (PCA)), a dimensionality reduction techniques that extract dominant patterns of variability from multivariate data. Given any space-time meteorological field, EOF analysis finds a set of orthogonal spatial patterns along with a set of associated uncorrelated time series or principal components (PCs). The orthogonal basis functions are chosen so they are orthonormal to each other and from the first onward they represent as much variance as possible. They allows to identify patterns which represent important fluctuation in the data. The technique guarantees that the fluctuation in time of the field is well defined by the fluctuation of the first few spatial patterns.

By construction, the EOF patterns and the principal components are independent. A well-known shortcoming of EOF analysis is that eigenvector are mathematical construct and two factors inhibit physical interpretation of EOFs: the orthogonality constraint and the fact that the derived patterns may be domain dependent. Indeed physical systems are not necessarily orthogonal and if the patterns depend on the region used they may not exist if the domain changes, so there is no guarantee that they represent physical/dynamical modes of the climate system. Still, even with these short comings, classical EOF (PCA) analysis has proved to be useful (National Center for Atmospheric Research Staff (Eds) 2013).

In the reported case the EOFs were found by computing the eigenpairs performing a singular value decomposition (SVD) of the spatially weighted anomaly data matrix of the monthly mean sea level pressure's values. SLP was chosen as the climate variable, but it would have been possible to perform the same calculations with the 500-hPa geopotential height (Z500), which is the gravitational potential energy of a unit mass at a particular location relative to mean sea level. The SVD is an algebraic technique that allows the factorization of a real or complex matrix. It generalizes the eigen-decomposition of a square normal matrix with an orthonormal eigen basis to any matrix *m x n*.

To obtain SLP anomaly's values, the climatological mean has been subtracted for each seasonal period from the seasonal time series at each grid point. Then the SLP anomaly has been detrended and weighted by the square root of the cosine of latitude.

The spatial weighting is used because spatial patterns should be invariant to how one chooses the grid locations, since the aim is to find properties of the continuous spatial field (e.g., "intrinsic EOFs"). Spatial weighting can be used for several reasons: to compensate for unequal distribution of grid points, to emphasize certain spatial regions, to account for variations in error covariances, to calculate patterns with more than one variable measured across the spatial domain (e.g., extended EOF analysis), or to equalize the variance at every grid point (e.g., EOFs based on the correlation matrix instead of the covariance matrix) (Baldwin et al. 2009).

The time period selected for the analysis of the observations extends from 1950 to 2023. In the case of the simulations, however, it was chosen to consider the entire span of the control, i.e. 250 years. The geographical domain chosen was the North Atlantic European region (20°N-90°N; 90°W-40°E).

Subsequently, using R[6] the PCA has been applied to the anomaly field obtaining an array of EOFs, an array of PCs, a vector of FVARs (Fraction of Explained Variance), an array of CORRs (Correlation maps) and the threshold for the correlation coefficient based on a two-tailed Student's t-test.
It's important to mention the fact that the principal component matrix has been standardized by dividing each component by its standard deviation. The standardization can be useful to compare the influence of different PCs or to interpret the regression coefficients. Indeed it might be helpful in regression analysis for the coefficients interpretation, that become more comparable across different variables with different scales, and for simplifying the comparison of the importance of different variables, as the coefficients are expressed in terms of standard deviations.
Lastly the array of PCs has been extracted to analyse and visualize the behaviour of the pattern of variability of interest.

3.3.3 Anomaly's spatial visualization related to NAO: linear regression and correlation

For displaying the spatial distribution of climate variable's anomaly, a linear regression was performed. The linear regression is a statistical model that explain how two variable are connected each other: it represents the impact of one variable on another. As said before, the anomalies are obtained first subtracting the climatological mean for each seasonal period from the seasonal time series and then detrending and weighting the obtained output. At that point a linear regression was performed between the anomaly at the current grid point and the selected standardized principal component. Than the regression coefficients, expressing the amplitude of the EOF pattern, were extracted.
In addition, also a correlation map between the anomaly and the principal component was calculated. The correlation is a statistic element that shows whether and how much two variables are correlated, so how much one variable changes as the other changes: it represents the strength of the association between them. The extraction of the correlation maps is useful to assess the statistical significance of the anomalies related to the dominant climate variability pattern.
In summary, the two main result obtained are:

- the array of regression coefficients that represents how strongly the variability of the field at one location is related to the dominant mode of variability represented by the chosen EOF mode;
- the array of correlation coefficient that provides information about the statistical significance of the anomalies concerning the EOF mode under analysis.

These values were finally extracted and transferred in Python[7] for plotting and visualising them.

3.3.4 Statistical significance

If a result is statistically significant, that means it's unlikely to be explained solely by chance or random factors. A statistically significant result has a very low chance of occurring if there were no true effects in a research study. In that specific case the statistical significance has been tested:

[6] R is a programming language and environment for statistical computing and graphics.
[7] Python is an interpreted, object-oriented, high-level programming language with dynamic semantics.

- for the values obtained from the difference between the climatology and the standard deviation calculated with ERA5 data and that calculated with EC-EARTH data;
- for correlation values between the anomaly and the principal component, to identify the regions of the regression coefficient matrix where the relationship is significant.

To determine the significance of climatology difference's value the *student's t-distribution* was used. The *t-distribution* is the distribution of *t-values* obtained performing the *t-tests* on all the samples of a population. Specifically a *t-test* is a type of statistical analysis used to compare the averages of two groups. It is often used in hypothesis testing to determine whether a process or treatment actually has an effect on the population of interest, or whether two groups are different from one another.

For determining the significance of the climatology difference's value, the two sample, two tailed *t-test* for unpaired data between climatology value from simulation and that from reanalysis was applied. Having two samples with different size the formula used to calculate the test statistic was:

$$t = \frac{\bar{X}_1 - \bar{X}_2}{\sqrt{\frac{\sigma_1^2}{n_1} + \frac{\sigma_2^2}{n_2}}}$$

where:
- $\bar{X}_1$ and $\bar{X}_2$ are the means of the two samples under analysis,
- σ_1^2 and σ_2^2 are the variances,
- $n_1$and n_2 are the sample sizes.

Using R a matrix of values of 1 and 0 was created based on the comparison between the *critical t-value* and the computed ones; than this matrix was used to mask that one contained the difference between the two climatology.

In the case of the standard deviation the concept is the same mentioned for climatology but the *f-distribution* and *f-test* were used instead, because applied for comparing two population variances. The formula for the *f-test* statistics is:

$$f = \frac{\sigma_1^2}{\sigma_2^2}$$

where:
- σ_1^2 is the variance of the simulated data and σ_2^2 is the variance of the observed ones.

The *Student's t-distribution* is also used to find the *critical t-value* to determine the significance of the regression values between the anomaly and the principal component. Here the calculation was performed with Python whit which the *critical t-value* identification was done using the percent point function (ppf) of the *t-distribution*. The input values were be the significance level equal to α = 0.05 (for a 95% confidence level) and the degree of freedom (DOF) obtained subtracting 1 from the total number of observation. Obtained the *critical t-value*, the *critical r-value* was computed

using the inverse of the formula used to calculate the t-statistic for testing the significance of the Pearson correlation coefficient *r* in the context of correlation analysis:

$$t = r \times \sqrt{\frac{(n-2)}{(1-r^2)}}$$

where:
- r is the correlation coefficient,
- n is the sample size.

In the end, the *r-value* was used to mask the correlation coefficient matrix to filter the regression coefficient matrix. In that way the regression coefficient is plotted only when the corresponding correlation coefficient is above the threshold and so also statistical significant.

4. Observed variability

4.1 The first 4 EOFs: main teleconnection patterns in NAE regions

The most relevant atmospheric circulation patterns to North Atlantic European weather and climate are analysed below using the ERA5 reanalysis.
The leading four pattern of North Atlantic European inter seasonal SLP variability are showing with the associated explained variance in Appendix 1. They are displayed in terms of amplitude, obtained by regressing the SLP anomalies upon the principal component time series from the chosen spatial domain determined by EOF analysis. Note that they are all plotted for what is conventionally considered to be the positive phase.

The leading pattern EOF1, expressing the maximum variance for all seasons, corresponds to the North Atlantic Oscillation (Josey et al. 2011; Lim 2015) through the entire annual cycle (Hurrell et al. 2003). Instead the behaviour of the second leading pattern EOF2 of seasonal mean SLP anomalies in North Atlantic European region changes with the season. Indeed it reflects the East Atlantic (EA) structure during winter (Josey et al. 2011; Lim 2015; Mikhailova & Yurovsky 2016) and it seems to represent the Scandinavian's signature (SCA) in the spring and autumn months. Also the third leading pattern EOF3 represents different mode of variability depending on the season: it seems to be the expression of SCA during winter (Bueh & Nakamura 2007; Josey et al. 2011; Lim 2015), of East Atlantic/West Russia (EA/WR) during spring and of EA during autumn. The last one considered is the EOF4 and it looks like the EA/WR pattern in winter (Josey et al. 2011; Lim 2015) and autumn. Since the EOF analysis depends sensitively on the boundaries chosen to define the domain (North 1984), assumes that the modes it explains are mutually orthogonal in space and time, and the first mode is the one that maximises the variance explained over the entire dataset, the results obtained with this procedure must be interpreted carefully (Dommenget & Latif 2002). This is why, for example, in the case of EOF2 in spring, it has been said that it appears to represent the signature of the SCA pattern: in fact, this mode of variability acts in the Kara-Barents Sea region and in Eurasia

(Santolaria-Otín et al. 2020), so that by using the boundaries of the NAE zone it is only possible to identify the influence that this pattern has in the region under investigation.

Focusing only on the winter season (when the atmosphere is most active dynamically and perturbations grow to their largest amplitudes) it's possible to recognize all the four principal pattern of variability acting in the NAE region (Figure 7).

The winter leading mode EOF1 accounts for 47 % of the variability and, as said before, it corresponds to the NAO. It's possible to notice an higher than normal surface pressure south of 55°N joint with a region of anomalously low pressure throughout the Arctic to enhance the climatological meridional pressure gradient. The largest amplitude anomalies occur in the vicinity of Iceland and near the Iberian Peninsula. During the positive phase stronger-than-average westerlies cross the middle latitudes of the Atlantic towards Europe, an anomalous southerly flow moves towards the Eastern U.S. and an anomalous northerly flow goes onto the Canadian Artic and the Mediterranean (Hurrell et al. 2003). The NAO's behaviour is explained better in the next section.

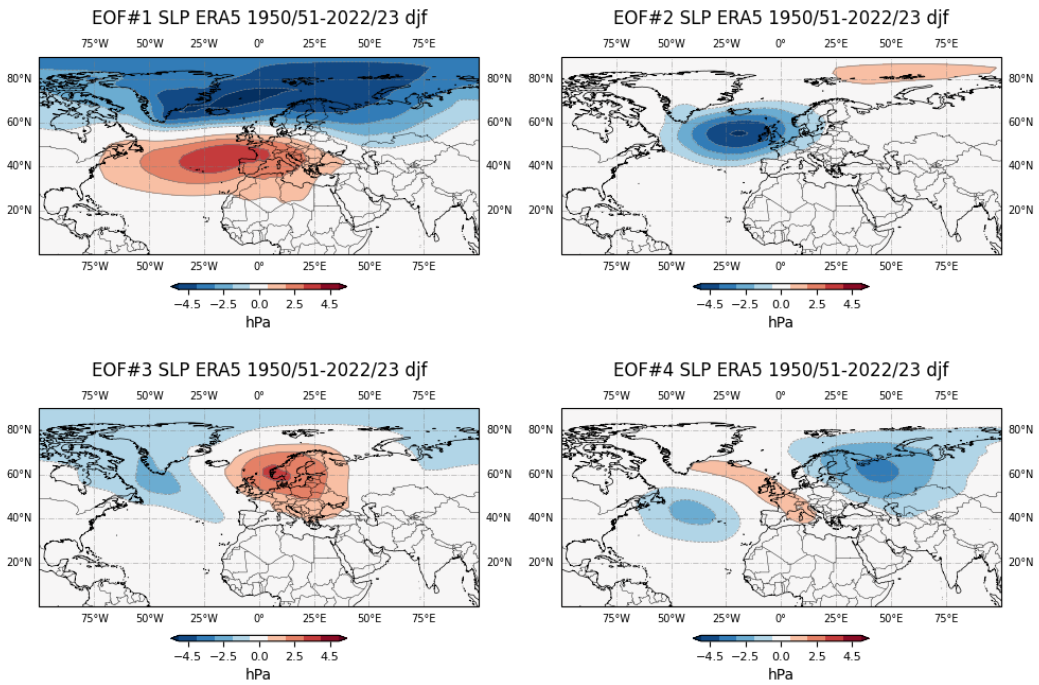

Figure 7 The leading four patterns of North Atlantic European region winter season (DJF) SLP variability, based on a 73 years (1950-2023) values of SLP anomalies from ERA5 as identified by regressing the SLP anomalies upon the principal component time series from the chosen spatial domain determined by EOF analysis.

The second winter leading mode EOF2 accounts for almost 17 % of the variability and it resembles the EA mode. It's represented by an extensive region of anomalously low pressure centred at about 55°N-20°W, which is approximately midway between the two centres of the NAO dipole. It gives rise to strong cyclonic wind forcing of the North Atlantic centred on this location (Josey et al. 2011). Voskresenskaya et al. (2009) have demonstrated that in the Atlantic-European region in winter the EA positive phase is dominated by the zonal circulation and no storms occur, while the negative one is characterized by meridional circulation type domination and the majority of storms develop in the Azov-Black Sea region (Mikhailova & Yurovsky 2016).

The atmospheric pressure anomalies in different EA phases are formed thanks to large-circulation changes. As an illustration of this (Figure 8), it should be noted that during the positive phase the

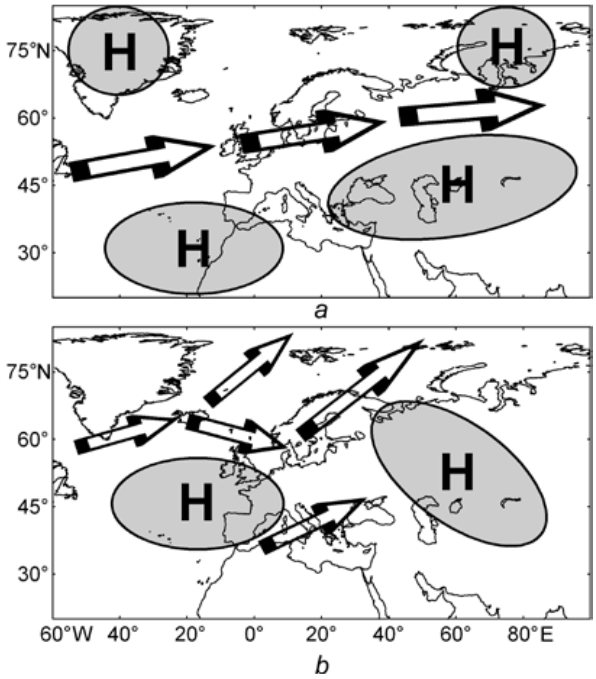

Figure 8 Principal storm-tracks of the extratropical cyclones (indicated by arrows) and position of the main anticyclones in the positive (a) and negative (b) phases in the EA winter. From Mikhailova et al. (2016).

south-eastern and the north-eastern parts of the region are respectively under the Siberian and the Scandinavian anticyclones influence. On the North, the Greenland anticyclones goes strong, a pathway for Atlantic cyclones appears and the North Atlantic surface positive temperature anomalies favour their intensification. Furthermore all these anticyclonic and cyclonic anomalies lead to enhanced westerly winds over the Atlantic-European region. Instead the cyclonic activity over the Mediterranean Sea is supressed and it results in precipitation deficit in the southern Europe and in the Black Sea region. Winter during the EA positive phase is mild and air temperature anomalies range from +0.5 to +3.5 °C (Mikhailova & Yurovsky 2016). When EA is in negative phase, there is a north-eastward movement of the Azores anticyclone and the north-eastern part of Atlantic/European region is affected by the Siberian anticyclones ridges. A relatively strong pressure gradient in the western Mediterranean is generated, with the potential to create a cold northerly airflow and to enhance ocean heat loss in this region (Josey et al. 2011). Storm tracks of Atlantic cyclones go along the northern periphery of any North Atlantic anticyclones and they bring precipitation to Russia, heat and moisture to Arctic region and colder winter in Europe.

As it turns, the EA as the NAO has a significant impact on the atmospheric circulation and the European climate. Specifically, it is shown to modulate precipitation to the South-West off the UK and across the Iberian Peninsula and to have influence upon the principal storm-tracks and jet stream position over the North Atlantic (Mikhailova & Yurovsky 2016).

The winter leading mode EOF3 accounts more or less for 12 % of winter variability and it looks like the SCA pattern. It projects itself on semi-permanent centres of action in the surface pressure pattern. In its positive phase a region of higher than normal surface pressure can be notice over the Scandinavian peninsula, extending towards northern Europe, and two weaker regions of lower than normal surface pressure form over the northeastern Atlantic and over central Siberia. These pressure anomalies lead to the weakening of the North-Atlantic storm track activity around Iceland and northern Europe and to the extension of the Atlantic jet stream eastwards, accompanied by an intensification of westerlies over southern Europe and the Eastern Mediterranean Sea. Westerly enhancement is also seen to the southeast of Lake Balkhash and Lake Baikal (in the North of East Asia). In contrast the westerlies are weakened significantly in the subpolar region from the North Atlantic along the Arctic coast. The positive phase is characterize by prominent anticyclonic anomalies around the Scandinavian Peninsula, giving rise in winter to below-normal temperatures across central Russia and western Europe, above-normal precipitations across Northeast Atlantic and South Europe and dry conditions over the Scandinavian region (Bueh & Nakamura 2007).

In SCA negative phase the Siberian high pressure pattern retreats towards east Asia and the Icelandic low extends eastwards into northern Europe, while the Azores high extend to the North. In contrast to the positive phase, the European trough deepens and weak pressure ridges are observed over the northeastern Atlantic and to the west of Lake Baikal. The Atlantic storm track extends north-eastwards and its activity enhances in a vast area from northern Europe to central Siberia. In this case the weakened northerly brings warmer conditions over western Russia and central Siberia (Bueh & Nakamura 2007).

The last winter leading mode analysed EOF4 accounts for almost 9 % of variability and it can be identified as the EA/WR pattern. It has two large-scale anomaly centres located just North of the Caspian Sea and western Europe, influencing the Mediterranean and Eurasian climate. During its positive phase two negative height anomaly occur, one over the Atlantic near 40°W and 40-45°N and the other over the western Russia, while a positive anomaly is found over central Europe. The EA/WR appears to originate in the North Atlantic and extends north-eastward across Europe and European Russia. Considering variables as temperature and precipitation, their geographical distribution reflects the upper level height anomaly distribution that has a wave structure spanning the Atlantic, Europe and western Russia. This wave structure shows a strong anticyclonic circulation over Europe and cyclonic circulation over western Russia in the event of positive EA/WR (Lim 2015). This corresponds to a meridional circulation over eastern Europe with southerly wind anomalies in winter and northerly wind anomalies between April and October (P. M. Craig & Allan 2022). The temperature anomaly pattern reflects the spatial distribution of circulation and temperature advection with the strongest response over Russia. So, during the EA/WR positive phase, positive anomalies are found over the eastern US, western Europe and Russia east of Caspian Sea. Instead eastern Canada, far eastern Europe including Ural Mountains, the Middle East and North-East Africa regions are characterized by negative anomalies. The distribution of precipitation anomalies is strongly linked to the anomalous SLP and lower-level circulation pattern: positive precipitation anomalies are found where negative SLP anomalies are located and vice versa. The mid-latitude Atlantic and central Russia are the main regions that have the above-average precipitation, while eastern Canada, part of North-East Africa and the European regions experience the below-average precipitation. A weak positive precipitation anomaly is observed over the eastern US, North-East Egypt and Israel (Lim 2015). The negative phase of the EA/WR is more or less a mirror image of the positive phase, with high pressure resident over western Russia and low pressure affecting much of Central and northwestern Europe. This pressure anomalies distribution leads to a strong cooling over Russia east of the Caspian Sea and a warming over Ural Mountains of northern Russia. Other impacts linked to the negative phase are the cooling over the eastern US, western Europe and northwestern Africa and a warming over eastern Canada and Europe, northeastern Africa and the Middle East. Concerning the precipitation, pronounced negative anomalies occur over the mid-latitude Atlantic and Central Russia, weaker negative anomalies interest the US region, while positive anomalies are mainly distributed over eastern Canada, the European region and northeastern Africa (Lim 2015).

The principal component time series of the four leading EOFs of NAE region sea level pressure is shown below (Figure 9). The period showing goes from 1950 to 2023 and notice that on the x-axis a value of for example 1950 indicates winter 1950-51.

The NAO exhibits considerable inter seasonal and interannual variability, and prolonged periods of both positive and negative phases of the pattern are common. The wintertime NAO also exhibits significant multi-decadal (low frequency) variability (Bell & Chelliah 2006; Hurrell 1995). For example, the negative phase of the NAO dominated from the mid-1950's through the 1978/79 winter (highlighted in blue in the plot). During this approximately 24-year interval, there were four prominent periods, each of at least three years, in which the negative phase was dominant. An evident transition to recurring positive phases of the NAO then occurred during the 1979/80 winter, with the atmosphere remaining locked into this mode through the 1994/95 winter season (highlighted in red in the plot). During this 15-year interval, a substantial negative phase of the pattern appeared only twice, in the winters of 1984/85 and 1985/ 86. After the 90s a trend's levelling off over the decade is evident (Hurrell et al. 2003).

The EA pattern index shows that in the period 1960-75 negative values dominate and then it seems to switch to a series of intense positive values that leads the linear trend of EA index to became positive. This EA pattern behaviour plays a significant role in fresh water flux variations to the eastern North Atlantic (Mikhailova & Yurovsky 2016).

Instead there are no clear trends in SCA and EA/WR pattern indices.

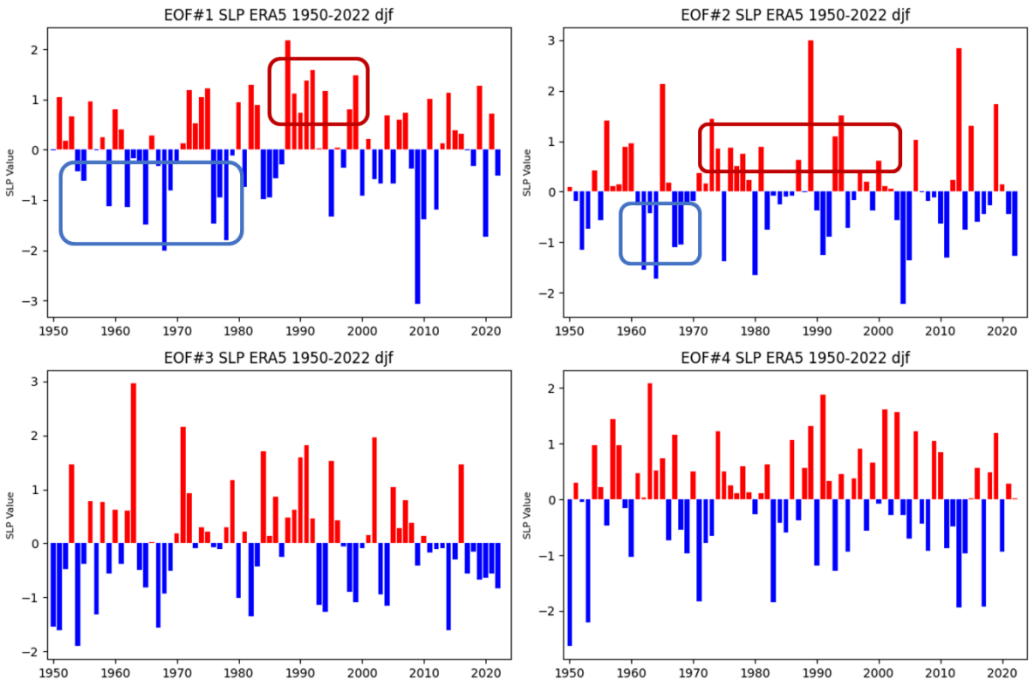

Figure 9 Standardized index of the mean winter four mode of variability constructed from the principal component time series of the four leading EOFs of the NAE region sea level pressure. The blue and red boxes qualitatively identify periods in which one phase persists over the other. ERA5 data from 1950 to 2023.

4.2 NAO's behaviour and its impact throughout the year

Since the behaviour of the NAO is influenced by variations and interactions between components in the climate system, it is useful to take a look at climatology and standard deviation of the most important climate variable, also to better understand the behaviour of field anomalies. The climatology is the average calculated at each grid point consisting of the latitude and longitude values over the selected time period. Instead the standard deviation (identified by the symbol σ) in general is a standardized measure that can be used to describe the dispersion pattern of all the observations in a normally distributed dataset. In this specific case the standard deviation values express the magnitude of the field anomalies, i.e. how strongly the field in question will oscillate around the mean if disturbed.

For the sake of clarity in all images shown from now on (unless otherwise specified), the climatic field under analysis is represented throughout the year: top left shows winter (December-January-February, DJF), top right is spring (March-April-May, MAM), bottom left is summer (June-July-August, JJA) and bottom right is autumn (September-October-November, SON).

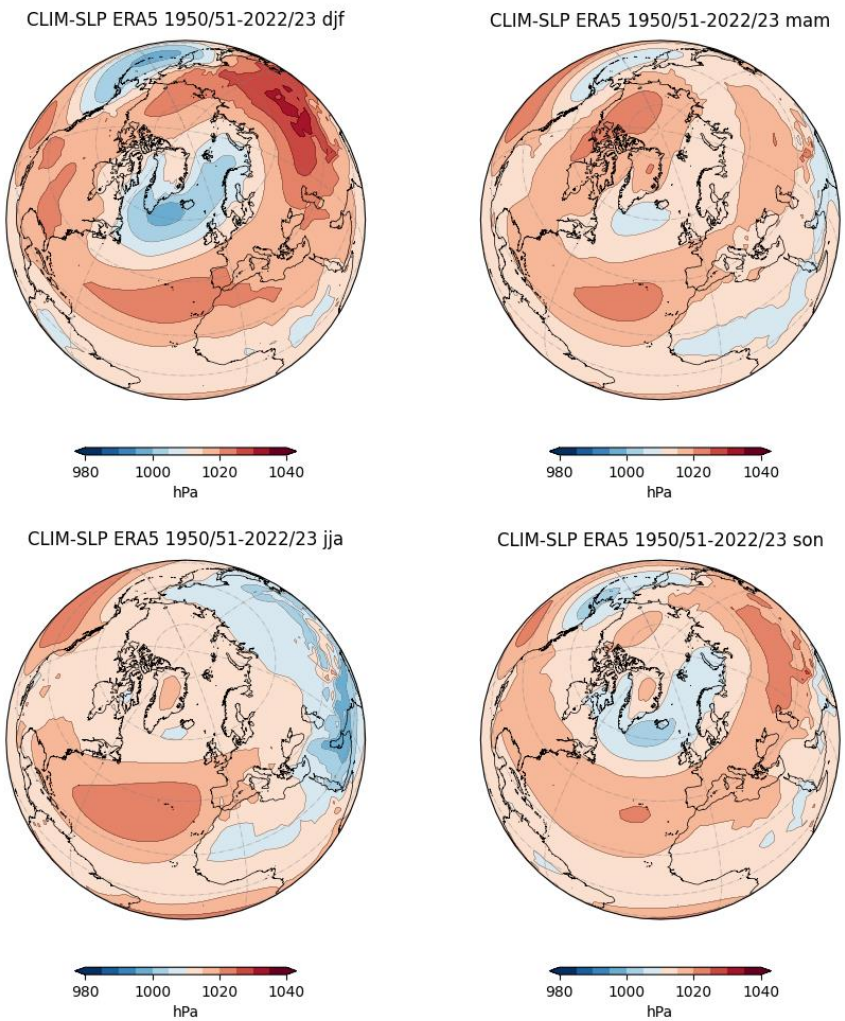

Figure 10 Climatology of SLP field (hPa) for DJF, MAM, JJA and SON seasons. ERA5 data from 1950 to 2023.

Figure 10 shows the SLP's climatology. In general the pattern has a cellular structure. A shifts in land-sea pressure distribution is evident due to the seasonal changes of insolation and to the different response of land and ocean to heating. Indeed the response to surface temperature seasonal variation by the ocean is smaller because there is a certain amount of energy into a deep layer with a large heat capacity and also because evaporation consumes much of the heat input. On the other side land surfaces have a much smaller capacity for storing heat and usually they are not sufficiently wet to balance the large summertime increase in insolation: for these reason lands warm up dramatically in summer and cool in winter. The pressure variations in mid-latitudes are associated with the dynamical response to the land-sea temperature and heating contrast. High surface pressure can be relate to low temperature and cold atmosphere and vice versa, low pressure regions generally occupy warm regions where the atmosphere is heated (*Global Physical Climatology*, 2016). Looking at the North Hemisphere in DJF it's possible to notice one prominent high-pressure cell, the Azores High, between the subtropics and temperate zone (Haarsma et al. 2019), which is distributed mostly eastwards in the Atlantic Ocean and it extends towards the Iberian Peninsula and North Africa. This cell prefers the eastern sides of the ocean basins where thermal and other forcing build higher pressure. Indeed it's reinforced by the upwelling of colder subsurface ocean water generated by the equatorward winds on the east side of the subtropical high. It is also influenced by the colder temperatures related to low stratus clouds that create a net radiative cooling of the air and by other factors such as the midlatitude storms track and tropical convection (Grotjahn 2015). The largest high-pressure formation, the Siberian anticyclone, is located mainly in the Asian continent and also extends slightly towards the Middle East. Other high-pressure centres of the same intensity as the one in the Atlantic Ocean and at the same latitude, are visible in the North American region. Instead, the main low-pressure centre is the Icelandic Low and is located in the northern Atlantic Ocean between Greenland and Iceland and then extends eastwards towards the Scandinavian peninsula and the Barents Sea. Finally, the second low-pressure formation that predominates the winter season is the high-latitude Aleutian centre positioned in the Pacific Ocean between North America and Russia.

The distribution and extent of these pressure centres varies quite a bit during the annual cycle. In the spring season, it can be seen that the high-pressure system in the Atlantic Ocean is weakened and localised further west. Similarly, the one over Russia, which was the most important one in DJF, loses a lot of intensity and is reduced. The same happen to the low-pressure centres. Instead there are a high-pressure system between North America/Greenland and the Arctic Ocean and a low-pressure one in the tropical region above the equator, which during winter was represented by a small formation in central Africa. In summer the land-sea pressure contrast is reversed in mid-latitudes, with the highest pressures over the oceans and the lowest pressures over the land areas (Global Physical Climatology 2016). It's also visible the expansion of the subtropical highs in the Northern Hemisphere. In particular, the high-pressure centre in the Atlantic persists, maintaining the central position it had acquired in spring and reaching the peak of its expansion. On the other hand, the high-pressure centre over Russia gives way to the low-pressure one, which, while it was weak and localised in the tropics during MAM, is now intensifying and affecting the Middle East and Northeast Asia due to the influence of the Asian summer monsoon (Global Physical Climatology 2016). While the low-pressure formation in the North Atlantic becomes minimal and resides in the

vicinity of Iceland. To conclude, in the autumn season, the distribution of centres of pressure is similar to the winter season, but weaker. It is in SON that the high-pressure system over the Atlantic Ocean reaches its lowest intensity.

In general, the distribution of sea level pressure in the winter season seems to resemble the distribution of the main Empirical Orthogonal Teleconnections (EOTs) of the NH winter SLP identified by Smoliak & Wallace (2015): the North Atlantic Oscillation/ Northen Hemisphere annular mode pattern that has three centre of actions, one in the Arctic and the other two over the Atlantic and the Pacific around 45°N; the Pacific-North America pattern with its primary centre of action in the vicinity of the climatological-mean Aleutian low; the Russian pattern that has the primary centre of action around 80°E over Urals.

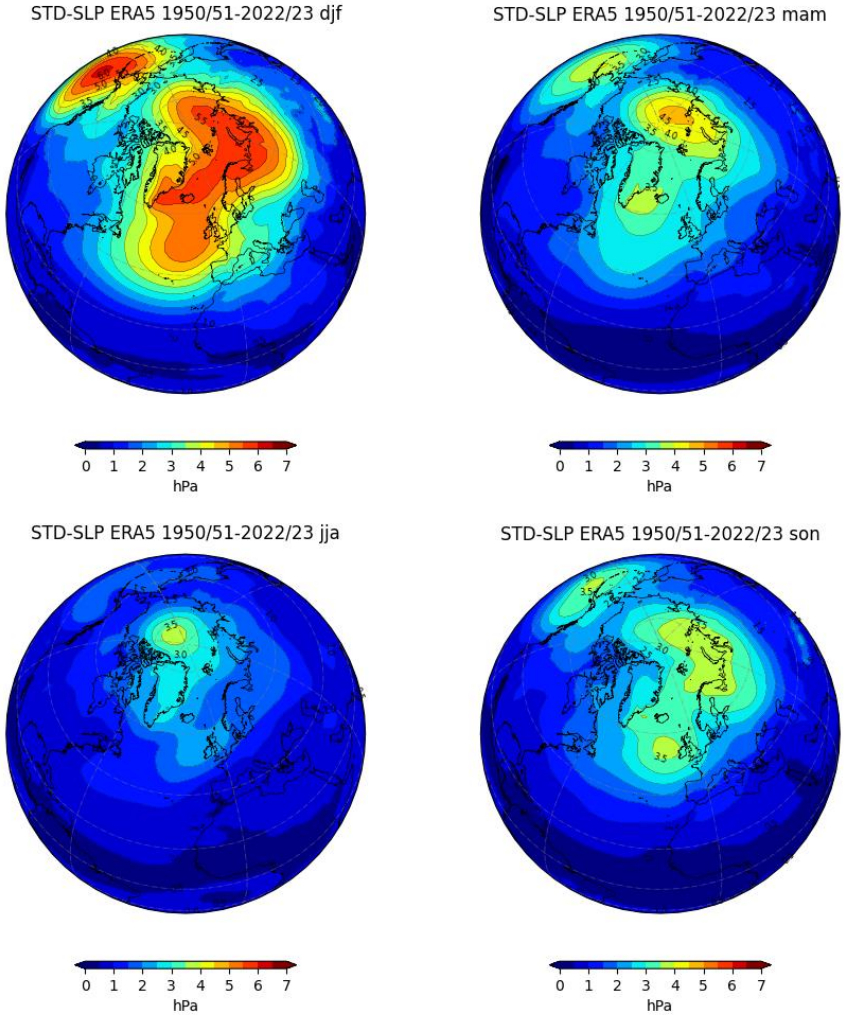

Figure 11 Standard deviation of SLP anomaly (hPa) for DJF, MAM, JJA and SON seasons. It has been calculated applying the standard deviation function to the detrended anomaly field (obtained by subtracting the climatology from the seasonal mean data for each year). ERA5 data from 1950 to 2023.

Figure 11 above represents the standard deviation related to the SLP anomaly's field, i.e. how much the variable oscillates around its mean value and how strong is the anomaly in a precise location. Looking at the seasonal behaviour, the greatest fluctuation of the SLP field around the mean due to the internal variability occurs during winter. There are two areas where this is evident. One is located in the North Pacific Ocean between North America and the Asian continent. The other is in the North Atlantic European region, and specifically the highest standard deviation values are between Iceland

and the Arctic Ocean, but also extends towards Greenland, England and northern Europe, the Scandinavian Peninsula and northern Russia. This particular area is where the dipole of pressure anomalies due to the NAO is located.

The oscillations already identified in winter also persist in spring, but they are less extensive and weaker: in fact, the maximum value is 4.5 hPa in contrast to the DJF season where values of 6 hPa were reached. In summer the influence of internal variability on sea level pressure anomalies reaches its minimum, and the only significant variation is concentrated in the Arctic Ocean. As for the fall season, oscillations return to greater values particularly in the Atlantic Ocean between Iceland and Ireland, in the Barents and Kara Sea area, and on the other side of the globe between North America and Asia.

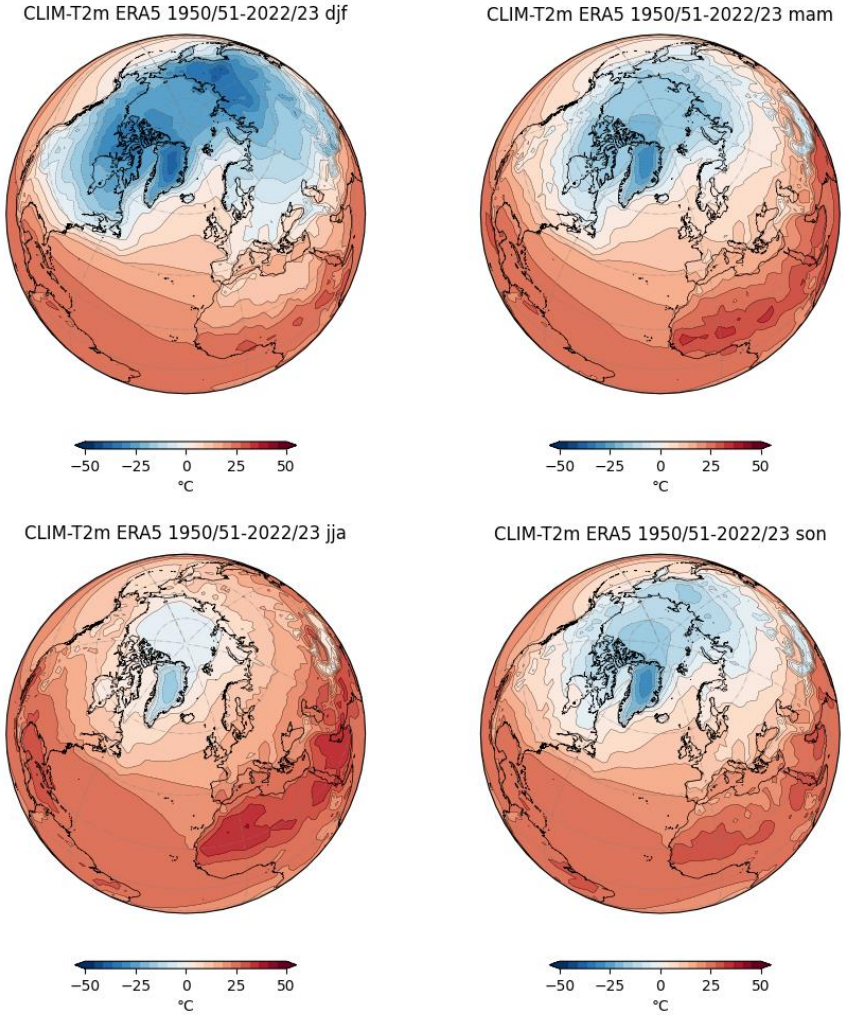

Figure 12 Climatology of t2m field (°C) for DJF, MAM, JJA and SON seasons. ERA5 data from 1950 to 2023.

The annual temperature distribution is controlled by the seasonal variations in amount of solar radiation received. As a general rule, regions close to the Equator have small annual variations in temperature because of the small variations in the amount of insolation received over a year. Yet, as one moves away from the Equator, relationships between the time of year, latitude, day length, and solar angle cause greater changes in insolation, and thus temperatures, on an annual basis. Indeed a net radiations surplus in the tropics is formed in all season and a poleward energy transport is required.

Due to the difference in specific heat between ocean and lands, in winter isotherms are deflected southward over land and northward over water and this means, as said before, that there are higher temperature over ocean and lower over land. The opposite situation happens in summer (Michael Pidwirny 2021). In addition, since the surface of the Southern Hemisphere is mostly covered by ocean, this also explains the small seasonal variation in temperatures in this section of the globe.
Along all the year the temperature's field, that follows the radiation behaviour, has notable zonally symmetry over the oceans (Grotjahn 2015).
During winter, as shown in Figure 12, the colder temperatures in middle latitudes are over the eastern sides of the continents and large ice-covered regions have the coldest temperature. It is also possible to identify the large temperature gradient underlying the formation of North Atlantic storms, the behaviour of which regulates the NAO.
In spring the area affected by cold temperatures shrinks particularly in northwest Europe and Russia reaching an average of around 0 °C. During summer, the coldest area of the Arctic reaches its maximum temperature and the hottest temperatures are located over the subtropical desert. In autumn, temperatures begin to cool again, allowing subzero temperatures to extend into the North Atlantic Ocean, northern Europe and Russia.

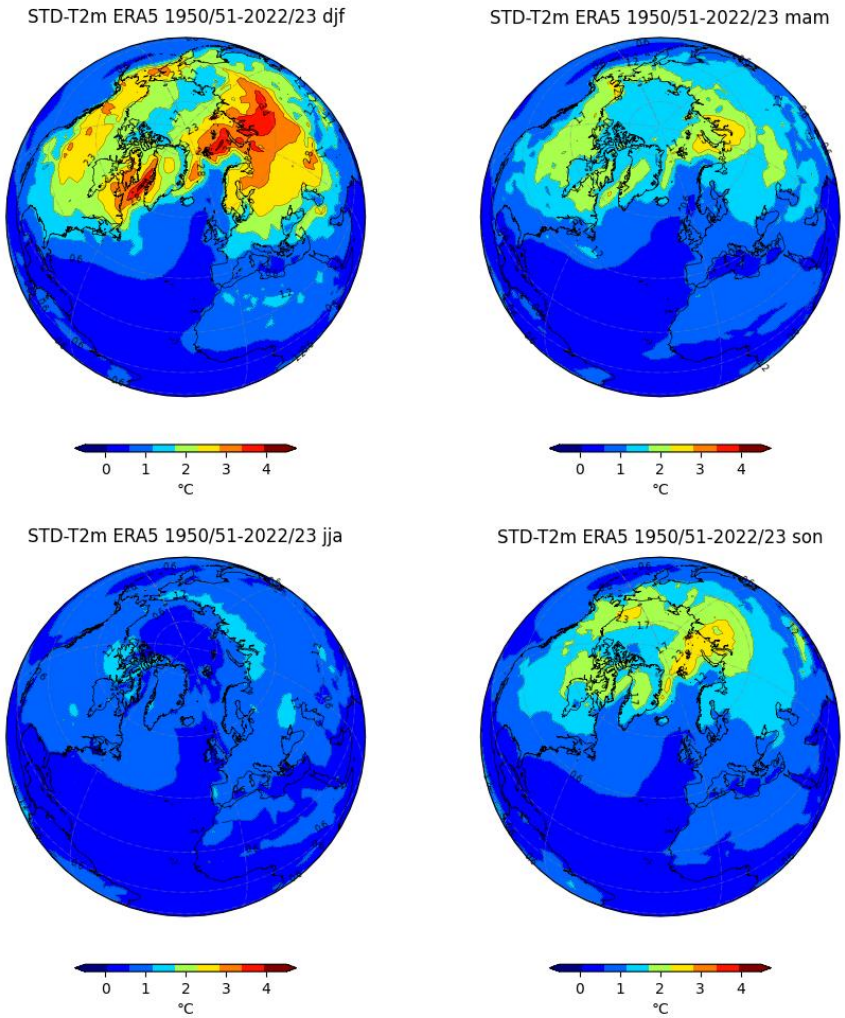

Figure 13 Standard deviation of t2m anomaly (°C) for DJF, MAM, JJA and SON seasons. It has been calculated applying the standard deviation function to the detrended anomaly field (obtained by subtracting the climatology from the seasonal mean data for each year).

Clearly the strongest difference in the pattern distribution happens between DJF and JJA: in winter there is a large variability between the Artic/North Atlantic region and Equatorial region; instead in summer all is more homogeneous.
Also in the case of variation of temperature anomaly's field the greater oscillations happen in DJF. Indeed in Figure 13 it's possible to notice high standard deviation value around the Arctic Polar Circle in winter. In particular, the largest oscillations are located over the Barents Sea and Siberia and in the area of the Atlantic Ocean between North America and Greenland. Even in the spring and fall seasons, variations are concentrated in the same area although the area affected is smaller and the magnitude is lower. Instead in JJA the standard deviation values reach the minimum indicating that the temperature's values fluctuates less around the mean.

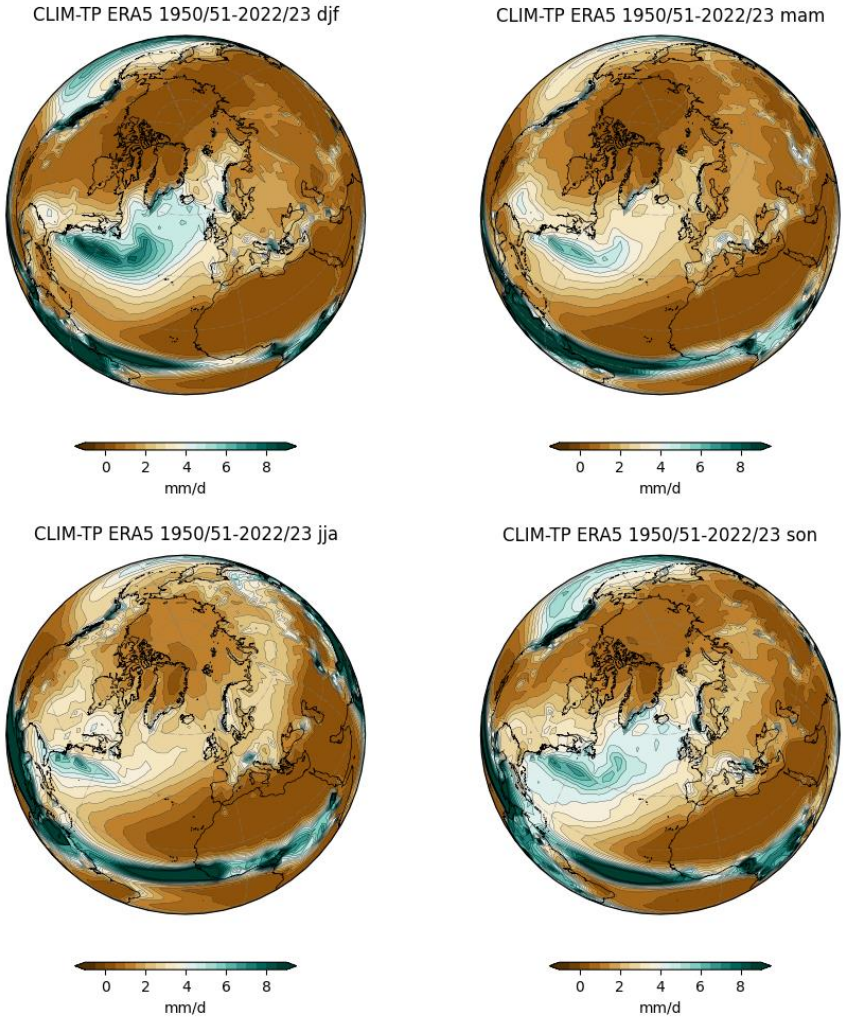

Figure 14 Climatology of TP field (mm/d) for DJF, MAM, JJA and SON seasons. ERA5 data from 1950 to 2023.

Figure 14 shows the seasonal mean precipitation distribution. Through all the annual cycle the largest precipitation occurs near the equator where the average water content of the air is high and tropical convective systems are responsible for the majority of the rainfall. Although not clearly visible from the maps, it is possible to discern a line of precipitation north of the Equator in the eastern halves of the Pacific and Atlantic oceans known as the Inter-Tropical Convergence Zone (ITCZ) that is associated with the rising branch of the Hadley cells.

In mid-latitudes of the NH, the precipitation is concentrated near the North America coast on the western margins of the Atlantic Ocean, where storm tracks are formed. Heavy precipitation verify also in mid-latitudes, West of the Rocky Mountains and the Andes, thanks to the westerly that flow over them and to the forced ascent of moist surface air. There is instead a decline in precipitation towards polar regions, because of the low temperatures and so low water-carrying capacity of the atmosphere (Global Physical Climatology 2016; Grotjahn 2015).

The precipitation distribution shows almost the same behaviour in all seasons with some differences. During the summer there is the northward migration of ITCZ consistent with the dominance of the winter hemisphere Hadley cell. In winter the centre of precipitation located at the western Atlantic Ocean is higher than in other seasons, in particular to respect the summer when it reaches its minimum and tends to move more toward the Southwest. As the other fields, also the precipitation distribution is more homogeneous during summer to respect winter and the difference between dry and wet areas is less pronounced all around the North Atlantic European region, with an amount of precipitation that is less over the Atlantic Ocean and more over the Arctic Ocean and North/Northeast Europe.

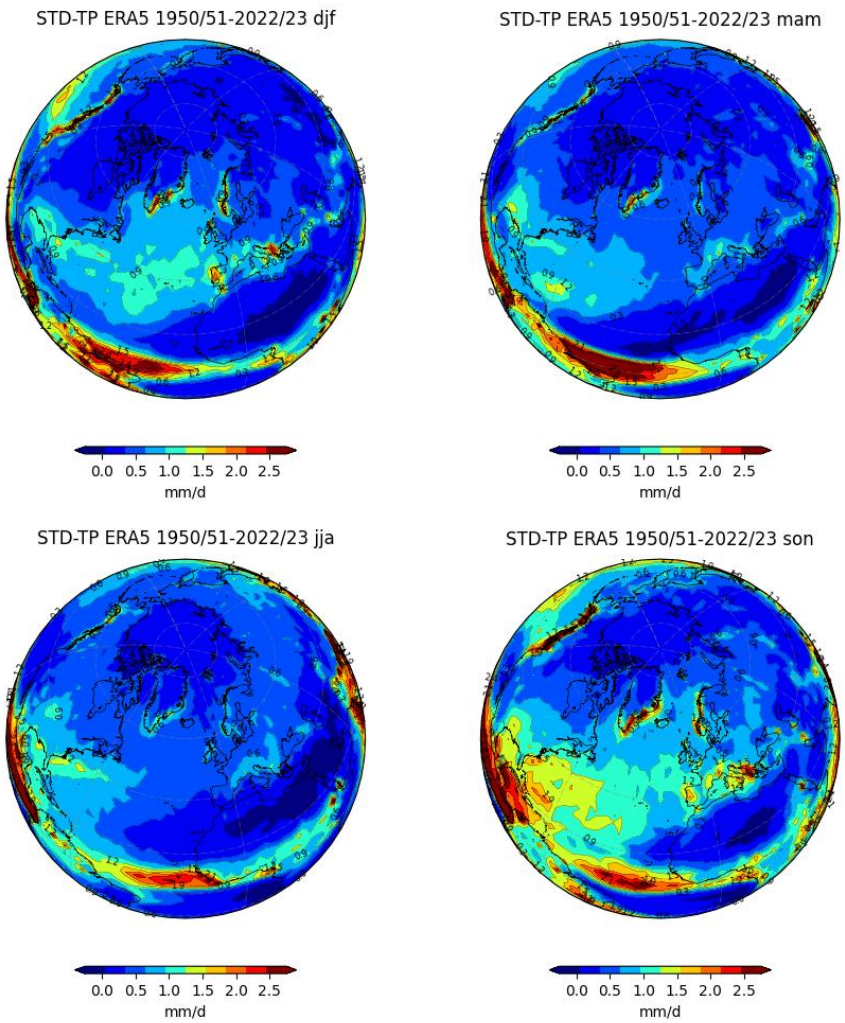

Figure 15 Standard deviation of t2m anomaly (mm/d) for DJF, MAM, JJA and SON seasons. It has been calculated applying the standard deviation function to the detrended anomaly field (obtained by subtracting the climatology from the seasonal mean data for each year).

Changes in the precipitation field anomaly in the North Atlantic European region are most pronounced during the autumn months (Figure 15). In fact, during SON the highest standard deviation values are located at the ITCZ and head north-eastward into the Atlantic Ocean from Central America. In addition, there are important variations in South/Southeast Europe, along the west coast of Norway, and in Southeast Greenland. Even during winter, variations are concentrated in the same areas, although those localized in the ITCZ and between Central American lands and the Atlantic Ocean are shifted southward and are much less pronounced. Oscillations in the North Atlantic and Europe also persist in the same locations, but are weaker. In contrast, in spring and particularly in summer, the oscillation of the field anomaly is less pronounced, and the ITCZ during JJA comes to occupy its northernmost position during the entire annual cycle.

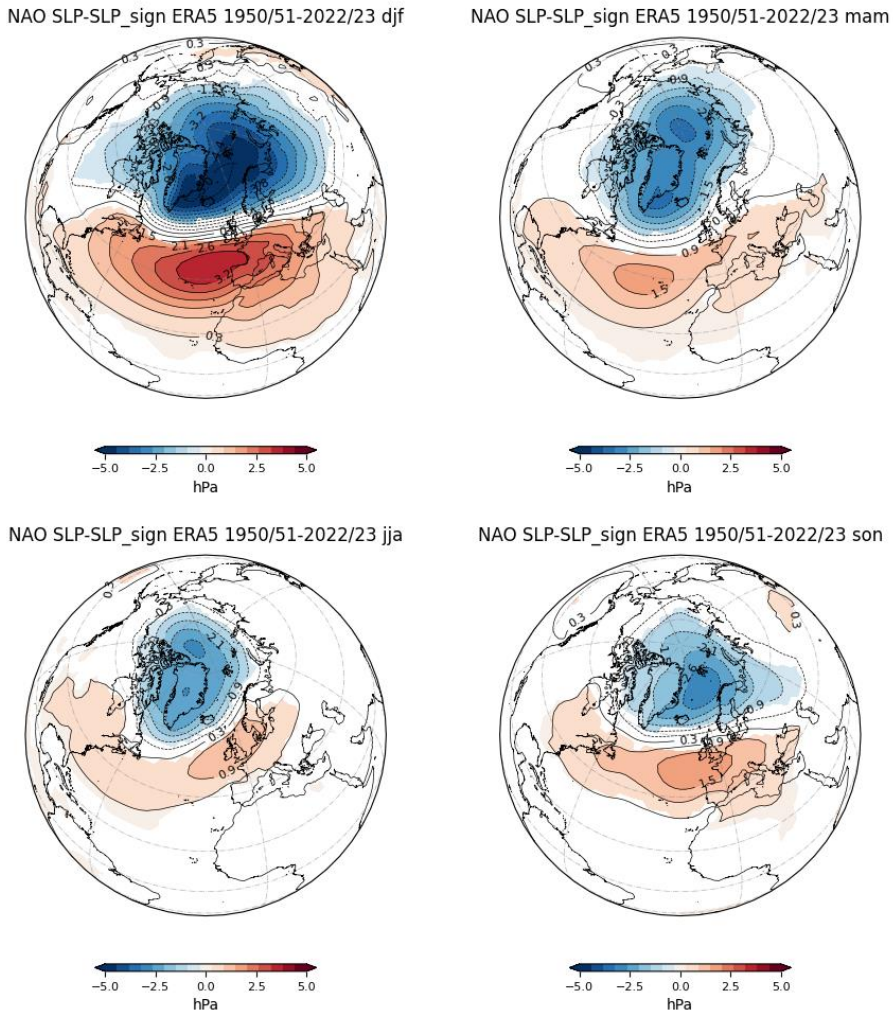

Figure 16 Seasonal SLP anomalies due to NAO in the North Atlantic European sector, based on 73 years (1950-2023) from ERA5 dataset. The patterns are identified by regressing the SLP anomalies upon the first principal component time series of the leading EOF1 for all seasons. Statistically significant areas at 95% confidence level based on a two-tailed t-test for correlation values between the SLP anomaly and the principal component are shaded.

In order to assess how the NAO and its influence on the surface climate in the NAE region have naturally varied from the recent past to the present day the results obtained using SLP, t2m and TP data from the ERA5 reanalysis model are investigated in this section.

The impact of the NAO in the area under analysis is visualised as the spatial distribution of the climate variable's anomaly related to its dynamics. To obtain it, as mentioned above, a linear

regression was made between the field anomaly due only to internal variability and the time series of the standardised leading PC, both calculated in the North Atlantic European sector. The maps show the 95 % statistically significant spatial distribution according to the *Student's t-test*, whereby the contour lines represent the entire anomalies and the shaded areas only the significant ones.
The largest SLP's anomalies are evident during the boreal winter months (DJF), but as said at the beginning of the chapter, this teleconnection pattern shows an evident surface pressure dipole throughout the year (Figure 16). Indeed the NAO is the only teleconnection pattern evident in all seasons in the NH. During the winter season it accounts for almost the half of the total variance in SLP over the North Atlantic (46.76 %) and appears with a slight Northwest-to-South-East orientation. During spring the pattern appears as a North-South dipole with two centres of larger low pressure anomalies (one near to Iceland and the other above Greenland in the Arctic Ocean) and a southern centre of action near the Azores. It can be notice that both the extent and the amplitude of SLP anomalies are smaller than in winter and in this case the leading EOF explains 37 % of the SLP variance. Large differences in the mean distribution of SLP are clear from boreal winter to boreal summer: indeed the amplitude, the extent and the percentage of total variability explained by the NAO reach their minimum during the summer season, when the centres of action are clearly North and East relative to winter. By fall the orientation of the NAO become more like that of winter, with the high pressure anomaly beginning to increase and move eastwards and the low pressure SLP anomaly comparable in position and magnitude to that of spring. That the spatial pattern of the NAO remains largely similar throughout the year does not imply that it also tends to persist in the same phase for long. To the contrary, it is highly variable, tending to change its phase from one month to another, and its longer-term behaviour reflects the combined effect of residence time in any given phase and its amplitude therein (Hurrell et al. 2003).
The difference in anomalies variance magnitude between JJA and DJF seasons is related to the difference in the distribution of solar radiation. Indeed in summer the thermal meridional gradient between the pole and the equator is lower than in winter and also the amount of energy transferred is smaller as is the pressure gradient in the region influenced by the NAO. It's possible to appreciate also an upward shift of the low anomaly's centre of action during the warmer months to respect the colder ones and it's related to the tilt of the earth's axis, which causes the Northern Hemisphere to receive more insolation than the Southern one during summer. This fact influences the extension and the strength of meridional cell and the mean meridional circulation that migrates further towards the pole during boreal summer (Lucas et al. 2022).
The temperature anomalies are driven by advection and so by changes in the surface wind and air-sea heat exchanges that are related with NAO variations. NAO-related temperature anomaly as well as the pressure anomaly is also more pronounced during the winter season, when, during the positive phase, enhanced westerly flow across the North Atlantic moves relatively warm maritime air over much of Europe and far downstream across Asia, while stronger northerlies over Greenland and northeastern Canada carry cold air southward and decrease temperatures over the Northwest Atlantic. The stronger clockwise flow around the subtropical Atlantic high-pressure centre leads to temperatures lower than normal over North Africa and Middle East and to temperature higher than normal over North America. The pattern shows in Figure 17 assumes a quadripolar behaviour with the two warm anomalies located over the Northeast of Europe and Russia and over the United States

respectively and the two cold ones over the North Canada and Greenland and over the North Africa and Middle East respectively (Hurrell et al. 2003).

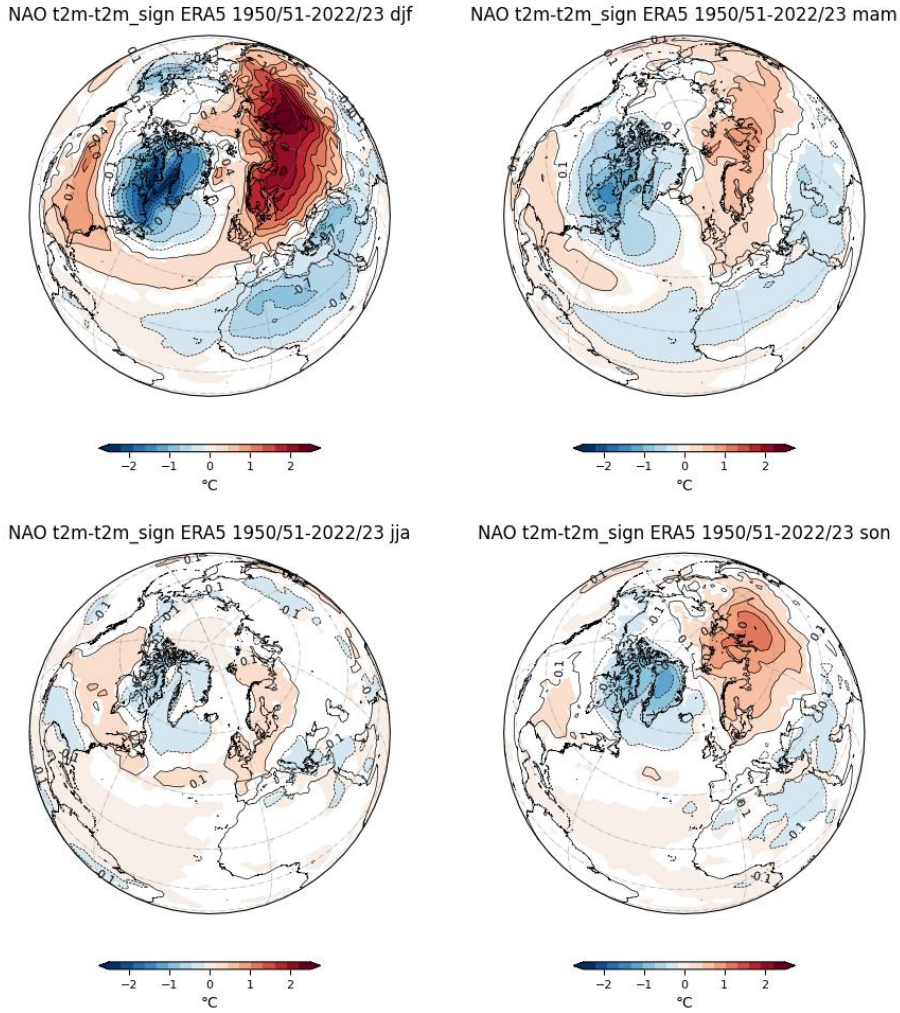

Figure 17 Seasonal t2m anomalies due to NAO in the North Atlantic European sector, based on 73 years (1950-2023) from ERA5 dataset. The patterns are identified by regressing the t2m anomalies upon the first principal component time series of the leading EOF1 for all seasons. Statistically significant areas at 95% confidence level based on a two-tailed t-test for correlation values between the t2m anomaly and the principal component are shaded.

The quadripolar subdivision can also be seen as a tripolar one, as has been pointed out by Visbeck et al. 2003, if the SST is analysed. The pattern of temperature change related to NAO is really important. In particular, it has long been recognized that fluctuation in SST and the strength of the NAO are related: the SST anomalies are driven by changes in the air-sea heat exchanges and surface wind-induced Ekman currents associated with NAO variations. The relationship is stronger when the NAO index leads an index of the SST variability by several weeks, which highlights the known results that large-scale SST over the extratropical oceans responds to atmospheric forcing on monthly and seasonal timescales. Also over longer periods, persistent SST anomalies seems to be related to persistent anomalous pattern of SLP (including that related to NAO), but on decadal timescales the mechanism whereby the atmosphere forces SST anomalies are different: the ocean adjusts dynamically to the overlying changes in wind stress curl, altering the horizontal and vertical oceanic heat transport that in turn impact SST (Hurrell 2015).

Continuing to analyse the interannual variability, during the spring season all the anomalies are weaker. In addiction which used to be the warmest in winter is reduced and now only affecting northern Europe and a small part of the northern Russia, the one that used to be the coldest is shifted southward and the other two are equal to zero. During the boreal summer the temperature anomalies are almost inexistent with only a very small region colder than normal between Canada and Greenland. Instead during autumn it can be notice the presence of two anomalies of a magnitude similar to spring, one warmer and the other colder than normal: respectively the first is over northern Russia and the second is over Greenland. The greater temperature anomalies difference that can be appreciated in winter is related to the fact that the temperature gradient between the pole and the equator during this season is more pronounced, resulting in greater variability in the data.

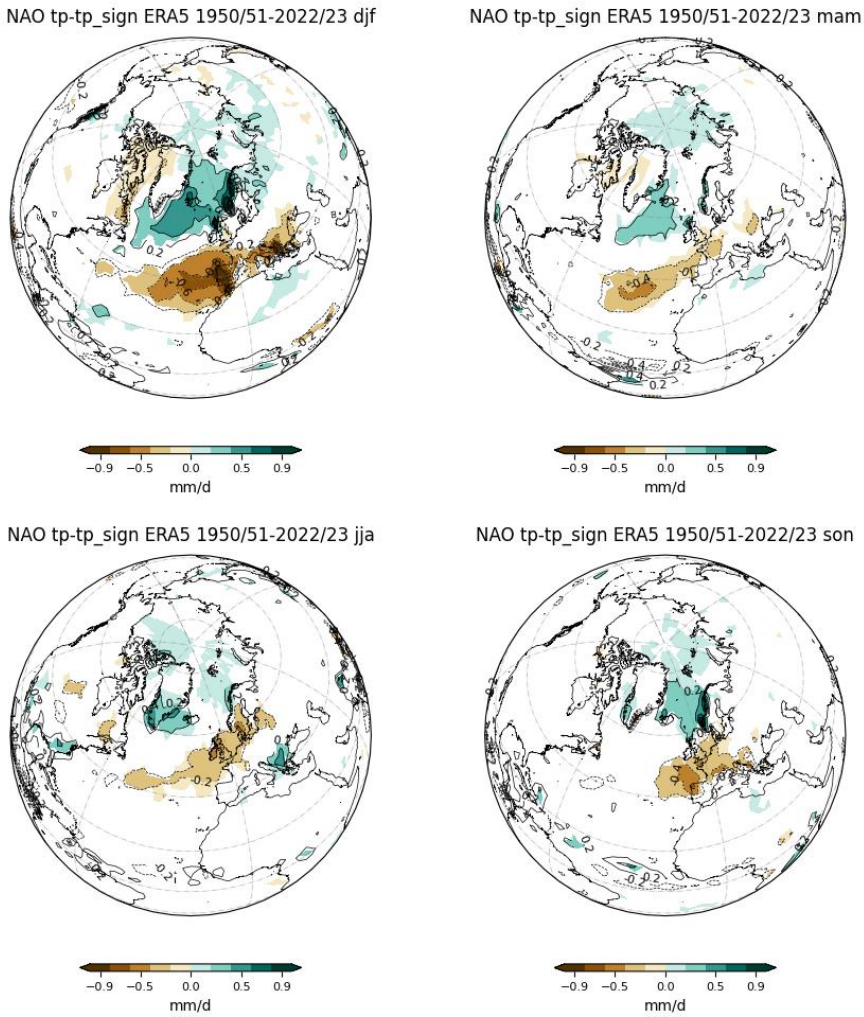

Figure 18 Seasonal TP anomalies due to NAO in the North Atlantic European sector, based on 73 years (1950-2023) from ERA5 dataset. The patterns are identified by regressing the TP anomalies upon the first principal component time series of the leading EOF1 for all seasons. Statistically significant areas at 95% confidence level based on a two-tailed t-test for correlation values between the TP anomaly and the principal component are shaded.

The behaviour of the NAO-related precipitation anomaly is closely linked to the behaviour of SLP anomaly as pressure gradients lead to the addition of water vapour to the atmosphere and consequently changes in circulation patterns, i.e. they drive fronts and storm systems. Indeed where the sea level pressure anomaly is low, the precipitation exceed the evaporation and on the contrary where the SLP anomaly is high, the evaporation exceed the precipitation. The larger amplitude anomaly occurs during winter and in this case, the great difference between winter and summer is less evident as the amplitude and extent of the summer anomaly are comparable to those of the spring and autumn seasons. The shift of the regions of more or less precipitation are connected to the shift of SLP dipole. Indeed changes in the mean circulation patterns over the North Atlantic associated with the NAO are accompanied by changes in the intensity and number of storms, their paths and weather. During winter a storm track connects the North Pacific and North Atlantic basins, with maximum storms activity over the oceans. Positive NAO winter are characterized by a north-eastward shift in the Atlantic storm activity with enhanced activity from Newfoundland into northern Europe and a modest decrease to the South. Furthermore the positive phase is associated with frequent storms in the vicinity of Iceland and the Norwegian Sea (Hurrell 2015). Indeed in Figure 18 a wet region over Iceland and part of the Scandinavian region and dry zones over the Greenland, the Canadian Arctic, the central/southern and eastern Europe are shown. In spring the wet anomaly is smaller and shifted westward as well as for the dry anomaly that now is located over the Azores archipelago. During the summer season both anomalies are shifted northward: the wet one is located over Greenland and the dry one over some of the North European countries. Instead in autumn precipitation exceeds evaporation over Iceland and a small part of Norway and the opposite happens over almost all the Central Europe.

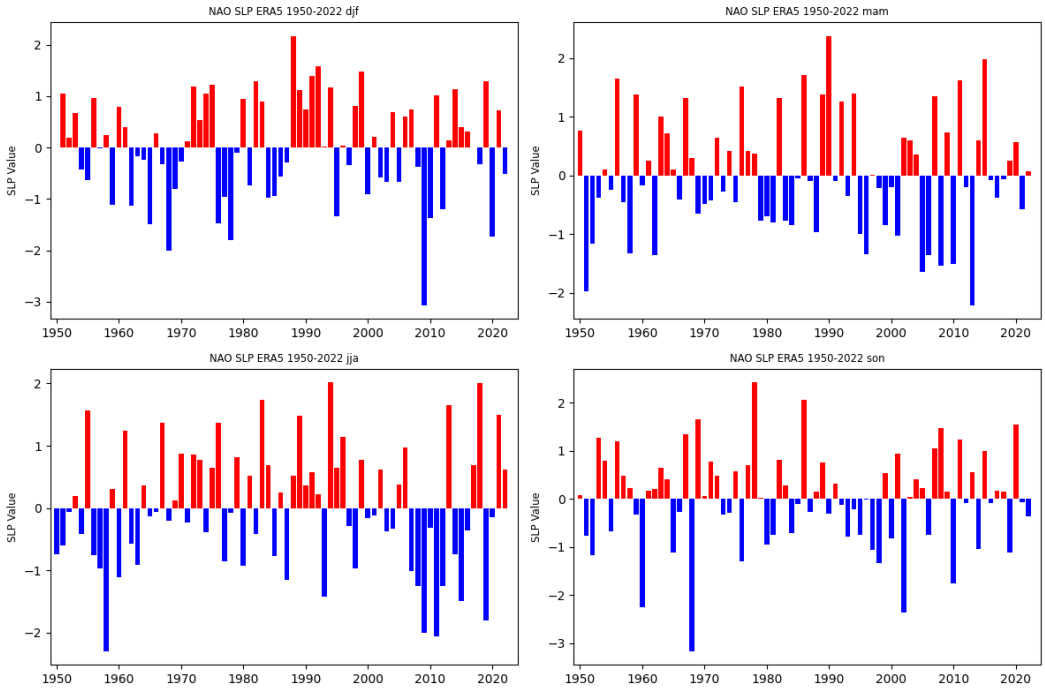

Figure 19 Standardized index of the mean seasonal NAO mode of variability constructed from the principal component time series of the first leading EOFs of the NAE region SLP. ERA5 data from 1950 to 2023

There is no universally accepted index to describe the temporal evolution of the NAO because there is no unique way to define its spatial structure. Most NAO indices are derived either from the difference in surface pressure anomalies between various northern and southern locations or from the PC time series of the leading EOF of SLP. Above (Figure 19) the second approach has been used: the advantage of PC time series method to respect the station based one is that the former is a more optimal representation of the full NAO spatial pattern cause the NAO centres of action tend to move through the annual cycle; but a disadvantage is that as the index is based on gridded SLP data, it can only be computed for short period of time depending on the data source. Looking at the PC time series of the NAO calculated in the NAE region for the whole year, it can be notice that there is a little evidence for the pattern to vary on any preferred time scale. Large changes can occur from one season of one year to the season of the next year and there is also a considerable amount of variability within a given winter season (Feldstein 2000; Nakamura 1996). This is consistent with the notion that much of the atmospheric circulation variability in the form of the NAO arises from processes internal to the atmosphere where a lot of process with different scales interact together to produce random variations. But as already noticed previously, there are periods when anomalous NAO-like circulation patterns persist over quite a few consecutive season as for winters from the late 1970s throughout the 1980s and into the 1990s. Thus, even though analysing the spectrum of the mean-winter NAO index Feldstein (2000) concluded that its evolution over time is associated with stochastic processes intrinsic to the atmosphere on a 10-day time scale, Feldstein (2000) himself stated that the role of external forces such as the ocean cannot be completely excluded. Indeed numerous studies have argued that external factors such as volcanic aerosols, anthropogenic influences in atmospheric composition, and variations in solar activity can influence NAO phase and amplitude. Furthermore a long-standing issue has been the extent to which the forced anomalous extratropical SST field feeds back to affect the atmosphere and so how much can influence the amplitude and the longer-term temporal evolution of the NAO. Moreover, it has been argued that interactions between troposphere and stratosphere can lend a low-frequency component of NAO variability. It is of interest to analyse these possible influences on the recurrence of a certain phase of the NAO because even a small portion of predictability can be useful considering the impact of the NAO on the climate of the NAE region (Hurrell 2015).

5. Simulated variability

5.1 Model biases: how the model simulates the North Atlantic climate

Climatology and standard deviation have been analysed not only to provide an overview of the variations and interactions between the different components of the climate system, but also because they are useful for detecting errors and distortions in simulations compared to observations.

The differences in the climatology and standard deviation for all three variables between the coupled mode simulation (a2am) and ERA5, between the atmosphere-only mode simulation (a2al) and ERA5 and between the two simulations are reported and analysed below. As mentioned before, the full range of differences is represented by the contour lines and the areas that are all coloured represent

the significant differences. Please note that significance was assessed on the basis of the *Student t-test* and *f-test* for climatology and standard deviation respectively.
From the ERA5 time series, it was chosen to consider the years 1978 to 2014 so that the results could be qualitatively compared with those obtained by R. Haarsma et al. (2020).
Maps showing the climatology and standard deviation for both simulations are also provided in the Appendix B.

Starting from the SLP's climatology, it can be seen that both simulations show biases of the order of about 6 hPa compared to the reanalysis model (Figure 20, *a* - *b*). In general, they are of greater intensity in the comparison between the coupled simulation and ERA5. Specifically in DJF there are three centres, one over the Kara Sea, one over the Atlantic Ocean south of Greenland and one, more extensive, over North Africa and a part of Middle East, where the simulated pressure is more positive than the observed one. Vice versa is the case of the centre over the Pacific Ocean between Russia and Canada, corresponding approximately to the region where the centre of action of the PNA resides. In spring, however, the intensity errors are milder: in the North Atlantic region, the simulation reports slightly higher values than ERA5 over Greenland and slightly lower along the Canadian coast and over the Arctic Ocean and Northern Europe. In North Africa it still simulates higher values, while the negative bias in the Pacific is smaller and, moving towards Russia, gives way to a positive bias along the West coast of the USA and Canada. In summer, the pattern of differences changes again. In this case, there are two centres of positive differences in favour of the simulation over the North Atlantic Ocean and the Arctic Ocean. In the Kara and Barents Seas, on the other hand, the simulated data are lower than the actual data. In the case of the autumn months, the differences are similar to those found for winter but shifted further South in the case of positive differences in the Scandinavian Peninsula and North Africa and further North in the case of large negative differences over Greenland and Arctic Ocean.
Analysing the comparison between the atmosphere-only simulation and observations, the biases in the climatology appear to be slightly lower in general. Overall, the largest discrepancies are seen in winter and autumn, which is also confirmed by Figure 20 (*c*). In winter, what is a large positive error in the case of the coupled simulation at the Kara Sea, is much less pronounced in the atmosphere-only simulation, where instead a negative error at Northern Europe gains significance. The important negative difference highlighted earlier in the Pacific becomes positive and more circumscribed in the case of a2al. In addition, the atmosphere-only simulation shows a large negative discordance from northern Canada to northern Russia via the Arctic Ocean. In JJA and MAM seasons, particularly in the NAE region, the two simulations behave very similarly. In autumn, on the other hand, there are differences: the area of more positive values found in the coupled simulation over the Scandinavian peninsula, here is stronger and is shifted eastwards; the negative difference over Greenland and the Atlantic Ocean is almost non-existent if the effect of the ocean is not taken into account.

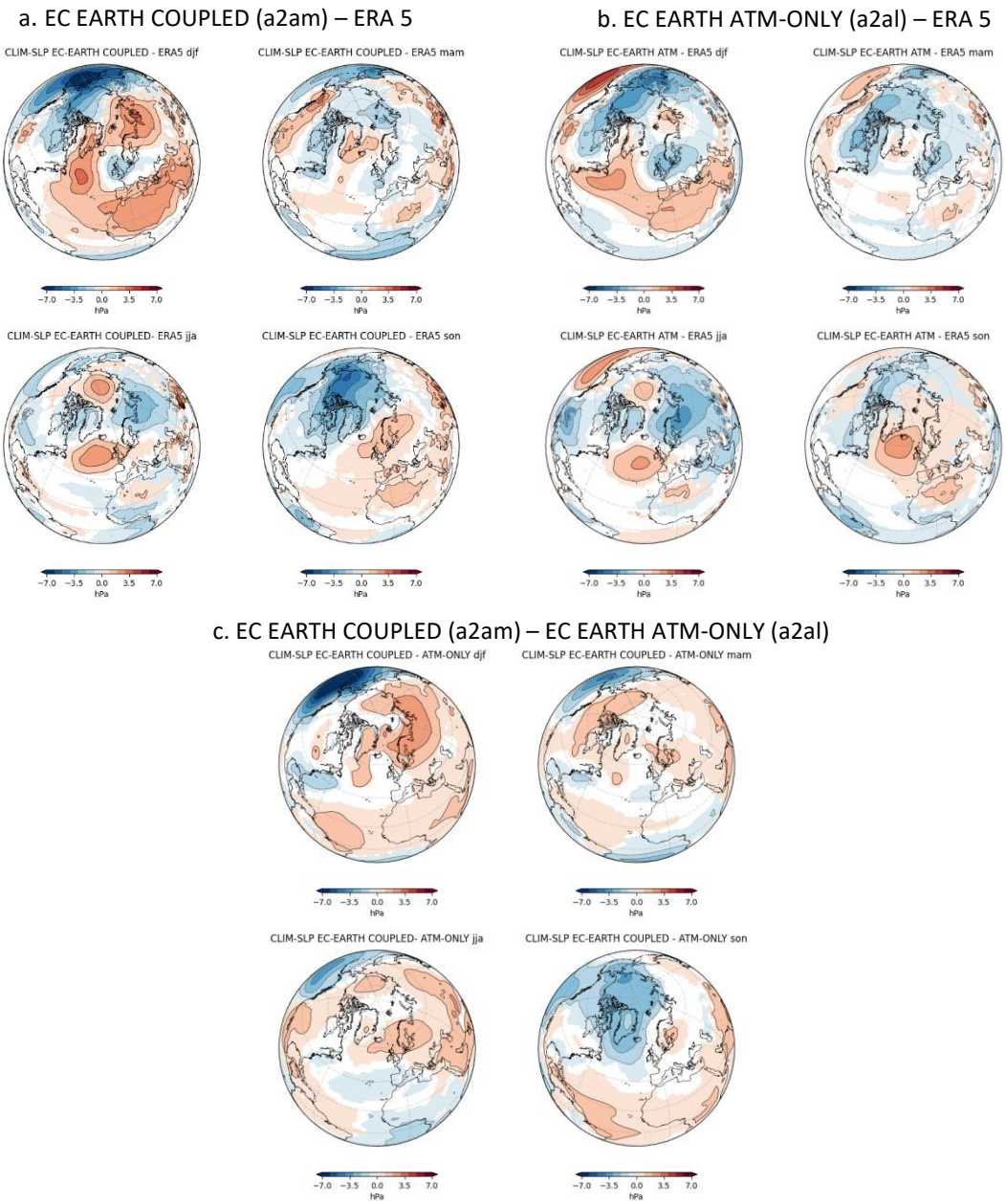

Figure 20 Difference between the SLP climatologies of the simulations and the reanalysis. In the case of ERA5, the period from 1978 to 2014 was considered. The contour lines show the entire field while the solid areas represent the significant differences according to a t-test at 95 % confidence level. Zero values are also shown. Top left a) is the difference between the climatology of the coupled simulation and that of the reanalysis model; top right b) is the difference between the climatology of the atmosphere-only simulation and that of the reanalysis model; bottom c) is the difference between the climatology of the coupled simulation and that of the atmosphere-only simulation.

As a further verification of the correctness of the simulations, a qualitative comparison was made between the results presented above and those obtained by R. Haarsma et al. (2020), in which the HighResMIP versions of EC-EARTH (EC-EARTH3P and EC-EARTH3P-HR) are described, analysing their performance and providing a basic validation. The comparison was made between the atmosphere-only simulation used in this research work and the atmosphere-only simulation used in the paper. However, it will be an exclusively visual and not strictly correct comparison as the configuration of the experiments is different. In the case of the simulation used here, the resolution is standard and, as reported in the data and methodology section, the SST is prescribed and calculated using the

climatology referring to the period 1988-2007; on the other hand, in the paper, the simulation is in high resolution and uses the SST for the period 1950-2014.

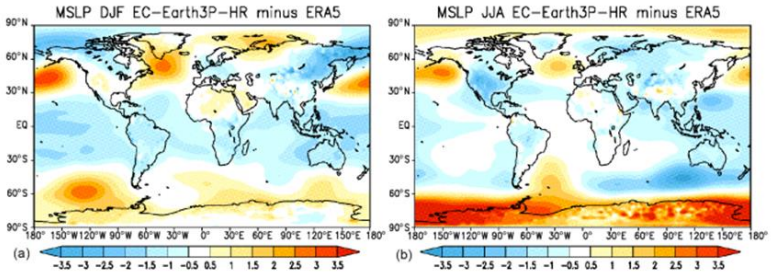

Figure 7. MSLP: bias (hPa) of EC-Earth3P-HR with respect to ERA5 for the period 1979–2014: **(a)** DJF and **(b)** JJA. Global means of MSLP for EC-Earth3P-HR are 1011.3 (DJF) and 1009.4 (JJA), and for ERA5 1011.53 (DJF) and 1011.24 (JJA). RMSEs of EC-Earth3P-HR with respect to ERA5 are 1.11 (DJF) and 1.27 (JJA).

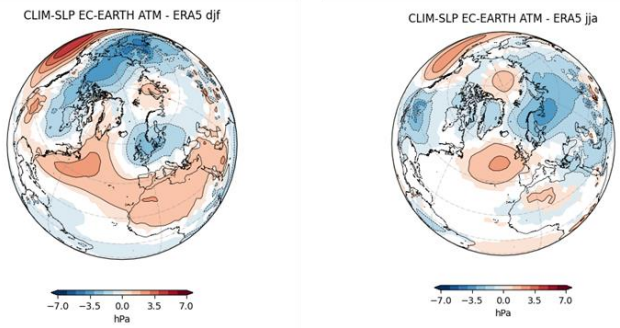

Figure 21 Comparison between the differences in pressure climatologies obtained in this research (below) and those obtained in Haarsma et al. (2020) (above).

Despite these differences, it can be observed (Figure 21) that the results look very similar. Note, for example, the positive bias in the area of the Atlantic Ocean South of Greenland, present both in winter and in summer both in the case under consideration and in the paper. Or the negative and positive biases located over Northern Europe and North Africa respectively during winter, but which disappear in summer in both simulations. However, differences can be seen in terms of biases magnitude as the upper and lower limits in the two cases are different. In any case, these dissimilarities could be attributed to the different initial configurations mentioned above.

Looking at the difference in standard deviation (Figure 22), it would seem that in winter, the coupled simulation performs better than the atmosphere-only simulation as it has fewer significant biases. However, this is no longer true when considering the other seasons, where the simulated variability is in excess in spring and autumn and in deficit in summer. This happens in both simulations, but when considering the effect of the ocean, the extent and intensity of the errors is greater. Specifically in spring, the coupled simulation shows a positive deviation from the mean in the central Atlantic ocean area, where the atmosphere-only one shows no biases. Looking at the comparison between the two experiments (Figure 22, *c*), it is interesting to note that most of the simulated excess ocean-related variability, resides near the tropics and where the NAO high pressure centre is located.

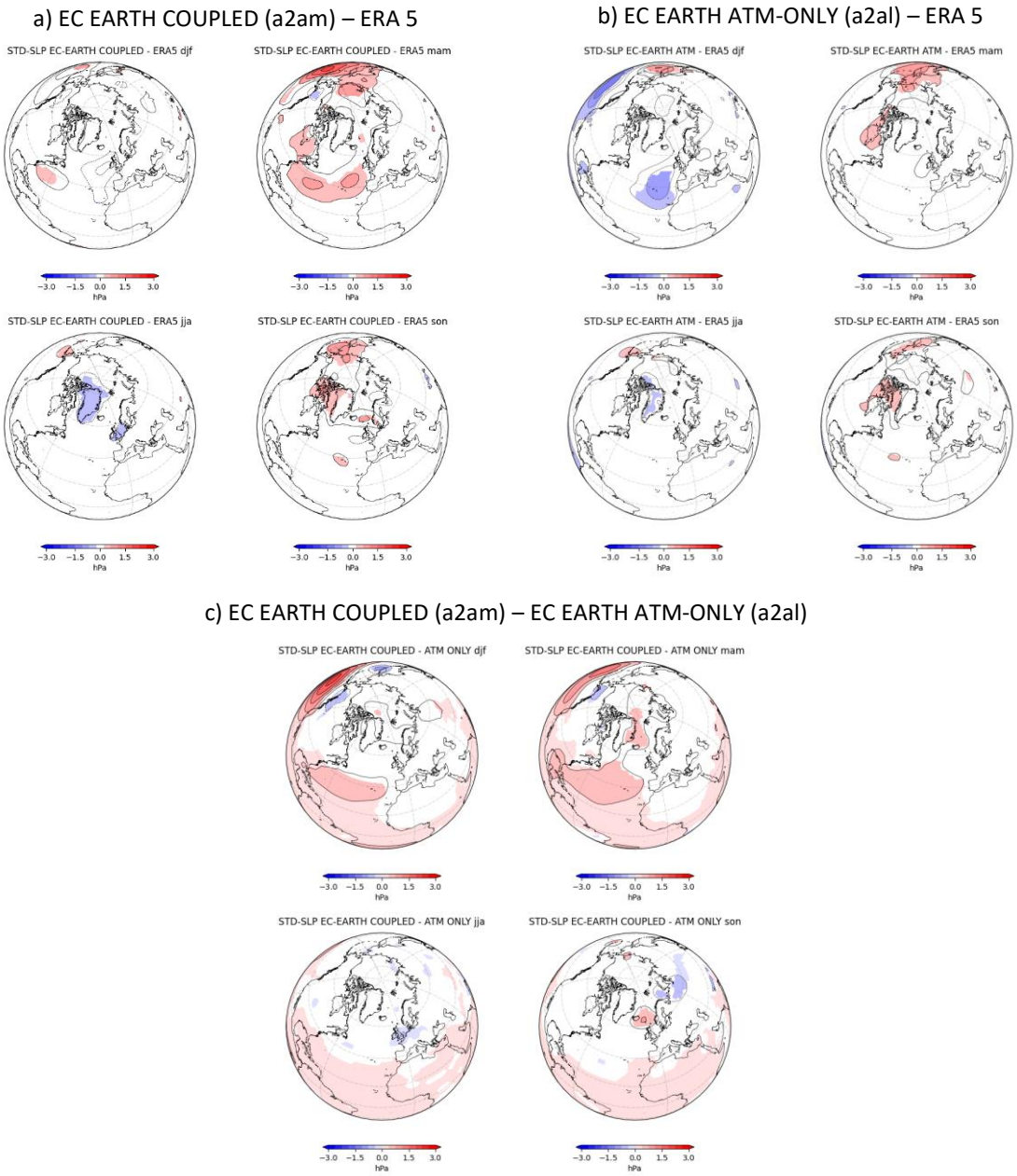

Figure 22 Difference between the SLP standard deviations of the simulations and the reanalysis. The contour lines show the entire field while the solid areas represent the significant differences according to a f-test at 95 % confidence level. Zero values are also shown. Top left a) is the difference between the standard deviation of the coupled simulation and that of the reanalysis model; top right b) is the difference between the standard deviation of the atmosphere-only simulation and that of the reanalysis model; bottom c) is the difference between the standard deviation of the coupled simulation and that of the atmosphere-only simulation.

Figure 23 shows the difference between the temperature climatologies. Beginning with the difference between the coupled simulation and ERA5 (Figure 23, *a*), a strong positive bias in the Arctic Circle region present year-round of the order of +7 °C is evident. Winter and autumn months show greater error intensity than summer and spring months. In DJF, warming affects Greenland, northern Canada and the East Coast bordering the United States, Alaska and northern Russia and extends into the Kara and Barents Seas. An additional positive error can be observed over India and parts of the Middle East, while over North Africa, Italy and Spain the simulation returns temperature values lower than observations on the order of -4/-4.5 °C. The spring season is the one in which the

described positive differences are less extensive and less intense, and the negative ones tend to narrow except for a negative difference Southeast of Greenland that strengthens slightly. In summer, on the other hand, negative biases are almost no existent, and more or less all lands in the Northern Hemisphere are affected by positive biases, less intense in the Arctic Circle and more pronounced over India, Middle East and Europe and over the North Pacific Ocean between America and Russia. Autumn is the season that shows the extent of the errors, which until now affected more land areas, above the Ocean: specifically, the highest warming is observed over the Arctic Ocean along the northern coasts of Siberia. In contrast, warmer areas in south-central Eurasia show minor differences in intensity. Also note the strong positive bias in the Atlantic Ocean at the Equator in Northeast Brazil.
Taking into account the differences between the atmosphere-only simulation and the reanalysis (Figure 23, *b*) and comparing them with those just described, it's clear that the positive biases are much less pronounced and in summer and autumn almost disappear. In fact, the DJF months again show positive biases over the Arctic Circle, but much more circumscribed and weak: the most prominent is the one at North Siberia. Instead, areas of Southern Europe, Scandinavian Peninsula, North Africa, Middle East, and West Coast of the United States are highlighted where the simulation returns colder values. Spring in this case shows the positive highest simulated values in the Arctic Circle at Greenland and northern Canada. Areas of colder values in the winter season persist and a new one emerges over China. In contrast, the bias of warmer values extends over India reaching higher values in summer. Again, summer is the season that shows the greatest extension of positive biases, although unlike the case where the ocean also plays a role, some negative biases persist here, such as the one over the Sahara Desert. In autumn months there are positive discrepancies in the North Pole area, but much slighter than in the previous case. On the other hand, the negative difference persist over North Africa and the positive one over Northeast Brazil.
The differences illustrated are also confirmed by the difference between the climatologies of the two simulations (Figure 23, *c*), so it is clear that in the case where the effect of the ocean is also considered, this leads to the simulation of higher average temperature values in the North Pole than in reality, and this may be due to problems in the configuration of the parameters representing the ocean and the coupling between it and the lands.

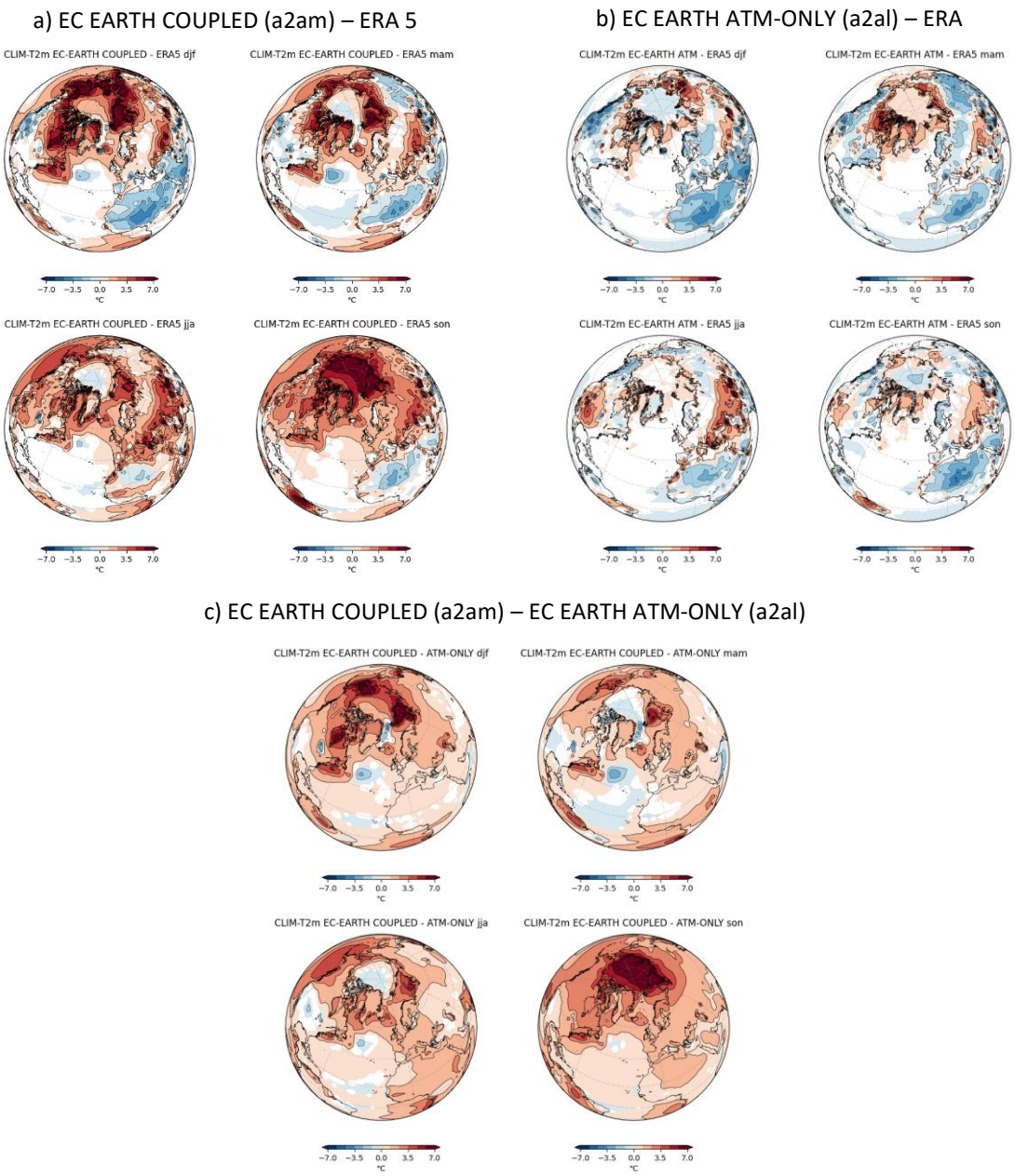

Figure 23 Difference between the t2m climatologies of the simulations and the reanalysis. In the case of ERA5, the period from 1978 to 2014 was considered. The contour lines show the entire field while the solid areas represent the significant differences according to a t-test at 95 % confidence level. Zero values are also shown. Top left a) is the difference between the climatology of the coupled simulation and that of the reanalysis model; top right b) is the difference between the climatology of the atmosphere-only simulation and that of the reanalysis model; bottom c) is the difference between the climatology of the coupled simulation and that of the atmosphere-only simulation.

The results were compared in a qualitative way with those obtained by R. Haarsma et al. (2020) and as can be seen in Figure 24, despite the differences in forcing conditions and resolution, the output is very similar. The positive and negative biases correspond for both seasons and the only difference is in the magnitude of the differences, which in some cases turns out to be stronger in the result obtained with the a2al simulation. For example, the negative biases over North Africa and along the West Coast of the United States for the winter season are consistent as are the positive biases in Middle East and in South-Central United States for the summer season.

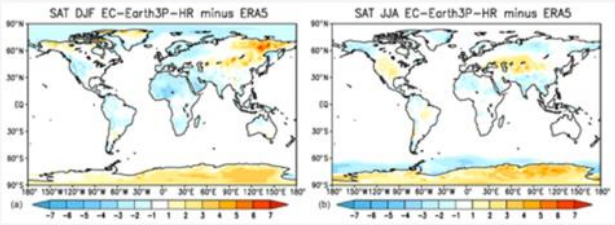

Figure 6 SAT: bias (°C) of EC-Earth3P-HR with respect to ERA5 for the period 1979–2014: **(a)** DJF and **(b)** JJA. Global means of SAT for EC-Earth3P-HR are 11.01 (DJF) and 15.85 (JJA), and for ERA5 12.43 (DJF) and 15.95 (JJA). RMSEs of EC-Earth3P-HR with respect to ERA5 are 1.25 (DJF) and 1.06 (JJA).

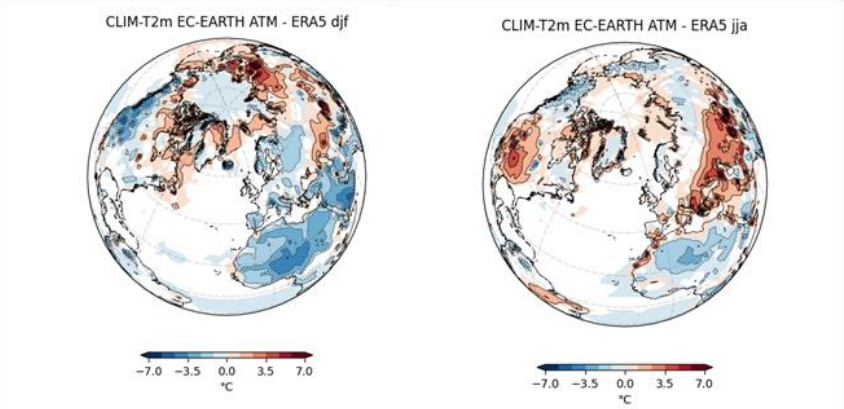

Figure 24 Comparison between the differences in temperature climatologies obtained in this research (below) and those obtained in Haarsma et al. (2020) (above).

Observing difference maps between temperature standard deviations of the three datasets (Figure 25), it is possible to find the highest values of variability in the observations: in winter and autumn in the case of the difference with the coupled simulation, and throughout the year in the case of the difference with the atmosphere-only simulation. The coupled simulation's significant errors are limited in extent and intensity. The season with the most biases is winter, during which negative differences of the order of -1 °C can be seen over the Arctic Circle lands and positive ones, of varying order of magnitude between +1/+3 °C, over the Norwegian Sea and Kara Sea and in the Arctic Ocean between Alaska and Russia. A negative difference East of the Caspian Sea and three positive differences in the Middle East, Mexico and between Brazil and Venezuela are also highlighted. In spring the positive differences persist and the negative ones are greatly reduced, and in summer the former extend and the latter disappear. In autumn, on the other hand, weak negative errors reappear in the land areas of the Arctic Circle to which is added an area of positive error throughout the Arctic Ocean. In contrast, the atmospheric-only simulation biases are almost all negative and except for winter, are mainly localized over water or at most along the coasts (Figure 25, *b*). In DJF, differences as low as -3 °C are noted around the Greenland coast and over the Barents Sea, while there are weaker ones extending over northern Canada, the Scandinavian Peninsula and Siberia. In spring the same negative errors persist above the surface of the seas and those on the earth's surface are reduced, and these disappear almost completely in summer followed by those in the Pole area. In JJA the extensive but weak negative biases are localized in the northern Atlantic and Pacific Oceans. In autumn, however, negative biases reappear on the surface of the Arctic Ocean, of the Barents Sea and of the sea around Greenland.

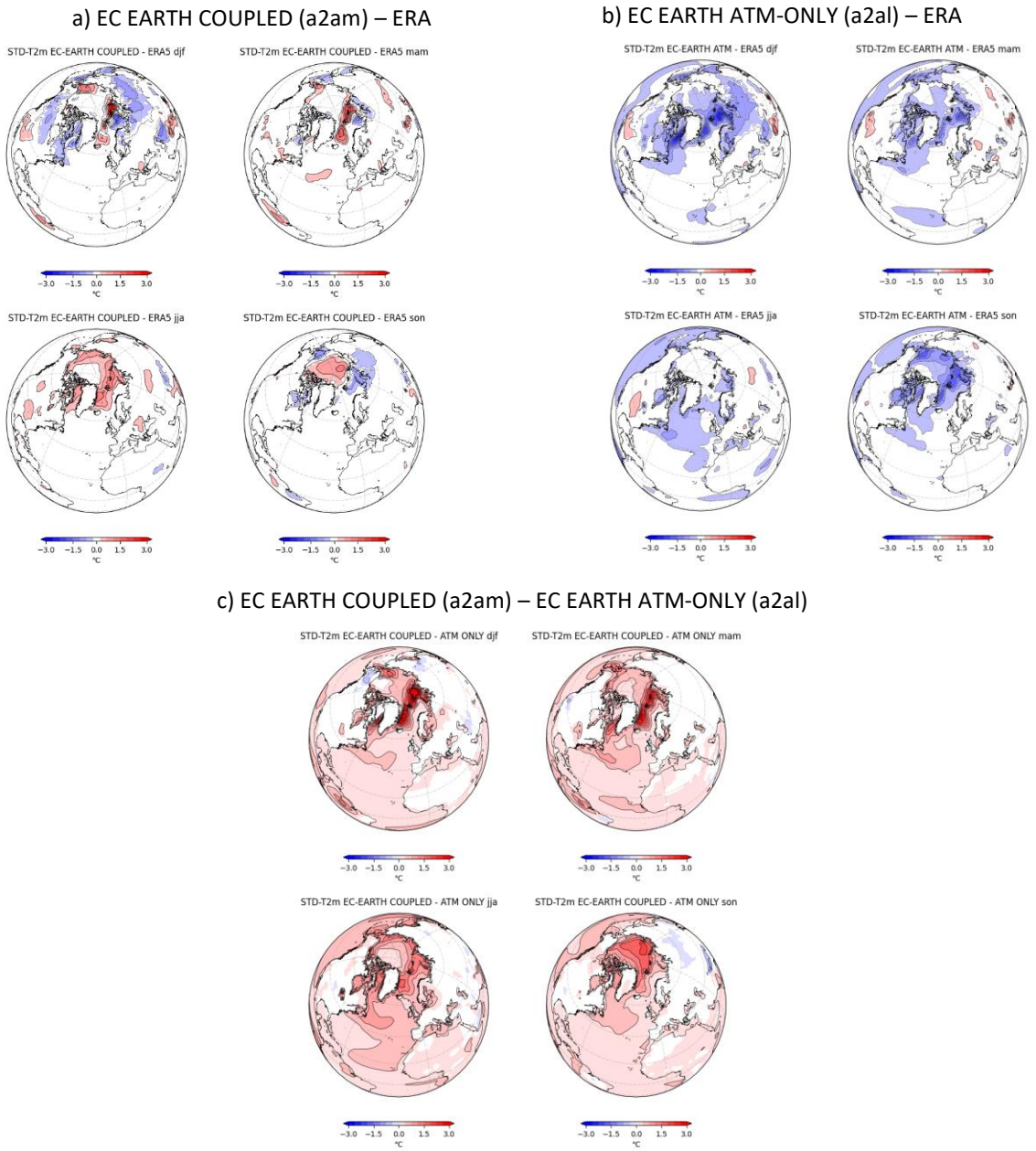

Figure 25 Difference between the t2m standard deviations of the simulations and the reanalysis. The contour lines show the entire field while the solid areas represent the significant differences according to a f-test at 95 % confidence level. Zero values are also shown. Top left a) is the difference between the standard deviation of the coupled simulation and that of the reanalysis model; top right b) is the difference between the standard deviation of the atmosphere-only simulation and that of the reanalysis model; bottom c) is the difference between the standard deviation of the coupled simulation and that of the atmosphere-only simulation.

The calculation of differences between the two simulations confirms that the significant biases all reside over the seas and oceans and that the ocean action allows for a simulation that can explain much more variability in the temperature field.

Based on these results, some considerations can be made. First of all, the fact that the experiment with only the simulated atmosphere shows less variance than the observations is consistent with the fact that its setup assumes fixed SST and SIC: in fact, in the reanalysis model, the variation in sea ice extent is a factor that greatly influences the variability of temperatures in the North Pole area.

Therefore, comparing the two simulations, it can be said that to achieve the same variability of observations in the temperature domain in the North Atlantic European region, sea ice variation (i.e., the effect of variation in the extent of SIC), and thus the action of the sea, is needed.
It would also appear that sea ice variation does not have a major influence on the variability of temperatures over the continents throughout the annual cycle. The only exception is the Scandinavian Peninsula and Siberia during winter, where the variation in the extent of ice cover is also high in the land regions around the Arctic Ocean and thus, it has consequences on temperature fluctuations.

Regarding differences in the climatology of total precipitation, in all three maps, the highest biases are concentrated in the ITCZ. In fact, as shown in Figure 26 simulations tend to shift the ITCZ southwards: the double ITCZ is a consequence of the strong warm temperature bias over the Southern Ocean leading to a greater southward shift of tropical rainfall and a more vigorous hydrological cycle (Döscher et al. 2022).
Observing the discrepancies of the coupled simulation versus the reanalysis (Figure 26, *a*), the most intense errors in the North Atlantic European zone are seen in the winter months, during which the ocean's contribution results in a dry zone (of the order of -2 mm/d) in the Atlantic Ocean and weaker ones are scattered over Middle East. The ocean also leads to wetter areas formations in the Greenland Sea and along the East coast of Canada and the United States. In spring, the aforementioned biases weaken and lose intensity and a new arid one emerges in the Atlantic Ocean, East of the US coast. During JJA differences between models change: errors in the area under analysis are mostly negative ones and are concentrated in central Europe and central Russia. There are also wet areas over Greenland and along the coast of the United States. Note that summer is the season during which the simulated ITCZ reaches its maximum southward shift. In September, October and November, the differences in the NAE region are fewer and weaker; the most noticeable ones are a dry zone in the mid-Atlantic and wetlands over Greenland.
In the case of the atmospheric-only simulation biases (Figure 26, *b*), in winter the dry zone that was in the centre of the Atlantic Ocean in the previous case is now weaker and shifted westwards. The positive biases, on the other hand, are no longer relevant. Spring has very few discrepancies and they are all very weak. Again, the North Atlantic European summer region has dry biases over central Europe and central Russia. In the case of autumn, errors are fewer and less intense and over the ITCZ, the differences are smaller and less pronounced.
It is possible to conclude that the effect of the ocean leads to more biases, which are more intense and more extensive, especially the positive ones, i.e. leading to wetter areas. This is confirmed by the map showing the significant differences between the two simulations (Figure 26, *c*), in which the presence of the wettest areas throughout the year along the US coastline can be seen. The most significant negative (dry) biases in winter, spring and autumn are present over the central Atlantic Ocean.

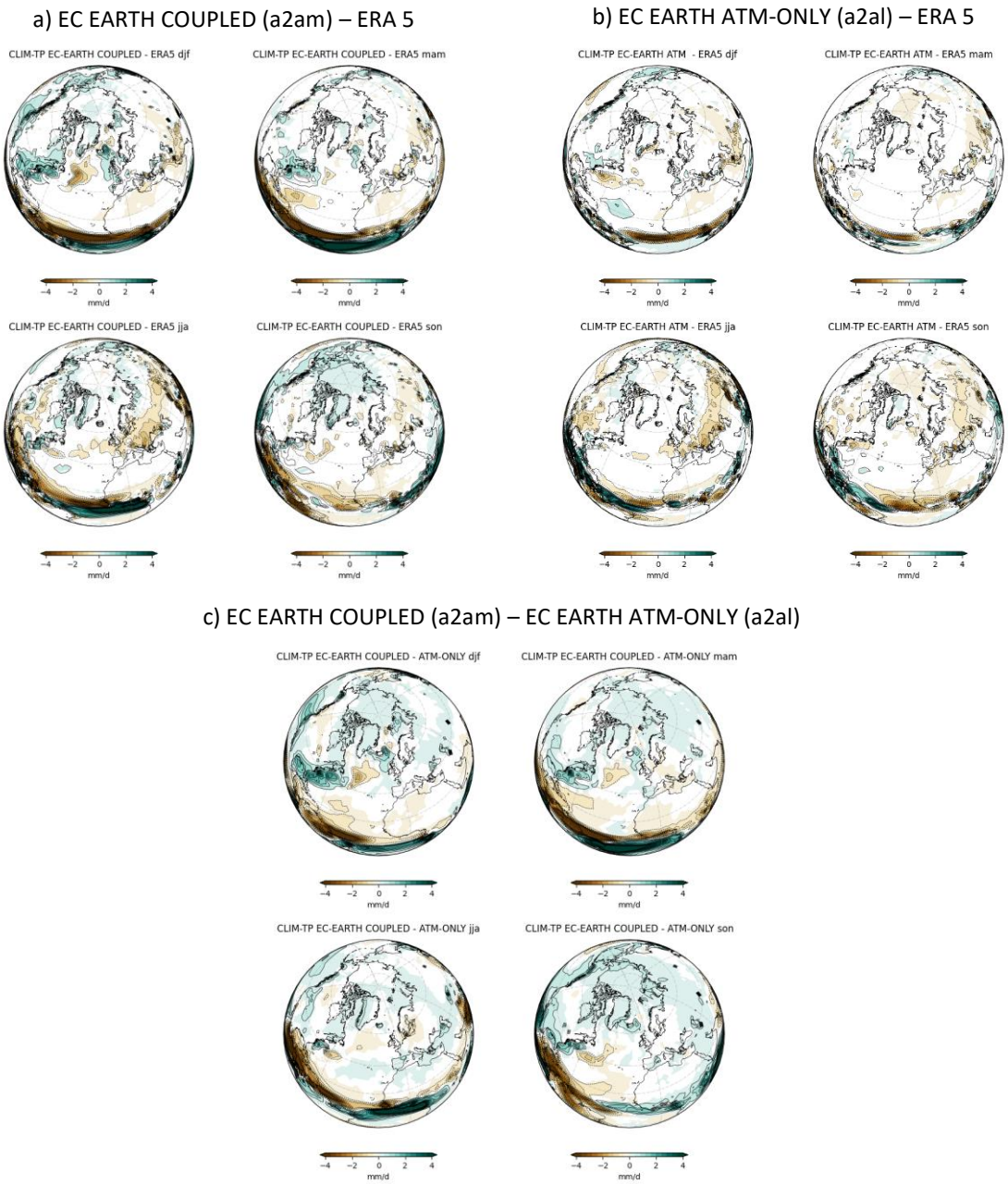

Figure 26 Difference between the TP climatologies of the simulations and the reanalysis. In the case of ERA5, the period from 1978 to 2014 was considered. The contour lines show the entire field while the solid areas represent the significant differences according to a t-test at 95 % confidence level. Zero values are also shown. Top left a) is the difference between the climatology of the coupled simulation and that of the reanalysis model; top right b) is the difference between the climatology of the atmosphere-only simulation and that of the reanalysis model; bottom c) is the difference between the climatology of the coupled simulation and that of the atmosphere-only simulation.

As a check on the correctness of the results, it was decided to compare the output with that obtained by Döscher et al. (2022), in which the Earth system model EC-EARTH3 for contribution to CMIP6 is documented. To do this, the annual average of the coupled simulation was subtracted from the annual average of precipitation over the period 1980-2010 by ERA5. Nevertheless, as in the previous cases, the comparison is only qualitative as the starting configurations of the simulations are different. However, the outputs seem to correspond quite closely (Figure 27): note for example in

both cases the presence of the arid zone in the middle of the North Atlantic Ocean or the wetter zone along the US coast or near Iceland.

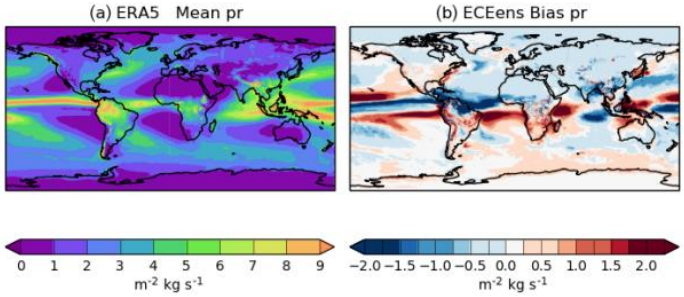

Figure 6. Mean precipitation for the period 1980–2010 for ERA5 **(a)**, precipitation anomaly with respect to ERA5 for EC-Earth3veg **(b)**, and zonal mean precipitation for ERA5 **(c)** (green), GPCPv2.2 (black), and EC-Earth3veg ensemble mean (blue).

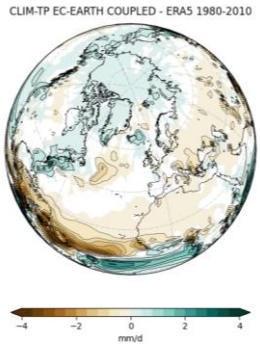

Figure 27 Comparison between the differences in temperature climatologies obtained in this research (below) and those obtained in Dösher et al. (2022) (above).

The comparison of the total precipitation weighted averages in the NAE region between the three datasets yields a different result depending on the season when considering only ERA5 and the coupled simulation (Figure 28). In fact, in winter and autumn (although in the latter case the gap is minimal) the reanalysis expresses more variability than the a2am simulation, while in spring and summer the opposite occurs. There are no significant differences between these two datasets, while between ERA5 and the atmosphere-only experiment the deviation is large and statistically significant throughout the entire year.

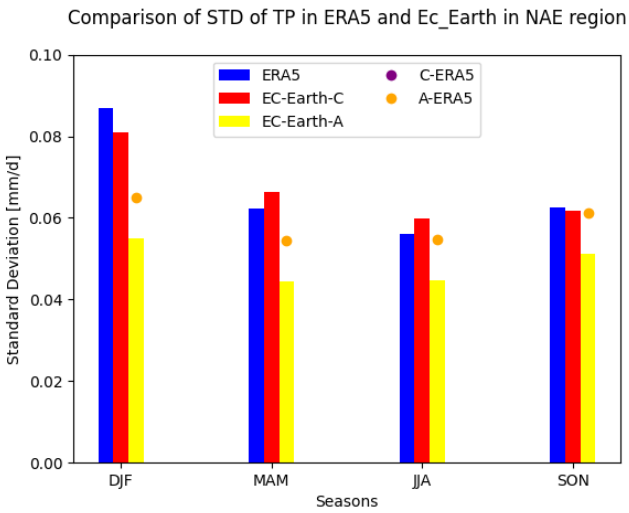

Figure 28 Bar plot of the TP standard deviation's weighted average in NAE region for the coupled and atmosphere only simulation and for ERA5. The orange and purple circle represent significative differences following the f-test.

Maps of significant biases in the simulations are shown in Figure 29. It was decided to disregard the large differences in the ITCZ and to set a range with lower maximum and higher minimum to show the significant errors in the area under analysis. Map *a* in Figure 29 shows the biases of the coupled model where winter is the season in which there are the most negative errors in the vicinity of the

NAE region: the weakest ones are concentrated over North Africa and Middle East (at the Sahara Desert and the Arabian Desert), while those of -0.25/-0.5 mm/d are located over Southern Europe. Instead, positive errors are concentrated in the Atlantic Ocean, east of Iceland and east of the US coast. In spring, the only negative errors that persist are those near the Sahara, while all others are reduced to almost zero. The positive ones remain at about the same winter location, extending slightly. In summer, the negative bias over North Africa diminishes and a new one arises in Eastern Europe, accompanied by a positive one in the South East. The positive bias in the Atlantic Ocean, East of America, persists and the one near Greenland strengthens. During autumn, the significant negative bias over North Africa and Eastern Europe diminishes, while a new one appears in the Atlantic Ocean, East of the United States. The positive bias over Greenland persists and widens.
Looking at map *b* in Figure 29, it is evident that the atmosphere-only simulation explains less variability than the year-round reanalysis. In fact, negative biases over Africa, Southern Europe and Eastern Europe are visible in all seasons. Positive biases are almost non-existent except for a more noticeable one in the Atlantic Ocean, West of the North African coast, probably related to the strong variability of the ITCZ. The fact that the ocean leads to greater variability, compared to the action of the atmosphere alone, especially in the central and North Atlantic region is confirmed by map *c* in Figure 29 in which the difference between the two simulations was calculated.

In this section, the differences between two simulations from EC-Earth (one in coupled air-sea mode, the other in atmosphere-only mode) and the ERA5 observations in representing the climate and its variability in the North Atlantic European region (and neighbouring regions) were examined. This was done because the ultimate goal is to use the experiments to assess how well they are able to represent the NAO and its associated variance and what the differences are if the effects of the ocean, in addition to atmospheric ones, and those of the radiative forcing are also taken into account.
The results obtained in the climatology were compared with those reported by R. Haarsma et al. (2020) and Döscher et al. (2022) to assess the consistency of the outputs. Although setting conditions of the experiments used in this analysis differed, visually and therefore qualitatively, it could be concluded that the performances obtained were rather similar in terms of the position and extent of the biases, whereas they differed in terms of intensity. This latter discrepancy could be related to the different initial conditions selected.
The second observation concerns the effect of the ocean on the climate of the North Atlantic area that can be deduced from the calculated difference between the climatologies of the variables of the two simulations. In the case of sea level pressure, it would appear that the effect is to increase the intensity of the pressure systems with a tendency to overestimate them, in particular during the winter months, by the order of 3.5 hPa/-5 hPa.
Biases in temperature result in a clear warming of the order of more than 7 °C of the subpolar region localised along coasts except in autumn when it also extends over the Arctic Ocean. While in the case of pressure the difference between the presence of ocean action and its absence is not particularly relevant, in the case of temperature it is a major bias. A possible hypothesis is that this is related to the choice of setting the radiative forcing at 2002, which in the case of the atmosphere-only simulation does not affect, because the SST and SIC parameters were also set, while in the case

of the coupled simulation it leads to over warming because the starting point is already warmer than the reanalysis point.

As far as precipitation is concerned, not taking the ITCZ into account, the effect is to intensify wet systems and dry systems by a maximum of +/- 3 mm/d, again resulting in an overestimation compared to observations.

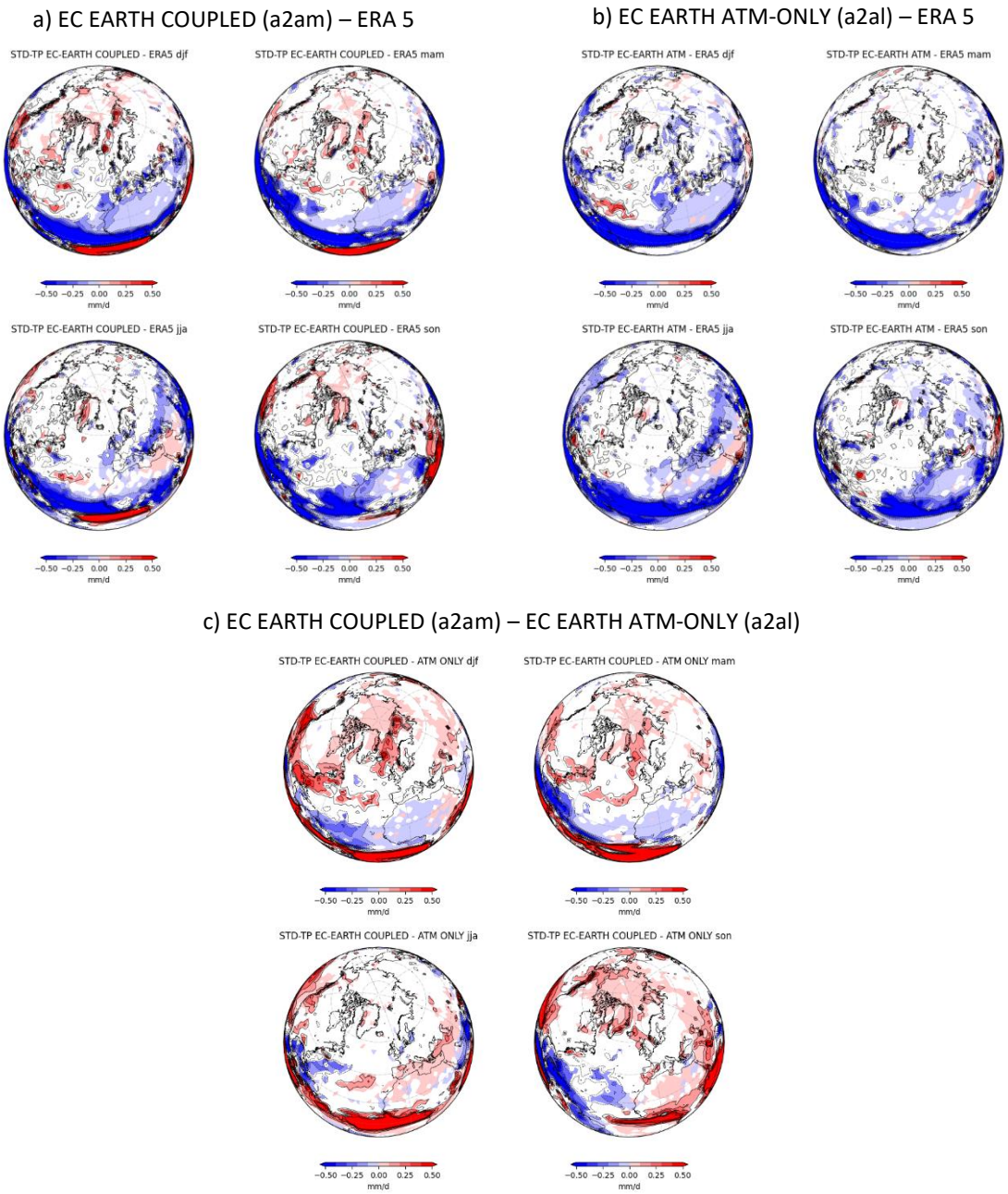

Figure 29 Difference between the TP standard deviations of the simulations and the reanalysis. The contour lines show the entire field while the solid areas represent the significant differences according to a f-test at 95 % confidence level. Zero values are also shown. Top left a) is the difference between the standard deviation of the coupled simulation and that of the reanalysis model; top right b) is the difference between the standard deviation of the atmosphere-only simulation and that of the reanalysis model; bottom c) is the difference between the standard deviation of the coupled simulation and that of the atmosphere-only simulation.

The analysis and comparison of standard deviations also assessed the effect of the ocean on climate variability in the region of interest. The variability of the SLP in winter seems to be better represented

by the coupled simulation as it has fewer significant biases than the atmosphere-only simulation. Although in general, the ocean results in an overestimation throughout the year. The increase in variability can also be seen from the calculation of the standard deviation difference between the two EC-EARTH simulations, where it is interesting to note that in the coupled simulation the enhanced variability is concentrated near the Azores high pressure system typical of the NAO.
The effect of the ocean is also relevant in the temperature variability, as the coupled simulation is more representative of the true deviation of temperatures from the mean, although it tends to underestimate it. However, the underestimation is not excessive and is not significant in spite of the one resulting from the atmosphere-only simulation, which reports much lower standard deviation values than the real ones, especially in summer. This is because the a2al experiment assumes that the SST and SIC variables are fixed (as seen in the Data and Methodologies section) and therefore, cannot represent the annual cycle of sea ice extension and reduction, which has a fundamental effect on temperature variability in the Arctic Circle region. In addition, by observing the distribution of differences in temperature variability in the two simulations, it can be concluded that, the continuous change during seasons of sea ice increase and decrease, has no major effect on temperature anomalies over the continents. The only exception is the winter season in which the difference in variability extends over the Scandinavian peninsula and northern Russia.
The coupled experiment is also a better estimate in the case of precipitation variability. In fact, the atmosphere-only simulation tends to underestimate it in all seasons in a statistically significant manner in contrast to the a2am simulation, which slightly overestimates it.
In order to better represent the climate anomalies in the North Atlantic European region, variability in the concentration of sea ice, i.e. the effect of the variation in its extent throughout the year, is required. Whereby, if the climate variability component is to be studied and analysed, the use of a coupled model is recommended.

5.2 The impact of air-sea coupling on the NAO

The NAO is a large-scale atmospheric phenomenon supplied mainly by stochastic interactions between atmospheric storms and both the climatological stationary eddies and the time mean jet stream (Hurrell et al. 2003). These mechanisms result in fluctuations of the NAO on a 10-day scale (Feldstein 2000). For these reasons, monthly and annual variations in the phase and amplitude of the NAO are difficult to predict. However, although the scientific community agrees that the NAO is an internal mode of variability within the atmosphere, there is evidence from both less and more recent studies that some external factors such as sea surface temperature, volcanic aerosol, stratospheric circulation and composition, sea ice and hemispheric snow cover as well as anthropological effects could influence the phase and amplitude of the NAO. Specifically, interactions between the atmosphere and the underlying surface or between the troposphere and stratosphere may cause a low-frequency component of the NAO variability (Budikova 2012; Feldstein 2000; Hurrell et al. 2003). This could result in a limited, but greater predictability of the phenomenon, which, given the large impact it has on the climate of the Northern Hemisphere, could be very useful within the debate on climate variability and change.

For instance, there have been conducted numerous studies about the potential predicting role of the reduction of sea ice concentration in the Barent-Kara Seas and an increase of snow cover extent across Siberia in autumn that would favour a negative NAO phase during the subsequent winter (e.g. García-Serrano et al. 2015; Santolaria-Otín et al. 2020; Scaife et al. 2014). The observational studies conclude that the november SIC in Barent-Kara Seas represents the most robust "potential" predictor of the winter NAO based on eastern Arctic SIC variability (e.g. García-Serrano et al. 2015; Koenigk et al. 2016; Santolaria-Otín et al. 2020).

The effect of air-sea coupling is one of the external factors that could have an influence on the NAO and studying it in more detail and understanding its interactions could be important to understand the details of the NAO amplitude and its evolution over the long term and thus increase its predictability. The scientific community agrees that the thermal anomalies in the upper ocean layer are dominated by atmospheric circulation, but the degree to which the extratropical SST field influences the atmosphere is still a topic under analysis and discussion. (Hurrell et al. 2003)

Following Bjerknes (1964) who discovered coupled atmosphere-ocean variability over the North Atlantic, Watanabe & Kimoto (2000) examined the possible presence of a positive atmosphere-ocean feedback over the same region using a series of general circulation model (GCM) experiments. In agreement with previous studies, coupled ocean-atmosphere fields showed greater interannual variability than uncoupled runs due to reduced local thermal damping. While their results confirmed the dominant role of the atmosphere in generating the SST anomalies, they also identified a zone of positive SST anomalies in the mid-latitudes zone that tends to stimulate the positive phase of the NAO, which consequently reinforces the tripolar SST anomaly: the results obtained manifest positive feedback at work in the coupled atmosphere-ocean patterns.

Czaja et al. (2003) also analysed the role of atmosphere-ocean coupling in influencing NAO variability. Assuming that extra-tropical climate variability, unlike that of the tropical Pacific, mostly reflects only processes within the atmosphere on a monthly or decadal time scale, it is clear that the atmospheric cap north of the equator is not an isolated system. Therefore, Czaja et al. (2003) question the possible effect of flux exchanges between the atmosphere and the ocean on the NAO. In doing so, they analyse the various mechanisms through which the Atlantic Ocean could impact the atmosphere, but the evidence from both observations and simulations shows that the relevance of these processes on NAO variability is low. However, this is related to the complexity of the air-sea interaction in the North Atlantic zone, which leads to numerous problems and difficulties in presenting firm conclusions on the impact of the Ocean on the NAO, so the authors conclude by leaving the issue open for further evaluation.

Indeed, a couple of years later Wu & Liu (2005) analysed the causes and mechanisms of decadal variability in the North Atlantic using a series of coupled ocean-atmosphere simulations. Their results highlight the critical role of ocean-atmosphere coupling in sustaining North Atlantic decadal oscillations at selected time scales. The negative feedback on SST anomalies, due to the NAO responding to the tripolar SST anomaly, can be obtained with both coupled and atmosphere-only models. However, stochastic atmospheric forcing fails to generate any preferred time scale. Thus, the authors conclude that decadal North Atlantic variability can be viewed as a coupled ocean-atmosphere mode under the influence of stochastic forces.

In 2017 Vannitsem & Ghil investigating ocean-atmosphere coupling in reanalysis data sets, confirm the existence, already found in the literature, of a common mode of atmosphere-ocean variability represented by a dominant low-frequency signal with a 25-30 year period. Furthermore, thanks to a new score to assess the internal nature of the common variability, they confirm the presence of coupled dynamics in the ocean-atmosphere system that impact the atmosphere at large scales and influence the predictability of the system.

Kim et al. (2018) explored the representation of low-frequency North Atlantic climate variability using large historical ensembles and pre-industrial control simulations performed with the Community Earth System Model (CESM). Their aim was to demonstrate the primary role of low-frequency NAO variability in generating other low-frequency variability in the North Atlantic. However, in their study they also suggest that the North Atlantic region acts as an active zone for ocean-atmosphere coupling, which in turn would affect low-frequency NAO variability. However, this assumption was not confirmed by model analyses, which were found to be deficient in estimating low-frequency NAO variability.

Further results in this topic were achieved by Peings & Magnusdottir (2014, 2016) and Peings et al (2016). Indeed, by analysing the relationships between the multidecadal scale SST fluctuations (Atlantic Multidecadal Oscillation, AMO) and the multidecadal winter fluctuations of the NAO, they obtained an interesting window of predictability for decadal forecasting given the fact that the AMO seems to anticipate the NAO by about 10-15 years. Furthermore, in both observations and simulations, they found that a positive AMO phase in winter leads to more frequent negative NAO phases accompanied by blocking episodes, which increase the occurrence of temperature extremes over the eastern US and Europe. Using different configurations of the Community Atmospheric Model version 5 (CAM5), to investigate the impact of Atlantic multi-decadal variability (AMV) in the winter atmospheric circulation, they obtained two main additional results: the NAO response in winter consists of a negative signal response to a warming North Atlantic ocean, and tropical and extratropical SST anomalies are necessary to obtain a significant modulation of the NAO with little influence from sea ice anomalies.

Peings et al. (2016) analysed the relationships between AMV and winter atmospheric circulation also in simulations of the fifth Coupled Model Intercomparison Project (CMIP5), and two models showed a small delayed signal suggesting a leading role of the ocean in decadal oscillations of the atmosphere, with two different potential mechanisms: through the latitude shift of the Atlantic ITCZ that can modulate NAO through a Rossby wave train emanating from the tropics, and through the decrease in storm track activity and the shift of intraseasonal weather regimes towards a negative NAO regime. These latter results lead one to hope for the possible long-term predictability of winter climate over the North Atlantic and adjacent areas, derived from the long-term fluctuations of the North Atlantic Ocean (provided that the AMV is correctly represented in the coupled models).

Again, Klavans et al. (2021) analysed the predictability of the NAO in climate models on a near-decadal scale. Building on the results of D. M. Smith et al. (2020), which showed that for the NAO, decadal predictive abilities only emerge in large multi-model ensembles, the authors concluded that the major source of NAO predictive ability is external radiative forces, but that ocean initialisation may also be important for some particular NAO events or for some specific regions such as the subpolar North Atlantic ocean. Finally, one of the most recent studies in this regard, conducted by

R. Wu et al. (2022), analyses the effect of air-sea coupling through the spatiotemporal evolution of atmospheric wind and surface sea temperature on the persistence or phase transition of the NAO during winter. What they obtained is that the persistence of the NAO during winter is associated with a strong coupling between the NAO and the tripolar North Atlantic anomaly of SST reacting on the NAO through the eddy-mean flow interaction. Thus, they concluded that the air-sea coupling is critical for the maintenance of the NAO phase throughout the winter season.

Although it is not easy to analyse and understand the effect of the ocean and the atmosphere and their coupling, it has been shown to be of paramount importance to deepen the knowledge in this regard in order to increase, even slightly, the ability to predict long-term climate variability in the North Atlantic area and in particular the NAO.
In the following, the spatial distributions of the climate variables SLP, t2m and TP related to the NAO in the observations and in the two EC-EARTH simulations are analysed and compared. In this way, it is possible to qualitatively assess the accuracy and correctness of the model in representing them. Furthermore, as the two simulations are in coupled atmosphere-ocean mode (a2am) and atmosphere-only mode (a2al) respectively, from their comparison it is possible to assess quantitatively, with regard to the explained variance, and qualitatively, with regard to the structure and intensity of the anomalies, what effect the ocean has on the behaviour of the NAO.
The method used is the one already mentioned in Sections 3.3 and 4.2, based on linear regression and Student t-test to highlight, as shaded areas, the areas that are statistically significant at 95 %.

Figure 30 shows the comparison between the SLP anomalies generated by the NAO dynamics, obtained using the datasets from the ERA5 reanalysis and from the two simulations from EC-EARTH. As already evidenced for the observations, also in the case of simulations, the largest fraction of variance is explained in winter and, in particular, the coupled simulation is able to account for a percentage of 45.81 %, which almost reaches the value of that represented by the reanalysis (46.76 %). While if the effect of the ocean is not taken into account, the percentage drops to 40.9 %. In spring and autumn, the a2am experiment is able to account for the largest fraction of variance, whereas the atmosphere-only simulation accounts for a smaller fraction than the reanalysis in spring and, conversely, a larger fraction in autumn. In summer, the coupled experiment represents a percentage of explained variance of 29.74 % compared to 32.8 % and 43.75 % for the a2al experiment and observations respectively. Therefore, particularly with regard to winter during which the atmosphere is dynamically more active, the simulation that includes the action of the ocean is able to account for a greater fraction of variability.

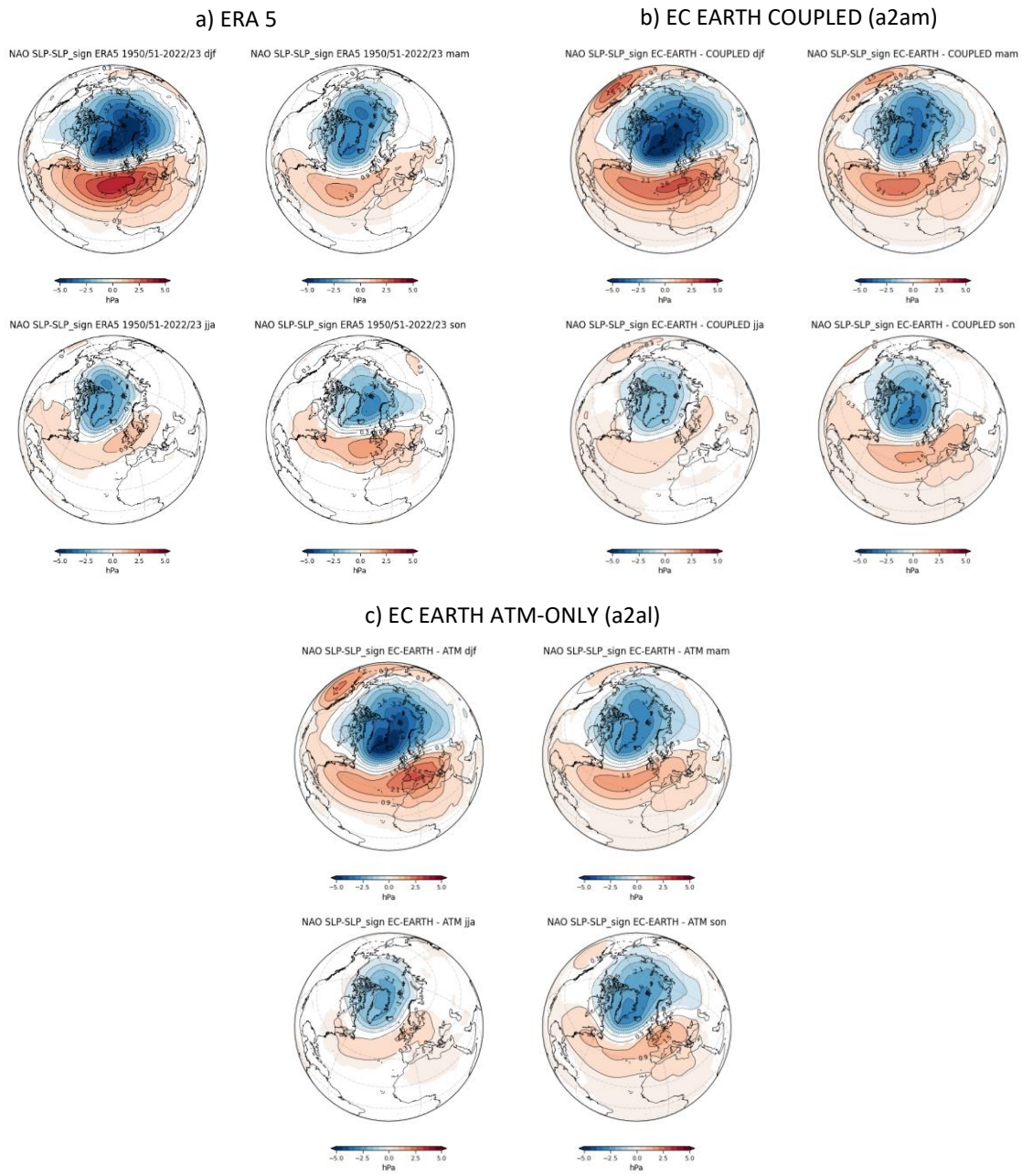

Figure 30 Seasonal SLP anomalies due to NAO in the North Atlantic European sector. The patterns are identified by regressing the SLP anomalies upon the first principal component time series of the leading EOF1 for all seasons. Statistically significant areas at 95% confidence level based on a two-tailed t-test for correlation values between the SLP anomaly and the principal component are shaded. Top left a) is the SLP anomaly from ERA5; top right b) is the SLP anomaly from the EC-Earth coupled simulation; bottom c) is the SLP anomaly from the EC-Earth atmosphere-only simulation.

Focusing on the a2am experiment (Figure 30 , *b*), we now describe the results obtained in terms of shape, position and intensity of the represented anomalies. Starting with winter, the map shows that the minimum intensity of the negative pressure anomaly centre is the same as that of the reanalysis, as is its orientation, since in both cases the anomaly tends to move eastwards. What varies slightly is the extent of the region of greatest intensity, which in the case of ERA5 has a more elongated structure directed towards North-East. On the other hand, analysing the positive anomaly, the intensity of the centre of pressure in the case of the simulation is lower (2.6 hPa vs. 3.2 hPa) and the size is smaller, giving the whole anomaly a weaker aspect overall. Another important difference lies

in the fact that the simulation also shows a second positive pressure anomaly in the North Pacific of the same sign as the one over the Atlantic. Thus, as also noted by McHugh & Rogers (2005) and Woollings et al. (2015), who used a series of Coupled ocean-atmosphere General Circulation Models (CGCM) to represent the NAO, the NAO SLP anomaly fields more closely resemble those of the Arctic Oscillation than the classical NAO pattern. The Arctic Oscillation has been defined as a large-scale annular variability mode that explains a certain fraction of variance in the Northern Hemisphere and is dominated by the regional NAO mode (Hurrell et al. 2003). However, more recently, it has been shown that the North Pacific and North Atlantic action centres in the mid-latitudes in the hemispheric signature of the NAO do not fluctuate in phase and thus, from this point of view, the AO would correspond to the circumglobally extension of the more regional NAO (García-Serrano & Haarsma 2017). Moving on to the analysis of the spring months, both the high pressure system over the Azores as well as the low pressure system over Iceland are in the same position as those of the observations, but have a greater and lower intensity respectively. Moreover, they are both more extensive: the negative one spreads towards the North of Russia and the positive one expands southwards, over North Africa, and westwards, over Central America. Also in spring, the presence of the high-pressure anomaly in the North Pacific (with the position of the centre more shifted towards the Asian continent than in the winter season) is emphasised, with a slightly lower intensity than the corresponding one in the Atlantic. In summer, the coupled simulation provides a less extensive and weaker representation of the anomaly dipole structure. In fact, the negative anomaly reaches a minimum of -1.5 hPa against the -2.1 hPa reached in the reanalysis model and, equally, the positive anomaly reaches a maximum of 0.3 hPa against the 0.9 hPa intensity in ERA5. The pattern of the low pressure system is very similar in the two models, while that of the high pressure system in the simulation is slightly more extended towards the East and South Atlantic and less extended westwards. We note once again the presence of the high pressure anomaly in the Pacific of the same intensity as that over the Azores. As far as autumn is concerned, there are differences in the position, intensity and extent of the anomalies pressure centres in the two models. In fact, the simulated Icelandic low centre, which reaches an intensity of -3.2 hPa, is shifted southwards and is located between Iceland and Greenland, unlike the observed one, which is of -2.6 hPa intensity and resides between Greenland and the North of the Scandinavian Peninsula. The structure differs because in the a2am experiment the anomaly is circular in shape and extends towards the Arctic Ocean, while in the reanalysis it has a less regular shape and extends towards Northern Europe and Northern Russia. As for the positive anomaly, on the other hand, the simulation returns a centre of pressure equal to that of the observations in terms of maximum intensity, but slightly different in terms of extension and position. Indeed, the former is smaller and more oriented westward (as does the rest of the simulated anomaly) and it arrives to influence a large part of North/Central America, unlike the observed anomaly, which stops in the first part of the United States facing the Atlantic Ocean.

The spatial distribution of the anomalies obtained with the a2al simulation is analysed below (Figure 30, *c*). Even in the case of the negative pressure system simulated by the atmosphere alone, the intensity and structure of the anomaly centre of action are very similar to observations ones. What varies slightly is the size of the latter, which, as in the coupled experiment, is less extensive towards the East. Similarities with the other experiment are also noted for the positive anomaly system: the centre of pressure reaches a maximum value of 2.6 hPa (to be compared with the 3.2 hPa of the

observations) and it is even less extended and more shifted eastwards than in the coupled simulation. Therefore, in general, the positive winter anomaly over the Azores due to atmospheric action alone is the weakest. The pressure system located in the Pacific is also of less magnitude, but its occurrence confirm the hypothesis that the model tends to represent the NAO in its extended version known as the AO. Continuing with the analysis, the negative spring anomaly simulated by the atmosphere alone has a more extensive shape than the observed one and its centre of pressure has a greater intensity compared to that simulated by the coupled experiment. The Azores high also resembles the shape and position of the one simulated by a2am, but differs in terms of the maximum strength reached, which is instead the same as that of the observations. The high pressure anomaly in the Pacific is also present in this case, but it is much weaker with a maximum value reached of 0.3 hPa compared to 1.5 hPa in the coupled simulation. The summer case is the only one in which the intensity of the anomalies simulated by the atmosphere reaches values more similar to those of the reanalysis. The shape and position of the Icelandic low are comparable in all three cases, while the structure of the positive anomaly in the case under analysis is comparable to that of ERA5, from which it differs only in the absence of influence over the United States. The autumn low-pressure system, obtained from the a2al experiment, appears larger and more extended towards both the Arctic Ocean and northern Russia, while the minimum intensity reached is the same as that of the observations, even though the centre of pressure is more shifted to the west, being over Greenland and Iceland. On the other hand, the high pressure system is less extended than in the other experiment. The amplitude of the centre of action is comparable with that of the other datasets, while there is a change in the position that in this case is located in Northern Europe, over northern France and Great Britain.

As with the pressure anomalies, the temperature anomalies are also more pronounced in winter compared to the other seasons of the year, and this is true for all three datasets used (Figure 31). Starting from results obtained with the coupled simulation (Figure 31, *b*), and more specifically from winter, the typical quadripolar structure of the temperature anomaly due to the NAO is clearly visible. The most obvious difference from observations lies in the fact that, both the centre of the negative anomaly over the Labrador Sea and the centre of the positive anomaly over the Scandinavian Peninsula, are weaker. In fact, the minimum temperature reached by the simulation is -1.6 °C compared to -2.2 °C for that depicted by the observations, and the same values, but with inverted signs, apply to maximums. Although the positions of the anomalies are similar, the structures and extents show some differences. For example, the simulated high temperature anomaly over northern Europe and northern Russia spreads less towards the Barents and Kara Seas and remains more localised over the land surface, with the most intense anomaly located over the Scandinavian Peninsula rather than over the northern Russia, as occurs for the observed one. The same happens in the case of the low temperature anomaly over North Africa and Middle East, which in ERA5 tends to extend westwards over the Atlantic Ocean and eastwards beyond the Caspian Sea. In spring, the cold anomaly in the vicinity of Canada and Greenland is still less extensive and less intense in the experiment, while the opposite is true for both warm temperature centres: both the one over Northern Europe and Russia and the one over the United States are more widespread and slightly more intense. The summer months are those in which the anomalies reach their minimum

size and strength. The simulated high-temperature systems differ from the observed ones in the direction of elongation: the one above the Scandinavian Peninsula tends to extend towards Eastern Europe instead of Western Europe, and the one above North America tends to extend towards the Atlantic Ocean instead of Canada. In the autumn season, the coupled simulation returns weaker temperature anomaly values at different locations than ERA5. Specifically, the warmest anomaly on the European continent has its centre of greatest intensity over the Scandinavian Peninsula, while in the observations it is located further east, over the northern Russia, towards which it widens. The other positive anomaly also shows differences as it is almost non-existent when looking at the reanalysis result and instead weakly covers the whole of Canada in the case of a2am. The two cold anomalies also have opposite behaviour in the two datasets, as the one simulated over Greenland is less intense and less extensive, while the one over North Africa is of equal intensity but more extensive.

Next is the analysis of the temperature anomalies spatial structures obtained with the atmosphere-only simulation (Figure 31, *c*). Beginning with the winter season, the quadripolar structure is also presented here, with the same position and size as previously achieved, but of lower intensity. The centre of the coldest anomaly over North of Canada is located at the same point as that simulated with the a2am experiment, while that of the warmest anomaly over northern Europe is distributed between the Scandinavian Peninsula and northern Russia, near the Kara Sea, with a maximum intensity of 1 °C. The other two poles in the South are even less extensive and weaker. In spring months, the same applies, so that, except for the positive anomaly in the North-East that widens towards the Arctic Ocean, all the others are smaller in size and less strong. The summer season is when, as in the other cases, they reach their lowest expansion and intensity, while in autumn the anomalous temperature systems begin to strengthen and widen again. It is interesting to note that in this season, the position and extension of the anomalies simulated by the atmosphere-only resemble those observed more closely: note, for instance, the centre of the positive anomaly to the North-East located over the north-eastern Russia as in ERA5 and not over the Scandinavian countries as in the a2am experiment.

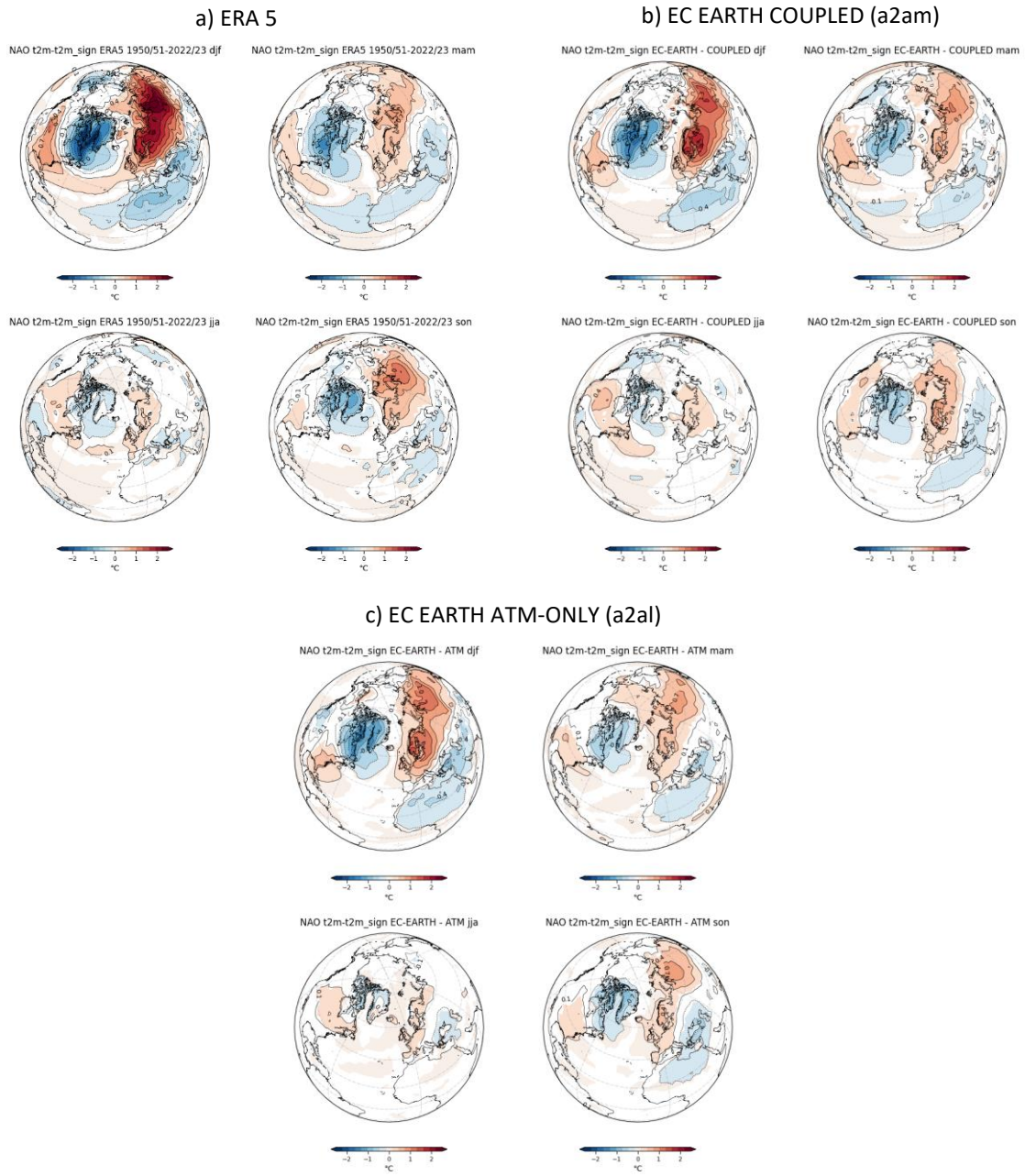

Figure 31 Seasonal t2m anomalies due to NAO in the North Atlantic European sector. The patterns are identified by regressing the t2m anomalies upon the first principal component time series of the leading EOF1 for all seasons. Statistically significant areas at 95% confidence level based on a two-tailed t-test for correlation values between the t2m anomaly and the principal component are shaded. Top left a) is the t2m anomaly from ERA5; top right b) is the t2m anomaly from the EC-Earth coupled simulation; bottom c) is the t2m anomaly from the EC-Earth atmosphere-only simulation.

The Figure 32 shows the comparison of the spatial distributions of precipitation anomalies due to the action of the NAO. In general, the simulated dipoles show a more elongated shape of the dry anomaly than the observed one. This is probably due to the way the model considers the eddy flow for the simulation of precipitation. In fact, the NAO-related precipitation anomalies are due to atmospheric interactions between the mean flow and eddies. The latter derive from the zonal wind in the Atlantic area and are characterised by a structure with a centre and edges, so it could be that the model, when considering the mechanisms required to represent precipitation, considers a larger section of the eddy flow than is necessary in reality.

Analysing the results obtained with the coupled simulation (Figure 32, *b*), it can be seen that in winter, the positive anomaly pole is in the same position and of the same intensity as the one obtained with the reanalysis, while the negative anomaly pole is also in the same position, but has half the intensity of the observed one. A further difference between the two datasets is the fact that the experiment simulates an additional significant negative anomaly in the Pacific Ocean, West of the US coast. Also in the case of the spring season, the major differences lie in the negative pole, which in the a2am experiment has the centre of the anomaly located over the West of the Iberian Peninsula and it tends to extend westwards in the Atlantic Ocean, while in ERA5 it is much smaller and located over the centre of the Ocean. Summer is the period in which the simulated dipole is much weaker than the observed one, while in autumn it recovers vigour even though it assumes a different location and shape from the reference: the positive system is more extended South of Iceland instead of to the North-East, and the negative one extends towards the Middle East and not towards the centre-north of Europe as is the case in ERA5.
Turning to the atmosphere-only simulation (Figure 32, *c*) and comparing it with the coupled one, the result in the winter season is practically the same as regards the positive pole, while the negative anomaly intensity and extension decreases even if it maintains the elongated shape mentioned above. Also without the intervention of the ocean, the model simulates the additional positive anomaly in the Pacific. In spring months, the dipole is the same as that obtained with the other simulation, with only the intensity of the negative centre decreasing. On the other hand, in summer and autumn, the a2al experiment seems to come closer to the results of the observations with regard to the negative precipitation anomaly intensity and position, respectively: indeed, in summer it reaches a minimum value of 0.2 mm/d and in autumn it is located over central and northern Europe.

From the analysis and results obtained, two conclusions are reached. The first is that in order to be able to explain a fraction of total variance due to the winter NAO mode more similar to the observations one, the coupled model is needed, namely the presence and influence of the ocean. This evidence is closely related to that already reached in section 5.1 regarding the need to consider the variation in sea ice extent (and hence ocean action) in order to best represent climate variability in the NAE region. Secondly, as previously shown by other studies (e.g. Czaja et al. 2003; Hurrell et al. 2003), and as can be seen if one calculates the autocorrelation of the time series of the NAO index, the air-sea coupling has no relevant effects on its dynamics in terms of variability time scales shorter than ten years and in terms of structure and position: therefore it can be confirmed that the mechanisms involved in the NAO are predominantly dominated by internal atmospheric processes.

Figure 32 Seasonal TP anomalies due to NAO in the North Atlantic European sector. The patterns are identified by regressing the TP anomalies upon the first principal component time series of the leading EOF1 for all seasons. Statistically significant areas at 95% confidence level based on a two-tailed t-test for correlation values between the TP anomaly and the principal component are shaded. Top left a) is the TP anomaly from ERA5; top right b) is the TP anomaly from the EC-Earth coupled simulation; bottom c) is the TP anomaly from the EC-Earth atmosphere-only simulation.

5.3 The impact of radiative forcing on NAO

Scientists are observing changes in the Earth's climate in every region and across the whole climate system, according to the latest Intergovernmental Panel on Climate Change (IPCC) Report (AR6 Working Group I, 2021). Climate change refers to long-term shifts in temperatures and weather patterns. Such shifts can be natural, due to changes in the sun's activity, or anthropogenic, primarily due to the burning of fossil fuels like coal, oil and gas (United Nations, n.d.). Scientists have showed that humans are responsible for most all the variations in climate over the last 200 years. Indeed many of these changes are unprecedented in thousands of years, and some of the changes already set in motion, such as continued sea level rise, are irreversible over a long period of time (AR6 Working Group I, 2021). A major effect of climate change is global warming, defined as the phenomenon of increasing average air temperatures near the surface of Earth over the past one to two centuries (Michael E. Mann, 2024). Human activities are causing an increase in greenhouse gases in the atmosphere, which in turns leads to a warming of the surface and lower part of the atmosphere relative to what would be expected in the absence or reduction of greenhouse gases (Michael E. Mann, 2024). When talking about a change in atmospheric temperature, this can be thought in terms of "radiative forcing." Indeed the radiative forcing is a measure of the influence a given climatic factor has on the amount of downward-directed radiant energy colliding with Earth's surface. The influence can be a "positive forcing", if it is exerted by climatic factors that contribute to the warming of Earth's surface, and a "negative forcing", if factors considered cause a cooling of the Earth's surface. In some cases, radiative forcing has a natural origin, such as during volcanoes eruptions where vented gases and ash block some portion of solar radiation from the surface. In other cases, radiative forcing has an anthropogenic origin due to the increase in carbon dioxide, methane, nitrous oxide and halogenated gases concentration (Michael E. Mann, 2024). It is now common knowledge that human activity has a great influence on the change in Earth's radiative balance. Indeed the total net increase in surface radiation due to anthropogenic activities, since the beginning of the Industrial Revolution, is 1.6 watts per square metre (Michael E. Mann, 2024). This global warming, and in general this climate change, caused to a large extent by humans, has major and sometimes irreversible effects on the climate, which in turn cause impacts on the environment and society. In addition to considering the most obvious and catastrophic consequences (such as droughts, fires, melting ice, etc.) (United Nations, n.d.) since the climate system is a complex gear in which every element is connected, it is also important to analyse the impacts that climate change, and more specifically, the variation of the radiative forcing, has on climate variability and on the NAO.

Actually, the NAO is a focus for researchers as it has a great influence on climate change and variability in the mid-latitudes (Huang et al., 2018). In turn, climate change itself can have an effect on this teleconnection pattern and therefore, in order to improve future climate predictions, it is necessary to understand the effect of climate change, intended as an increase in radiative forcing, on the NAO. Nathan P. Gillet et al. (2003) review that in recent decades the boreal winter NAO index has increased substantially and this changes has been associated with over half the Eurasian winter surface temperature increase and much of the observed trend in precipitation over Western Europe. There is considerable disagreement about the relative roles of all forcings (natural and

anthropogenic), but most authors agree that GHGs are likely to be at least partly responsible for the long-term trend in the winter NAO index. Indeed, even if natural forcings may have also had an impact on the atmospheric circulation, some authors have argued that greenhouse gas-induced changes in the meridional temperature gradient in the lower stratosphere, may be responsible for the upward NAO index trend. In addition, it has been proven in some studies, that changes in the NAO are also manifested in a shift in the position of the action centres, but overall the mechanisms of response to greenhouse gases remains open to debate (Gillett et al., 2003). Yu Huang et al. (2018) investigated changes of the winter NAO variability in response to different climate forcings and their possible causes through a set of atmosphere-only timeslice experiments, forced by SST from coupled runs. They found that the effects of uniform SST warming and CO_2 direct radiative forcing could lead to intensification of winter NAO variability, although they do not consider the ocean-atmosphere coupling. Instead C. M. McKenna et al.(2022) showed, using a large number of coupled simulation from different climate models, that the increase in the winter NAO plays a role in the decrease in winter precipitation in the South of Europe. This is an important result because it suggests that uncertainty in southern Europe precipitation changes could be partly reduced with improved understanding of future NAO changes. Ramón Fuentes-Franco et al. (2023) also analysed the correlation between NAO and precipitation in the case of a high emissions scenario. Using coupled models, unlike Yu Huang et al. (2018), they observed a weakening of NAO variability in the second half of the 21st century accompanied by an increase in the correlation between extreme precipitation events and the NAO index.

Therefore it is clear that the impact of the radiative forcing on the NAO is an issue under analysis and there are still no definite results. However, given the influences that the NAO has on climate, and in particular on precipitation, in the European region, it is necessary to gain a deeper understanding of the correlation between the two, when temperatures rise due to a change in radiative forcing. In this way, the ability to predict precipitation trends and consequently the environmental, social and economic impacts they have, can be enhanced. In the following, it was decided to investigate the effect of the radiative forcing on the climate and its variability in the North Atlantic-European region, also taking into account the effect of air-sea coupling. To do this, they were compared the control simulations at present conditions (i.e. radiative forcing set to the year 2002), already seen in the previous section, with two other simulations at future conditions (i.e. radiative forcing set to the year 2050). The initial conditions of future simulations are derived from a long transient run performed forced with SSP2-4.5 scenario, as has already been explained in the data and methodology section.

Before analysing the specific effect of the NAO on future climate, it is interesting to assess the changes that the increased radiative forcing may cause in the mean and variability of climate in the North Atlantic European region, whether the effect of the ocean, or only that of the atmosphere, is taken into account.

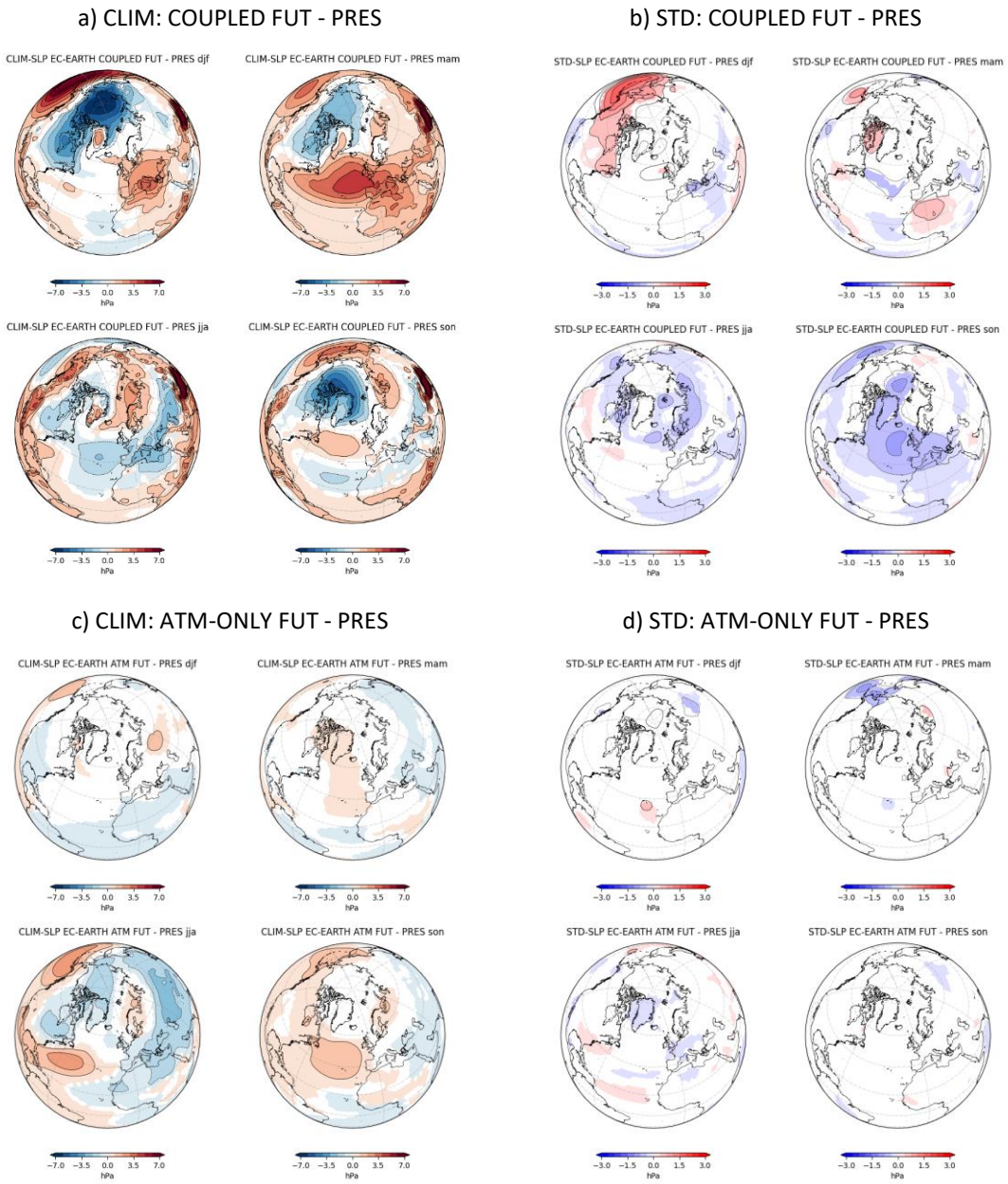

Figure 33 Difference between the SLP climatologies of the present and future simulations. The present simulations have radiative forcing fixed at the year 2002; the future ones have the radiative forcing fixed at the year 2050. The contour lines show the entire field while the solid areas represent the significant differences according to a t-test at 95 % confidence level. Zero values are also shown. Top left a) is the difference between the future and present climatology of the coupled simulations; top right b) is the difference between the future and present standard deviation of the coupled simulations; bottom left c) is the difference between the future and present climatology of the atmosphere-only simulation; bottom right d) is the difference between the future and present standard deviation of the atmosphere-only simulation.

Figure 33 shows the differences between future and present in the climatology and standard deviation of the SLP in both coupled and atmospheric-only simulations. Looking at the difference in the coupled means (Figure 33, *a*), in winter, spring and autumn, negative pressure systems appear less intense in the future than in the past and, conversely, positive pressure systems increase their intensity. Furthermore, in spring the anticyclone located west of Europe in the Atlantic Ocean becomes wider, while in autumn it is the cyclone located in the Arctic Circle that expands. In winter and spring, there is also a very famous pattern: the intensification of the anticyclonic system over the Mediterranean, which, together with changes in regional circulation, was observed to lead to variations in European precipitation (Tuel & Eltahir, 2020). The changes observed in climatology,

should be consistent with those emerging in variability. Indeed for instance, if one looks at Figure 33 (*b*) can be seen that, in winter, the increase in magnitude of the anticyclone in the Pacific is accompanied by an increase in variability, while, in autumn, the decrease in intensity of the cyclone in the Arctic Circle goes together with a decrease in variability. In the case of the atmosphere-only simulation, on contrast, variations in the mean and especially in future variability compared to the present are minimal, and the only season with more changes is summer.

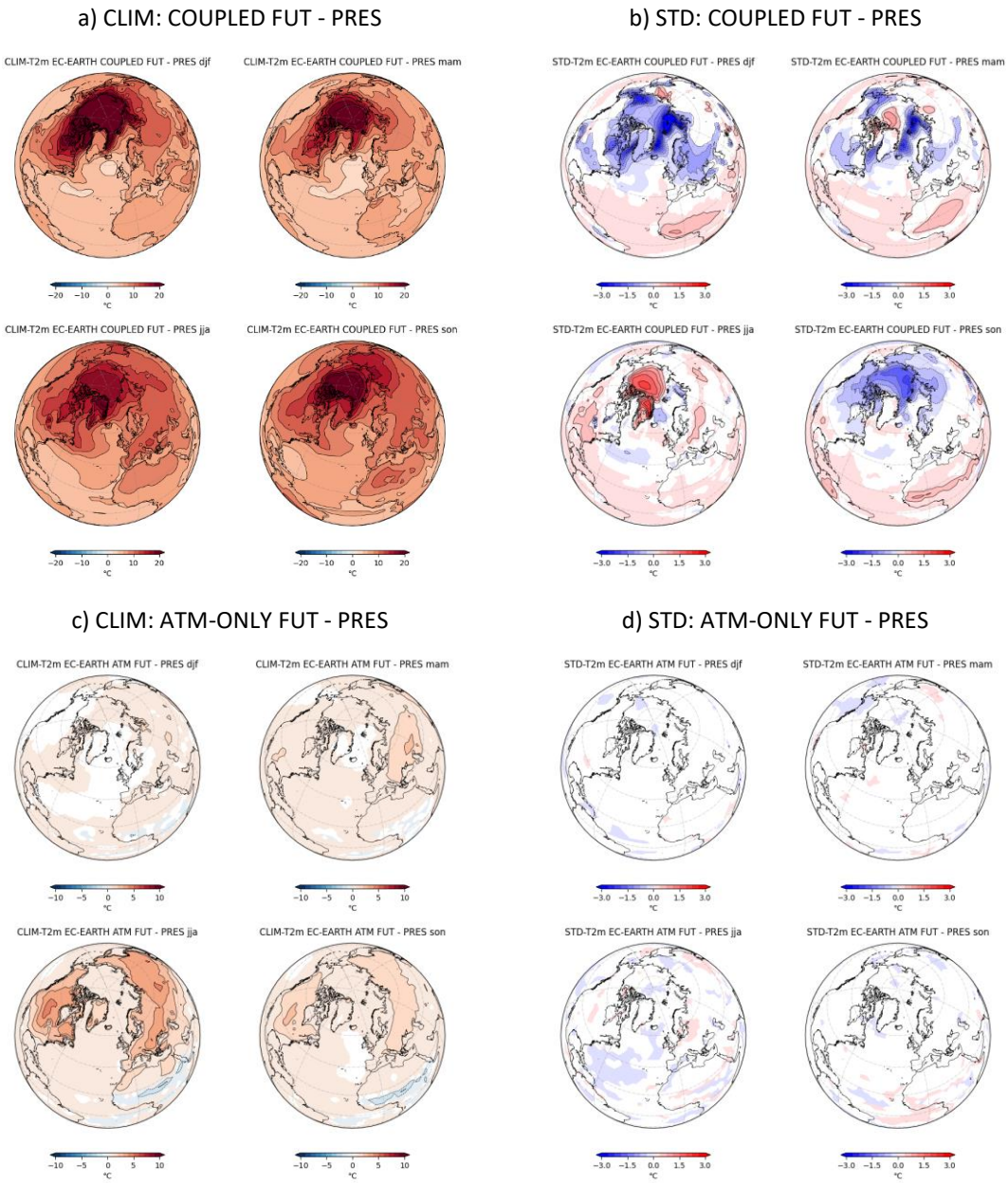

Figure 34 Difference between the t2m climatologies of the present and future simulations. The present simulations have radiative forcing fixed at the year 2002; the future ones have the radiative forcing fixed at the year 2050. The contour lines show the entire field while the solid areas represent the significant differences according to a t-test at 95 % confidence level. Zero values are also shown. Top left a) is the difference between the future and present climatology of the coupled simulations; top right b) is the difference between the future and present standard deviation of the coupled simulations; bottom left c) is the difference between the future and present climatology of the atmosphere-only simulation; bottom right d) is the difference between the future and present standard deviation of the atmosphere-only simulation.

Differences in climatology and standard deviation of temperature at two meters above the surface are analysed in Figure 34. When the effect of the ocean is taken into account, warming is evident in all seasons, particularly in the Arctic Circle area, where there is an increase of more than 25 °C in winter. The atmosphere becomes super warm and, consequently, it seems much more stable. Observing the winter variability of the temperature field, in fact, it is possible to notice a strong decrease in the Arctic Circle region and Northern Europe. In particular, the centres where a greater decrease is noticeable are above the Greenland Sea and above the Barents and Lara Seas. If one looks at the map of the standard deviation of the temperature in the future coupled simulation (Appendix B), compared to the present one, it is clear that in winter, over the Arctic Ocean, the standard deviation values are almost zero. In contrast, in summer, the conditions become the opposite and, always considering the North Pole region where in the present there is practically no variability, in the future it increases by about 2 °C. The decrease in standard deviation in winter could be an indication that, if there is sea ice, it is less variable than in the present and probably also less thick. On the other hand, the increase in variability in summer could be related to the total melting of the sea ice, which would allow a release of heat as a result of the descent of solar radiation. However, in order to be able to draw firm conclusions, the variable SIC must be observed in future analyses. In future autumn, as in winter, variability decreases, while in spring it decreases except in a small region north of Greenland. Considering other areas instead, in North Africa the standard deviation assumes positive values in all seasons; in Northern Europe, on the other hand, the anomalies are negative in all seasons except summer, with an extension to a large part of European countries in winter months; Eurasia, on the other hand, shows no variations, indicating that this area appears to be somehow independent of what happens in the Arctic due to the change in the radiative forcing. In the case of the atmosphere-only simulation, the same argument holds true for sea-level pressure; in fact, variations in mean and climatic variability are minimal and only appear in the summer climatology over Eurasian and North American lands.

Figure 35 shows the differences between future and present in total precipitation. As in the previous section, the maximum and minimum of the standard deviation range have been reduced, in terms of absolute value, in order to display the variations in the North Atlantic European zone. Starting with the coupled simulation climatology, rainfall appears to increase in the ITCZ and the North Atlantic region throughout the year. This evidence goes along with the fact that the future climate has a warmer atmosphere, which will therefore be able to hold a higher percentage of humidity (i.e. water vapour), which once condensed will turn into more rain. Indeed the Clausius−Clapeyron equation implies that air can hold 7% more moisture per degree of warming and daily rainfall extremes roughly scale with this factor (Robinson et al., 2021). However, dynamical changes can also influence the frequency and intensity of precipitation and thus disrupt the Clausius-Clapeyron expected change. For example, changes in extratropical storm tracks will affect rainfall in mid-latitude regions (Lehmann et al., 2015), as seems to be the case in the North American region, where, particularly in summer, there is a decrease in precipitation. Lands in the Mediterranean region also show a decrease in rainfall, especially in summer. Behind this drying appears to be the intensification of the anomalous ridge, already commented on in the analysis of changes in the SLP variable. In particular, changes in the large-scale flow of the upper troposphere, together with the reduction of the regional land-sea temperature gradient, have been identified as the two main

causes of this Mediterranean precipitation pattern (Tuel & Eltahir, 2020). In agreement with variations in the mean, precipitation variability will became more in all season in the Arctic Polar region and in Northern Europe, but it became less in Southern Europe and in North Africa. In the case of the atmosphere-only simulation, the differences between present and future are again much smaller compared to the coupled one. The most noticeable ones always occur in summer, in particular in the tropical zone, where the Clausius-Clapeyron relationship also applies in this case, as the atmosphere in this area is generally warmer than in the rest of the world and, thus, can contain more moisture and more rain.

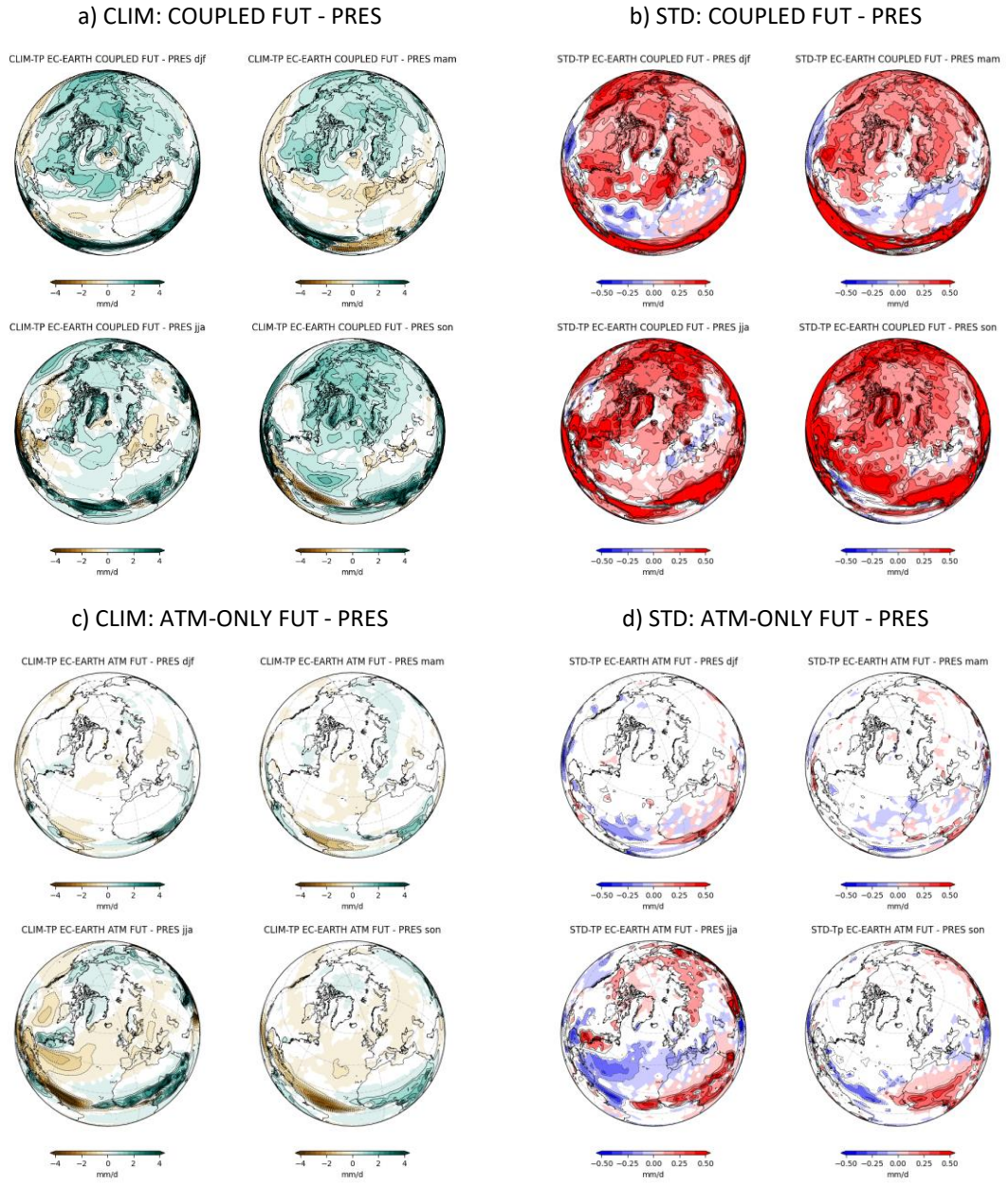

Figure 35 Difference between the TP climatologies of the present and future simulations. The present simulations have radiative forcing fixed at the year 2002; the future ones have the radiative forcing fixed at the year 2050. The contour lines show the entire field while the solid areas represent the significant differences according to a t-test at 95 % confidence level. Zero values are also shown. Top left a) is the difference between the future and present climatology of the coupled simulations; top right b) is the difference between the future and present standard deviation of the coupled simulations; bottom left c) is the difference between the future and present climatology of the atmosphere-only simulation; bottom right d) is the difference between the future and present standard deviation of the atmosphere-only simulation.

Focusing now on the NAO, Figure 36 shows the comparison of the spatial structure of the NAO-related SLP anomaly in the future and in the present, in the case of both coupled and atmospheric-only simulations. Starting with the comparison of simulations that take the air-sea coupling into account (Figure 36, *a-b*), it can be seen that the fraction of variance explained in the future winter and autumn is a few percentage points lower than in the corresponding present seasons. Furthermore, the north lobe appears weaker and, in winter, the centre of action of the south lobe is moved westwards, while in autumn it decreases in intensity. Comparing the spring and summer seasons, on the other hand, it can be seen that, in spring in particular, there is a large increase in the percentage of variance explained with respect to the present conditions. Also in this case there is a westward shift of the centre of action of the Azores high system, accompanied in spring also by a slight increase in the intensity of the centre of pressure of the Icelandic low system and of the Pacific high one. Turning now to the comparison of the atmosphere-only simulations (Figure 36, *c-d*), in which only the composition of the atmosphere varies and not the SST, it is observed that in future DJF the low pressure system centre of action stretches towards North-East, while the high system one is shifted towards West. In addition, both lobes of the dipole have the centre of greatest intensity extended, while that of the high pressure system in the Pacific appears reduced and less intense. In future spring the pattern is very similar to the present one and only a reduction in the magnitude of the positive system is noticeable, whereas in summer the low system is weaker and the high one is wider and stretched towards North-East. Finally in SON the Icelandic-low is more focused on the Arctic Circle and the Azores-high is less intense. As for the fraction of variance explained, this is always lower except in winter where it shows a small increase. In particular, it is interesting to note that, in the winter months, the two future simulations are able to attribute a very similar fraction of variance to the NAO-related SLP anomaly and this means that the main agents in the strengthening of the winter anticyclonic circulation are processes within the atmosphere. The only differences between the two future DJF simulations lie in the fact that, in the atmosphere-only simulation, the centre of action of the low-pressure system is stretched towards the Barents and Kara Seas, while that of the high-pressure system is smaller and shifted eastwards. As far as the other seasons are concerned, in spring both lobes of the dipole are less intense, the fraction of variance explained is much lower and the high pressure centre in the Pacific seems to be unaffected by the NAO, contrary to the coupled simulation. In summer and autumn, what changes is the position and extent of the high pressure centre, so that in both cases it shifts to the northeast. Therefore, the main differences between the two future simulations lie in the percentage of variance explained and the intensity of the anomalies. In winter, the spatial structure of the SLP linked to the NAO can be represented by an atmosphere-only model, as the ocean seems to have no influence, whereas the same is not valid for the other future seasons, particularly spring.

The comparison of present and future spatial structures of NAO-related temperature anomalies is shown in the Figure 37. Concerning the coupled experiments (Figure 37, *a-b*), the quadripolar pattern appears less intense in all seasons and it's particularly evident in winter over high latitude, consistent with the weakening of Icelandic-low system as it has been seen that NAO-related temperature variations are governed by advection. The only exceptions are in spring, where the two poles in the east are more intense and in summer, where there are major cold anomalies above the Arctic Circle.

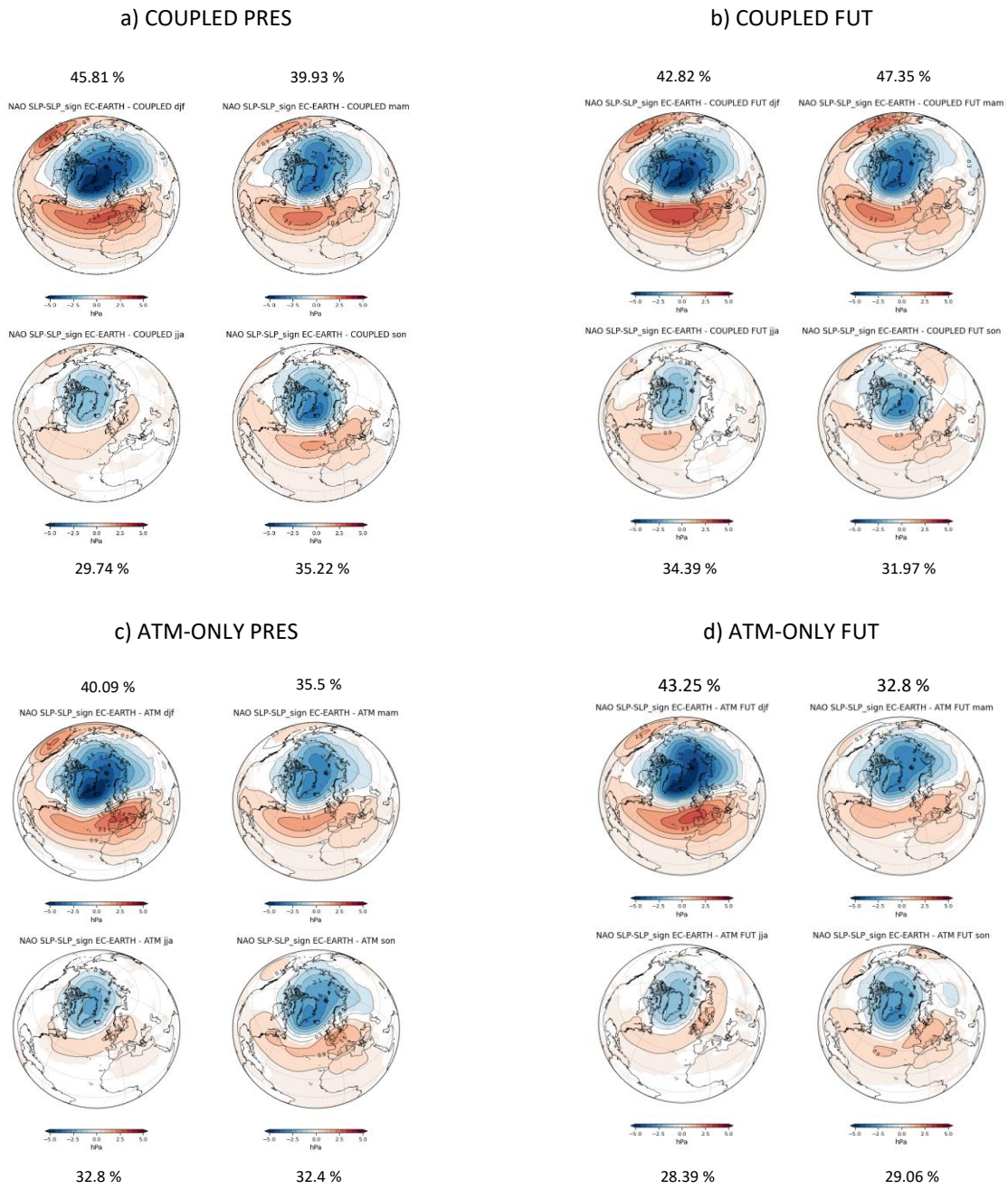

Figure 36 Seasonal present and future SLP anomalies due to NAO in the North Atlantic European sector. The patterns are identified by regressing the SLP anomalies upon the first principal component time series of the leading EOF1 for all seasons. Statistically significant areas at 95% confidence level based on a two-tailed t-test for correlation values between the SLP anomaly and the principal component are shaded. Top left a) is the SLP anomaly from the EC-EARTH present coupled simulation; top right b) is the SLP anomaly from the EC-EARTH future coupled simulation; bottom left c) is the SLP anomaly from the EC- EARTH present atmosphere-only simulation; bottom right d) is the SLP anomaly from the EC- EARTH future atmosphere-only simulation.

Analysing atmosphere-only experiments (Figure 37, *c-d*), in future DJF the quadripolar structure is slightly more intense in particular when considering the two anomalies over high latitudes. During MAM the warm anomaly over North Europe and Russia is more intense, while the others are similar. In summer there are only small differences on position and extension and in autumn the two temperature anomalies at high latitudes are weaker. In spring and summer, all the poles of the quadripolar structure show a lower intensity than in the coupled experiment, while in autumn the

warm anomaly at high latitudes is larger and extended towards Russia and the cold one over North Africa is reduced and concentrated over the Mediterranean Sea. It is thus possible to conclude that in order to best represent temperature anomalies, the ocean is necessary. Indeed, in a future where air-sea coupling is taken into account, the atmosphere is warmer than in the case where the sea is not taken into account, and this leads to a reduction in variability, as has already been observed in the mean and standard deviation of the temperature field.

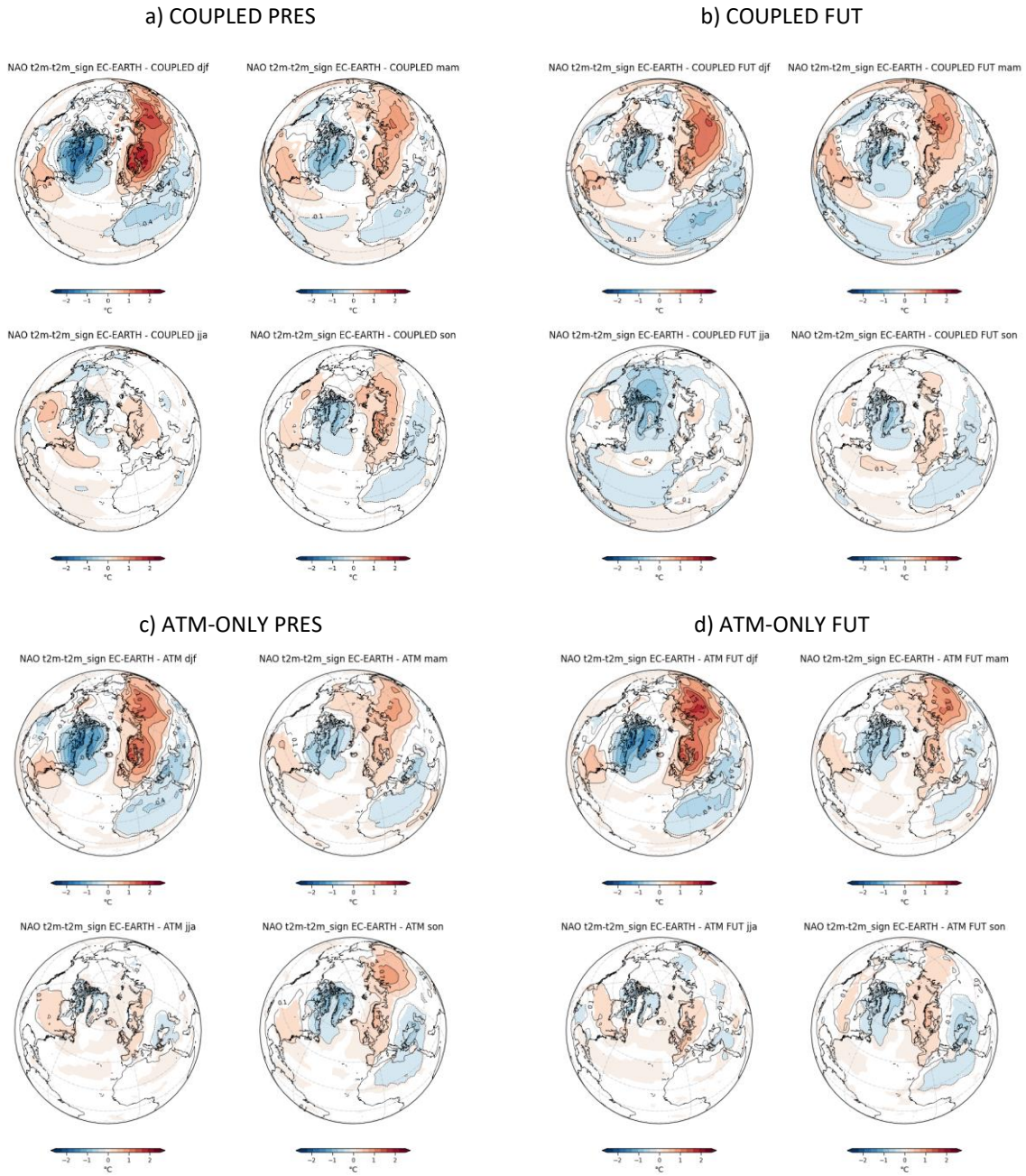

Figure 37 Seasonal present and future t2m anomalies due to NAO in the North Atlantic European sector. The patterns are identified by regressing the t2m anomalies upon the first principal component time series of the leading EOF1 for all seasons. Statistically significant areas at 95% confidence level based on a two-tailed t-test for correlation values between the t2m anomaly and the principal component are shaded. Top left a) is the t2m anomaly from the EC-EARTH present coupled simulation; top right b) is the t2m anomaly from the EC-EARTH future coupled simulation; bottom left c) is the t2m anomaly from the EC- EARTH present atmosphere-only simulation; bottom right d) is the t2m anomaly from the EC- EARTH future atmosphere-only simulation.

In the case of the total precipitation anomalies related to the NAO (Figure 38), in winter and spring, the coupled dipole, appears more intense and wider, in particular the dry pole. In fact, the negative anomaly shows a two contours difference to respect the present day simulation, proving that, in future, the influence of NAO on rainfall will became stronger. Furthermore, this influence, also seems to extend toward the ITCZ especially during winter and spring months. The intensity of the dipole over Europe also seems to increase in summer, while in autumn the magnitude is the same as the present conditions, but the extent of the anomalies is greater. If, on the other hand, the two atmosphere-only simulations are observed (Figure 38, *c-d*), no major differences in the intensity and extent of the anomalies are shown. Indeed, looking at the comparison between the two future experiments, in winter the intensity of the dipole in the coupled simulation is greater. The centre of action of the coupled dry anomaly is shifted westward and located in the middle of the ocean, while the humid one is shifted eastward. Spring is the season when the simultaneous action of the atmosphere and ocean linked to the NAO mode has a major influence on precipitation in the North Atlantic European region. Indeed the anomaly intensity and extension are really greater when the ocean plays a role and also the ITCZ seems to be much influenced by the NAO, compared with the other experiments. During summer the coupled dry anomaly is shifted westward and a dry anomaly also over the Terranova and Labrador region appears. In autumn both the dry and wet anomalies are more intense and larger in the coupled simulation and the wet pole is shifted towards North and East. Again, as with temperature, it can be concluded that ocean action is required to fully capture changes in climatology and variability, including NAO-related one, of precipitation.

A number of conclusions can be drawn from the analysis and results obtained. Comparing the future spatial structure of the SLP anomalies, represented by the coupled model, with that represented by the atmosphere-only model, it is concluded that in order to represent the NAO itself, the pattern and the fraction of variance explained, the role of the ocean is not necessary. Consistent with this result, the future winter NAO explains the same fraction of variance in both simulations. Particularly in a world where the radiative forcing and consequently the temperature increases, the pattern of the NAO is largely driven by processes within the atmosphere alone. On the other hand, it was shown how, in order to capture all the warming and all the variations in precipitation in the entire climate system of the North Atlantic region, it is necessary to consider the action of the ocean. In fact, it was explained that due to the Clausius-Clapeyron relation, a warmer atmosphere is associated with more water vapour. But this moisture must have a precise origin and this is represented by the ocean. In fact, thanks to the action of the latter, it is possible to represent the increase in average precipitation and in the consequent anomalies and, vice versa, the decrease in variability in the case of temperatures that tend to increase and stabilise. These generally valid changes have a regional effect on the behaviour of the spatial structures of the NAO-related anomalies. Moreover, unlike in winter, in spring the NAO pattern itself and the fraction of variance explained increase greatly when the effect of the ocean is taken into account. Hence, if one wants to better study the NAO in other seasons than winter and in a future world affected by global warming, it is convenient to use a coupled model. Results show that the ocean role, in relation to the change in radiative forcing, in accounting for the totality of changes in climate variables patterns

(both global and related to the NAO), is useful for improving future predictions of climate in the region under analysis and of its subsequent impacts.

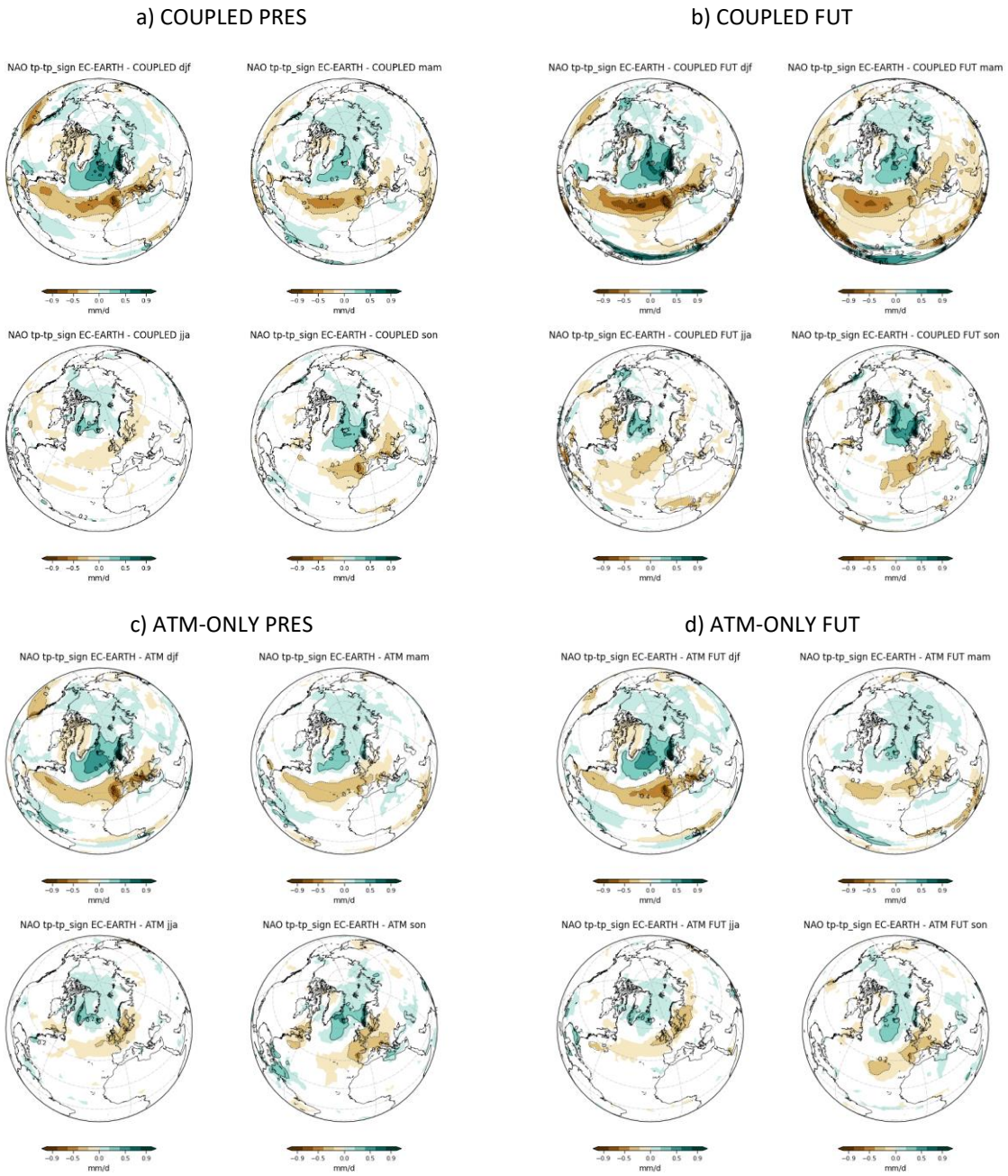

Figure 38 Seasonal present and future TP anomalies due to NAO in the North Atlantic European sector. The patterns are identified by regressing the TP anomalies upon the first principal component time series of the leading EOF1 for all seasons. Statistically significant areas at 95% confidence level based on a two-tailed t-test for correlation values between the TP anomaly and the principal component are shaded. Top left a) is the TP anomaly from the EC-EARTH present coupled simulation; top right b) is the TP anomaly from the EC-EARTH future coupled simulation; bottom left c) is the TP anomaly from the EC- EARTH present atmosphere-only simulation; bottom right d) is the TP anomaly from the EC- EARTH future atmosphere-only simulation.

6. Conclusions

In this analysis, both observed and simulated variability related to the NAO were analysed. To do this, the ERA5 (1950-2023) reanalysis and a series of simulations calculated with the standard configuration of the global climate model EC-EARTH3 for CMIP6 were used, respectively. Using the latter, the impact of two external factors on the NAO was also assessed, namely the impact of air-sea coupling and that of radiative forcing change. First, by comparing the averages and standard deviations of some climate variables obtained from the simulations with those obtained from previous studies, which also used EC-EARTH, the model biases were assessed. Although the initial conditions used in the two cases under comparison were different, the performance of the model was qualitatively similar in terms of position and extent of biases. Furthermore, the error analysis, and in particular the comparison between a simulation with fixed and one with variable SIC, also showed that, in order to obtain a faithful representation of temperature variability in the North Atlantic European region, the annual variation of SIC must also be taken into account and, consequently, the effect of the ocean should be considered.

This result was also confirmed by the comparison between the coupled simulations (in which the ocean effect is accounted for) and the atmosphere-only simulations, performed with the aim of assessing the impact of air-sea coupling. Indeed, the analysis showed that to obtain all the variability associated with the winter NAO, the coupled experiment is necessary. On the other hand, it turned out that the air-sea coupling does not have a strong influence on the dynamics of the NAO in terms of structure and position and, therefore, it is possible to confirm the result known from the literature, that the mechanisms involved in the NAO are dominated mainly by processes within the atmosphere. To assess the effect of the radiative forcing change, in conjunction with the effect of air-sea coupling, simulations under present conditions (year 2002) and those under future conditions (year 2050) were compared. Again, the ocean does not appear to play a major role in governing the winter NAO dynamics, as the structure of the future pattern and its impact on precipitation and temperature are similar in the coupled and air-atmosphere-only experiments. However, in order to capture all the variations in climatology and variability related to changing radiative forcing and to explain the magnitude of the NAO-related anomalies, it is necessary to consider the action of the ocean, as was already evident from the analysis of the present conditions. Indeed, it is only through the effect of the air-sea coupling that it is possible to represent the future increase in amplitude of the NAO-related anomalous precipitation dipole and, conversely, the future decrease in amplitude of the NAO-related anomalous temperature quadripole. The result obtained on the importance of the ocean role, in accounting for the totality of changes in climate variables patterns (both global and related to the NAO), is useful for improving future predictions of climate in the region under analysis and of its subsequent impacts.

7. References

AR6 Working Group I. (2021, August 9). *Climate change widespread, rapid, and intensifying – IPCC*. https://www.ipcc.ch/2021/08/09/ar6-wg1-20210809-pr/

Aumont, O., Ethé, C., Tagliabue, A., Bopp, L., & Gehlen, M. (2015). PISCES-v2: an ocean biogeochemical model for carbon and ecosystem studies. *Geoscientific Model Development*, *8*(8), 2465–2513. https://doi.org/10.5194/gmd-8-2465-2015

Baldwin, M. P., Stephenson, D. B., & Jolliffe, I. T. (2009). Spatial Weighting and Iterative Projection Methods for EOFs. *Journal of Climate*, *22*(2), 234–243. https://doi.org/10.1175/2008JCLI2147.1

Balsamo, G., Viterbo, P., Beljaars, A., van den Hurk, B. J. J., Hirschi, M., Betts, A., & Scipal, K. (2008). A revised hydrology for the ECMWF model: Verification from field site to terrestrial water storage and impact in the Integrated Forecast System. In *ECMWF Technical Memoranda* (Issue 563, p. 28). ECMWF. https://doi.org/10.21957/yzyeh0vlw

Barsugli, J. J., & Battisti, D. S. (1998). The Basic Effects of Atmosphere–Ocean Thermal Coupling on Midlatitude Variability*. *Journal of the Atmospheric Sciences*, *55*(4), 477–493. https://doi.org/10.1175/1520-0469(1998)055<0477:TBEOAO>2.0.CO;2

Bell, G. D., & Chelliah, M. (2006). Leading Tropical Modes Associated with Interannual and Multidecadal Fluctuations in North Atlantic Hurricane Activity. *Journal of Climate*, *19*(4), 590–612. https://doi.org/10.1175/JCLI3659.1

Benedict, J. J., Lee, S., & Feldstein, S. B. (2004). Synoptic View of the North Atlantic Oscillation. *Journal of the Atmospheric Sciences*, *61*(2), 121–144. https://doi.org/10.1175/1520-0469(2004)061<0121:SVOTNA>2.0.CO;2

Bjerknes, J. (1964). *Atlantic Air-Sea Interaction* (pp. 1–82). https://doi.org/10.1016/S0065-2687(08)60005-9

Boussetta, S., Balsamo, G., Beljaars, A., Kral, T., & Jarlan, L. (2013). Impact of a satellite-derived leaf area index monthly climatology in a global numerical weather prediction model. *International Journal of Remote Sensing*, *34*, 3520–3542.

Budikova, D. (2012). Northern Hemisphere Climate Variability: Character, Forcing Mechanisms, and Significance of the North Atlantic/Arctic Oscillation. *Geography Compass*, *6*(7), 401–422. https://doi.org/10.1111/j.1749-8198.2012.00498.x

Bueh, C., & Nakamura, H. (2007). Scandinavian pattern and its climatic impact. *Quarterly Journal of the Royal Meteorological Society*, *133*(629), 2117–2131. https://doi.org/10.1002/qj.173

Bueler, E., & Brown, J. (2009). Shallow shelf approximation as a “sliding law” in a thermomechanically coupled ice sheet model. *Journal of Geophysical Research: Earth Surface*, *114*(F3). https://doi.org/10.1029/2008JF001179

Climate Prediction Center Internet Team. (2008, May 8). *NOAA / National Weather Service/ Center for Weather and Climate Prediction*. https://www.cpc.ncep.noaa.gov/data/teledoc/teleintro.shtml

Copernicus Climate Change Service. (n.d.). https://climate.copernicus.eu/

Craig, A., Valcke, S., & Coquart, L. (2017). Development and performance of a new version of the OASIS coupler, OASIS3-MCT_3.0. *Geoscientific Model Development*, *10*(9), 3297–3308. https://doi.org/10.5194/gmd-10-3297-2017

Craig, P. M., & Allan, R. P. (2022). The role of teleconnection patterns in the variability and trends of growing season indices across Europe. *International Journal of Climatology*, *42*(2), 1072–1091. https://doi.org/10.1002/joc.7290

Czaja, A., Robertson, A. W., & Huck, T. (2003). *The role of Atlantic Ocean-atmosphere coupling in affecting North Atlantic oscillation variability* (pp. 147–172). https://doi.org/10.1029/134GM07

Delaygue Gilles. (2019). Climate variability: the example of the North Atlantic Oscillatio. *Encyclopedia of the Environment*. https://www.encyclopedie-environnement.org/en/climate/climate-variability-example-north-atlantic-oscillation/

Dommenget, D., & Latif, M. (2002). A Cautionary Note on the Interpretation of EOFs. *Journal of Climate*, *15*(2), 216–225. https://doi.org/10.1175/1520-0442(2002)015<0216:ACNOTI>2.0.CO;2

Döscher, R., Acosta, M., Alessandri, A., Anthoni, P., Arsouze, T., Bergman, T., Bernardello, R., Boussetta, S., Caron, L.-P., Carver, G., Castrillo, M., Catalano, F., Cvijanovic, I., Davini, P., Dekker, E., Doblas-Reyes, F. J., Docquier, D., Echevarria, P., Fladrich, U., … Zhang, Q. (2022). The EC-Earth3 Earth system model for the Coupled Model Intercomparison Project 6. *Geoscientific Model Development*, *15*(7), 2973–3020. https://doi.org/10.5194/gmd-15-2973-2022

Dutra, E., Balsamo, G., Viterbo, P., Miranda, P. M. A., Beljaars, A., Schär, C., & Elder, K. (2010). An Improved Snow Scheme for the ECMWF Land Surface Model: Description and Offline Validation. *Journal of Hydrometeorology*, *11*(4), 899–916. https://doi.org/https://doi.org/10.1175/2010JHM1249.1

European Centre for Medium-Range Weather Forecasts. (n.d.). https://www.ecmwf.int/en

Feldstein, S. B. (2000). The Timescale, Power Spectra, and Climate Noise Properties of Teleconnection Patterns. *Journal of Climate*, *13*(24), 4430–4440. https://doi.org/10.1175/1520-0442(2000)013<4430:TTPSAC>2.0.CO;2

Feldstein, S. B., & Franzke, C. L. E. (2016). Atmospheric Teleconnection Patterns. In *Nonlinear and Stochastic Climate Dynamics* (pp. 54–104). Cambridge University Press. https://doi.org/10.1017/9781316339251.004

Folland, C., Karl, T. R., Christy, J. R., Clarke, R. A., Gruza, G. V, Jouzel, J., Mann, M., Oerlemans, J., Salinger, M., & Wang, S.-W. (2001). *: Observed Climate Variability and Change.* (pp. 99–181).

Fuentes-Franco, R., Docquier, D., Koenigk, T., Zimmermann, K., & Giorgi, F. (2023). Winter heavy precipitation events over Northern Europe modulated by a weaker NAO variability by the end of the 21st century. *Npj Climate and Atmospheric Science*, *6*(1), 72. https://doi.org/10.1038/s41612-023-00396-1

García-Serrano, J., Frankignoul, C., Gastineau, G., & de la Cámara, A. (2015). On the Predictability of the Winter Euro-Atlantic Climate: Lagged Influence of Autumn Arctic Sea Ice. *Journal of Climate*, *28*(13), 5195–5216. https://doi.org/10.1175/JCLI-D-14-00472.1

García-Serrano, J., & Haarsma, R. J. (2017). Non-annular, hemispheric signature of the winter North Atlantic Oscillation. *Climate Dynamics*, *48*(11–12), 3659–3670. https://doi.org/10.1007/s00382-016-3292-3

Gillett, N., Graf, H.-F., & Osborn, T. (2003). Climate Change and the North Atlantic oscillation. *The North Atlantic Oscillation: Climatic Significance and Environmental Impact, 193-209 (2002)*, *134,*. https://doi.org/10.1029/134GM09

Global Physical Climatology. (2016). Elsevier. https://doi.org/10.1016/C2009-0-00030-0

Grotjahn, R. (2015). *GENERAL CIRCULATION OF THE ATMOSPHERE | Mean Characteristics*. https://api.semanticscholar.org/CorpusID:126982391

Haarsma, R., Acosta, M., Bakhshi, R., Bretonnière, P.-A., Caron, L.-P., Castrillo, M., Corti, S., Davini, P., Exarchou, E., Fabiano, F., Fladrich, U., Fuentes Franco, R., García-Serrano, J., von Hardenberg, J., Koenigk, T., Levine, X., Meccia, V. L., van Noije, T., van den Oord, G., … Wyser, K. (2020). HighResMIP versions of EC-Earth: EC-Earth3P and EC-Earth3P-HR – description, model computational performance and basic validation. *Geoscientific Model Development*, *13*(8), 3507–3527. https://doi.org/10.5194/gmd-13-3507-2020

Haarsma, R. J., García-Serrano, J., Prodhomme, C., Bellprat, O., Davini, P., & Drijfhout, S. (2019). Sensitivity of winter North Atlantic-European climate to resolved atmosphere and ocean dynamics. *Scientific Reports*, *9*(1), 13358. https://doi.org/10.1038/s41598-019-49865-9

Huang, Y., Ren, H.-L., Chadwick, R., Cheng, Z., & Chen, Q. (2018). Diagnosing Changes of Winter NAO in Response to Different Climate Forcings in a Set of Atmosphere-Only Timeslice Experiments. *Atmosphere*, *9*(1). https://doi.org/10.3390/atmos9010010

Hurrell, J. W. (1995). Decadal Trends in the North Atlantic Oscillation: Regional Temperatures and Precipitation. *Science*, *269*(5224), 676–679. https://doi.org/10.1126/science.269.5224.676

Hurrell, J. W. (2015). CLIMATE AND CLIMATE CHANGE | Climate Variability. In *Encyclopedia of Atmospheric Sciences* (pp. 47–60). Elsevier. https://doi.org/10.1016/B978-0-12-382225-3.00109-2

Hurrell, J. W., Kushnir, Y., Ottersen, G., & Visbeck, M. (2003). *An overview of the North Atlantic Oscillation* (pp. 1–35). https://doi.org/10.1029/134GM01

Jan Dutton. (2021, March 11). *The East Atlantic – Western Russia Pattern: 4 Important Impacts*. WCS Blog. https://www.worldclimateservice.com/2021/11/03/east-atlantic-western-russia/

Josey, S. A., Somot, S., & Tsimplis, M. (2011). Impacts of atmospheric modes of variability on Mediterranean Sea surface heat exchange. *Journal of Geophysical Research*, *116*(C2), C02032. https://doi.org/10.1029/2010JC006685

Kim, W. M., Yeager, S., Chang, P., & Danabasoglu, G. (2018). Low-Frequency North Atlantic Climate Variability in the Community Earth System Model Large Ensemble. *Journal of Climate*, *31*(2), 787–813. https://doi.org/10.1175/JCLI-D-17-0193.1

Klavans, J. M., Cane, M. A., Clement, A. C., & Murphy, L. N. (2021). NAO predictability from external forcing in the late 20th century. *Npj Climate and Atmospheric Science*, *4*(1), 22. https://doi.org/10.1038/s41612-021-00177-8

Koenigk, T., Caian, M., Nikulin, G., & Schimanke, S. (2016). Regional Arctic sea ice variations as predictor for winter climate conditions. *Climate Dynamics*, *46*(1–2), 317–337. https://doi.org/10.1007/s00382-015-2586-1

Kushnir, Y., Robinson, W. A., Bladé, I., Hall, N. M. J., Peng, S., & Sutton, R. (2002). Atmospheric GCM Response to Extratropical SST Anomalies: Synthesis and Evaluation*. *Journal of Climate*, *15*(16), 2233–2256. https://doi.org/10.1175/1520-0442(2002)015<2233:AGRTES>2.0.CO;2

Lehmann, J., Coumou, D., & Frieler, K. (2015). Increased record-breaking precipitation events under global warming. *Climatic Change*, *132*(4), 501–515. https://doi.org/10.1007/s10584-015-1434-y

Lim, Y.-K. (2015). The East Atlantic/West Russia (EA/WR) teleconnection in the North Atlantic: climate impact and relation to Rossby wave propagation. *Climate Dynamics*, *44*(11), 3211–3222. https://doi.org/10.1007/s00382-014-2381-4

Lindeskog, M., Arneth, A., Bondeau, A., Waha, K., Seaquist, J., Olin, S., & Smith, B. (2013). Implications of accounting for land use in simulations of ecosystem carbon cycling in Africa. *Earth System Dynamics*, *4*(2), 385–407. https://doi.org/10.5194/esd-4-385-2013

Lucas, C., Rudeva, I., Nguyen, H., Boschat, G., & Hope, P. (2022). Variability and changes to the mean meridional circulation in isentropic coordinates. *Climate Dynamics*, *58*(1–2), 257–276. https://doi.org/10.1007/s00382-021-05903-9

Madec, G. (2008). *NEMO ocean engine*. https://api.semanticscholar.org/CorpusID:129226551

Madec, G. (2015). *NEMO ocean engine Version 3.6 stable Note du Pole de modelisation de l'Institut Pierre-Simon Laplace* (Vol. 27). IPSL.

McHugh, M. J., & Rogers, J. C. (2005). Multi-model representation of the North Atlantic Oscillation in the 20th and 21st centuries. *Geophysical Research Letters*, *32*(21). https://doi.org/10.1029/2005GL023679

McKenna, C., & Maycock, A. (2022). *The role of the North Atlantic Oscillation for projections of winter mean precipitation in Europe*. https://doi.org/10.1002/essoar.10511064.2

Michael E. Mann. (2024). Global warming. *Encyclopedia Britannica*. https://www.britannica.com/science/global-warming

Michael Pidwirny, U. of B. C. (2021). *Physical Geography Lab Manual: The Atmosphere and Biosphere*. Our Planet Earth.

Mikhailova, N. V., & Yurovsky, A. V. (2016). The East Atlantic Oscillation: Mechanism and Impact on the European Climate in Winter. *Morskoy Gidrofizicheskiy Zhurnal*, *4*. https://doi.org/10.22449/0233-7584-2016-4-27-37

Nakamura, H. (1996). Year-to-Year and interdecadal variability in the activity of intraseasonal fluctuations in the Northern Hemisphere wintertime circulation. *Theoretical and Applied Climatology*, *55*(1–4), 19–32. https://doi.org/10.1007/BF00864700

National Center for Atmospheric Research Staff (Eds). (2013, July 22). *The Climate Data Guide: Empirical Orthogonal Function (EOF) Analysis and Rotated EOF Analysis.* https://climatedataguide.ucar.edu/climate-data-tools-and-analysis/empirical-orthogonal-function-eof-analysis-and-rotated-eof-analysis

Nigam, S., & Baxter, S. (2015). GENERAL CIRCULATION OF THE ATMOSPHERE | Teleconnections. In *Encyclopedia of Atmospheric Sciences* (pp. 90–109). Elsevier. https://doi.org/10.1016/B978-0-12-382225-3.00400-X

North, G. R. (1984). Empirical Orthogonal Functions and Normal Modes. *Journal of the Atmospheric Sciences*, *41*(5), 879–887. https://doi.org/10.1175/1520-0469(1984)041<0879:EOFANM>2.0.CO;2

Palmeiro, F. M., García-Serrano, J., Rodrigo, M., Abalos, M., Christiansen, B., & Yang, S. (2023). Boreal winter stratospheric climatology in EC-EARTH: CMIP6 version. *Climate Dynamics*, *60*(3), 883–898. https://doi.org/10.1007/s00382-022-06368-0

Peings, Y., & Magnusdottir, G. (2014). Forcing of the wintertime atmospheric circulation by the multidecadal fluctuations of the North Atlantic ocean. *Environmental Research Letters*, *9*(3), 034018. https://doi.org/10.1088/1748-9326/9/3/034018

Peings, Y., & Magnusdottir, G. (2016). Wintertime atmospheric response to Atlantic multidecadal variability: effect of stratospheric representation and ocean–atmosphere coupling. *Climate Dynamics*, *47*(3–4), 1029–1047. https://doi.org/10.1007/s00382-015-2887-4

Peings, Y., Simpkins, G., & Magnusdottir, G. (2016). Multidecadal fluctuations of the North Atlantic Ocean and feedback on the winter climate in CMIP5 control simulations. *Journal of Geophysical Research: Atmospheres*, *121*(6), 2571–2592. https://doi.org/10.1002/2015JD024107

Rafferty J. P. (2023). North Atlantic Oscillation. *Encyclopedia Britannica*. https://www.britannica.com/science/North-Atlantic-Oscillation

Rivière, G. (2009). Effect of Latitudinal Variations in Low-Level Baroclinicity on Eddy Life Cycles and Upper-Tropospheric Wave-Breaking Processes. *Journal of the Atmospheric Sciences*, *66*(6), 1569–1592. https://doi.org/10.1175/2008JAS2919.1

Robinson, A., Lehmann, J., Barriopedro, D., Rahmstorf, S., & Coumou, D. (2021). Increasing heat and rainfall extremes now far outside the historical climate. *Npj Climate and Atmospheric Science*, *4*(1), 45. https://doi.org/10.1038/s41612-021-00202-w

Rousset, C., Vancoppenolle, M., Madec, G., Fichefet, T., Flavoni, S., Barthélemy, A., Benshila, R., Chanut, J., Levy, C., Masson, S., & Vivier, F. (2015). The Louvain-La-Neuve sea ice model LIM3.6: global and regional capabilities. *Geoscientific Model Development*, *8*(10), 2991–3005. https://doi.org/10.5194/gmd-8-2991-2015

Santolaria-Otín, M., García-Serrano, J., Ménégoz, M., & Bech, J. (2020). On the observed connection between Arctic sea ice and Eurasian snow in relation to the winter North Atlantic Oscillation. *Environmental Research Letters*, *15*(12), 124010. https://doi.org/10.1088/1748-9326/abad57

Scaife, A. A., Arribas, A., Blockley, E., Brookshaw, A., Clark, R. T., Dunstone, N., Eade, R., Fereday, D., Folland, C. K., Gordon, M., Hermanson, L., Knight, J. R., Lea, D. J., MacLachlan, C., Maidens, A., Martin, M., Peterson, A. K., Smith, D., Vellinga, M., … Williams, A. (2014). Skillful long-range prediction of European and North American winters. *Geophysical Research Letters*, *41*(7), 2514–2519. https://doi.org/10.1002/2014GL059637

Shindell, D. T., Miller, R. L., Schmidt, G. A., & Pandolfo, L. (1999). Simulation of recent northern winter climate trends by greenhouse-gas forcing. *Nature*, *399*(6735), 452–455. https://doi.org/10.1038/20905

Smith, B., Wårlind, D., Arneth, A., Hickler, T., Leadley, P., Siltberg, J., & Zaehle, S. (2014). Implications of incorporating N cycling and N limitations on primary production in an individual-based dynamic vegetation model. *Biogeosciences*, *11*(7), 2027–2054. https://doi.org/10.5194/bg-11-2027-2014

Smith, D. M., Scaife, A. A., Eade, R., Athanasiadis, P., Bellucci, A., Bethke, I., Bilbao, R., Borchert, L. F., Caron, L.-P., Counillon, F., Danabasoglu, G., Delworth, T., Doblas-Reyes, F. J., Dunstone, N. J., Estella-Perez, V., Flavoni, S., Hermanson, L., Keenlyside, N., Kharin, V., … Zhang, L. (2020). North Atlantic climate far more predictable than models imply. *Nature*, *583*(7818), 796–800. https://doi.org/10.1038/s41586-020-2525-0

Smoliak, B. V., & Wallace, J. M. (2015). On the Leading Patterns of Northern Hemisphere Sea Level Pressure Variability*. *Journal of the Atmospheric Sciences*, *72*(9), 3469–3486. https://doi.org/10.1175/JAS-D-14-0371.1

Straile, D., Livingstone, D. M., Weyhenmeyer, G. A., & George, D. G. (2003). *The response of freshwater ecosystems to climate variability associated with the North Atlantic Oscillation* (pp. 263–279). https://doi.org/10.1029/134GM12

The PISM Team: PISM. (2019). *A Parallel Ice Sheet Model*.

Thompson, D. W. J., Lee, S., & Baldwin, M. P. (2003). *Atmospheric processes governing the Northern Hemisphere annular mode/North Atlantic Oscillation* (pp. 81–112). https://doi.org/10.1029/134GM05

Tuel, A., & Eltahir, E. A. B. (2020). Why Is the Mediterranean a Climate Change Hot Spot? *Journal of Climate*. https://api.semanticscholar.org/CorpusID:218914968

United Nations. (n.d.). *What Is Climate Change?* Retrieved February 26, 2024, from https://www.un.org/en/climatechange/what-is-climate-change

van den Hurk, B. J. J., Viterbo, P., Beljaars, A., & Betts, A. (2000). Offline validation of the ERA40 surface scheme. In *ECMWF Technical Memoranda* (Issue 295). ECMWF. https://doi.org/10.21957/9aoaspz8

van Noije, T. P. C., Le Sager, P., Segers, A. J., van Velthoven, P. F. J., Krol, M. C., Hazeleger, W., Williams, A. G., & Chambers, S. D. (2014). Simulation of tropospheric chemistry and aerosols with the climate model EC-Earth. *Geoscientific Model Development*, *7*(5), 2435–2475. https://doi.org/10.5194/gmd-7-2435-2014

Vancoppenolle, M., Fichefet, T., Goosse, H., Bouillon, S., Madec, G., & Maqueda, M. A. M. (2009). Simulating the mass balance and salinity of Arctic and Antarctic sea ice. 1. Model description and validation. *Ocean Modelling*, *27*(1–2), 33–53. https://doi.org/10.1016/j.ocemod.2008.10.005

Vannitsem, S., & Ghil, M. (2017). Evidence of coupling in ocean-atmosphere dynamics over the North Atlantic. *Geophysical Research Letters*, *44*(4), 2016–2026. https://doi.org/10.1002/2016GL072229

Visbeck, M., Chassignet, E. P., Curry, R. G., Delworth, T. L., Dickson, R. R., & Krahmann, G. (2003). *The ocean's response to North Atlantic Oscillation variability* (pp. 113–145). https://doi.org/10.1029/134GM06

Wallace, J. M., Thompson, D. W. J., & Beresford, P. (2015). GENERAL CIRCULATION OF THE ATMOSPHERE | Overview. In *Encyclopedia of Atmospheric Sciences* (pp. 33–42). Elsevier. https://doi.org/10.1016/B978-0-12-382225-3.00153-5

Watanabe, M., & Kimoto, M. (2000). Atmosphere-ocean thermal coupling in the North Atlantic: A positive feedback. *Quarterly Journal of the Royal Meteorological Society*, *126*(570), 3343–3369. https://doi.org/10.1002/qj.49712657017

Winkelmann, R., Martin, M. A., Haseloff, M., Albrecht, T., Bueler, E., Khroulev, C., & Levermann, A. (2011). The Potsdam Parallel Ice Sheet Model (PISM-PIK) – Part 1: Model description. *The Cryosphere*, *5*(3), 715–726. https://doi.org/10.5194/tc-5-715-2011

Woollings, T., Franzke, C., Hodson, D. L. R., Dong, B., Barnes, E. A., Raible, C. C., & Pinto, J. G. (2015). Contrasting interannual and multidecadal NAO variability. *Climate Dynamics*, *45*(1–2), 539–556. https://doi.org/10.1007/s00382-014-2237-y

World Climate Research Programme CMIP6. (2021, December 17). *Climate Model - Surface Temperature Change: SSP2 (Middle of the Road) - 2015 - 2100*. https://sos.noaa.gov/catalog/datasets/climate-model-surface-temperature-change-ssp2-middle-road-2015-2100/

Wu, L., & Liu, Z. (2005). North Atlantic Decadal Variability: Air–Sea Coupling, Oceanic Memory, and Potential Northern Hemisphere Resonance*. *Journal of Climate*, *18*(2), 331–349. https://doi.org/10.1175/JCLI-3264.1

Wu, R., Dai, P., & Chen, S. (2022). Persistence or Transition of the North Atlantic Oscillation Across Boreal Winter: Role of the North Atlantic Air-Sea Coupling. *Journal of Geophysical Research: Atmospheres*, *127*(23). https://doi.org/10.1029/2022JD037270

Zeke Hausfather. (2018, April 19). *Explainer: How 'Shared Socioeconomic Pathways' explore future climate change*. https://www.carbonbrief.org/explainer-how-shared-socioeconomic-pathways-explore-future-climate-change/

Zhang, S., Liu, Z., Zhang, X., Wu, X., Han, G., Zhao, Y., Yu, X., Liu, C., Liu, Y., Wu, S., Lu, F., Li, M., & Deng, X. (2020). Coupled data assimilation and parameter estimation in coupled ocean–atmosphere models: a review. *Climate Dynamics*, *54*(11–12), 5127–5144. https://doi.org/10.1007/s00382-020-05275-6

Appendix

Appendix A

The leading four pattern of North Atlantic European inter seasonal SLP variability

46.76 %

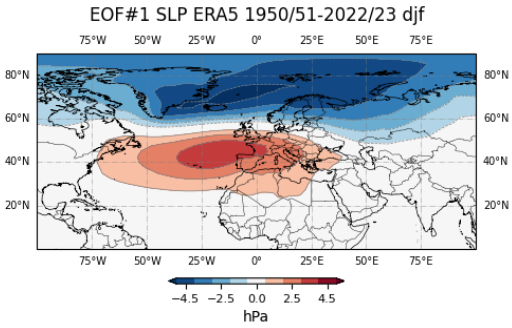

37.02 %

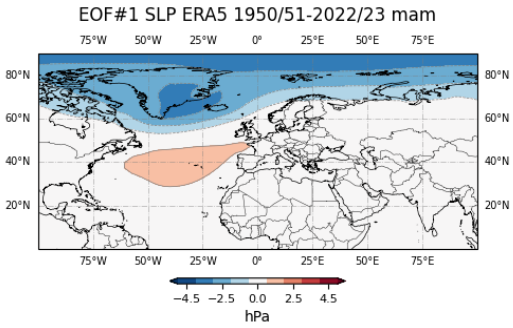

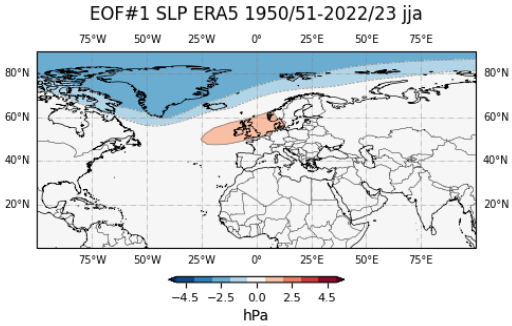

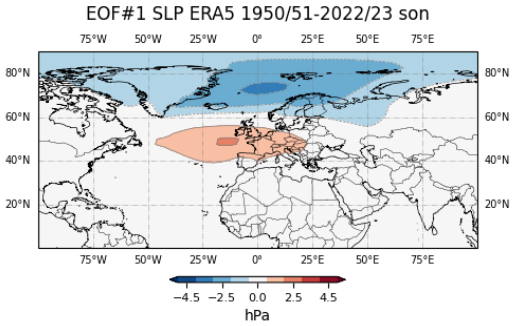

43.75 %

27.29 %

16.57 %

16.51 %

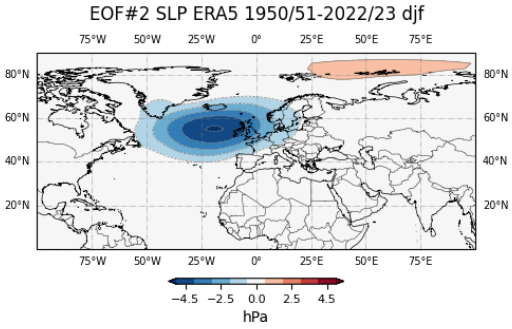

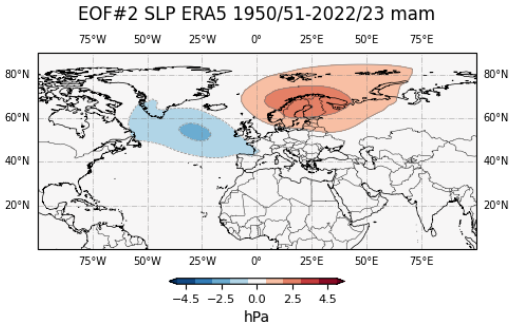

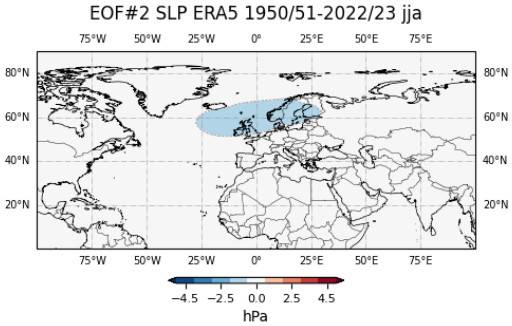

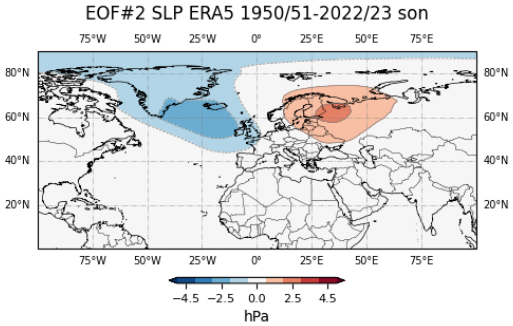

10.85 %

21.02 %

11.93 %

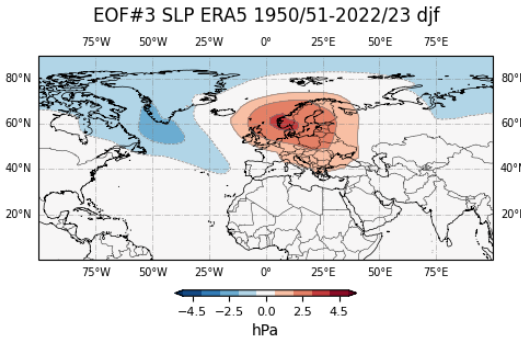

11.49 %

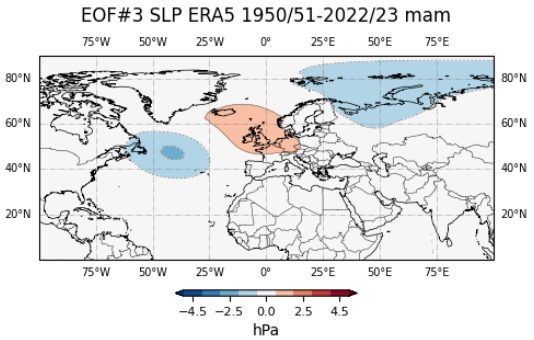

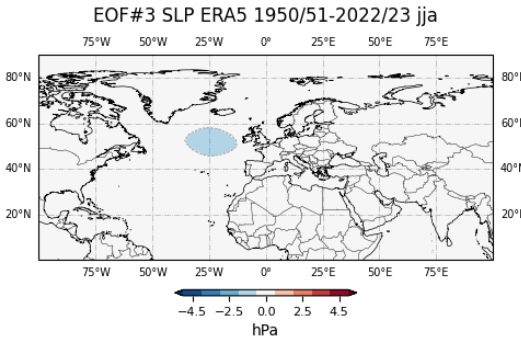

7.98 %

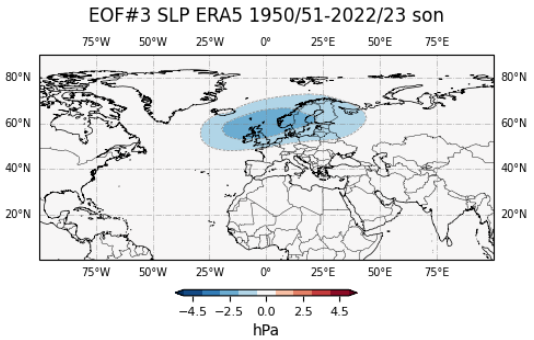

12.95 %

8.85 %

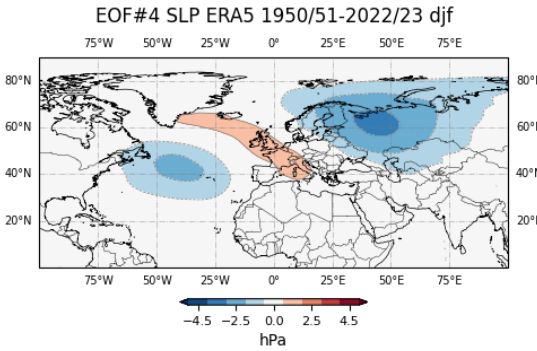

8.60 %

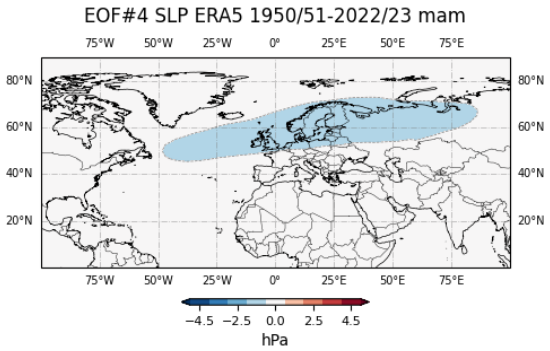

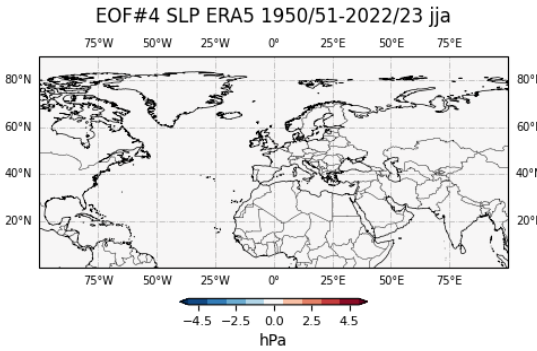

6.73 %

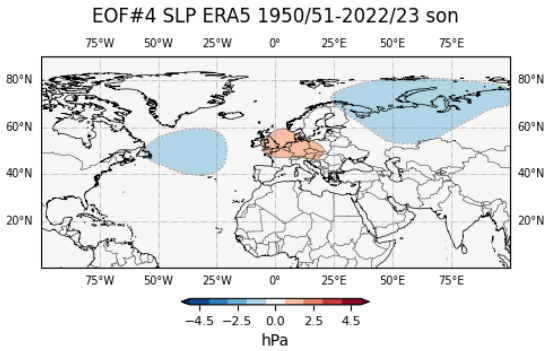

9.06 %

Figure 39 The first four EOFs in the NAE region, based on a 73 years (1950-2023) values of SLP anomalies from ERA5 as identified by regressing the annual SLP anomalies upon the principal component time series from the chosen spatial domain determined by EOF analysis. EOF1, EOF2, EOF3 and EOF4 are represented from top to bottom respectively.

Appendix B

1. The climatologies and standard deviations for ERA5, EC-Earth coupled and atmosphere-only present simulation

1.1 SLP

Climatology

ERA 5 DATA

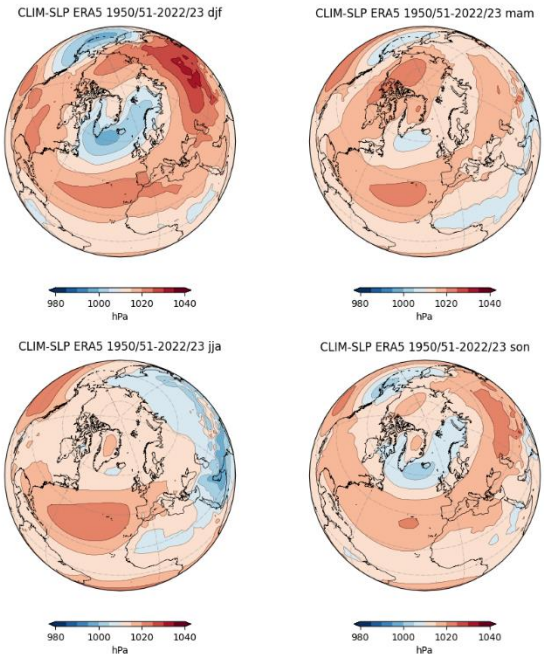

EC EARTH (a2am) – COUPLED

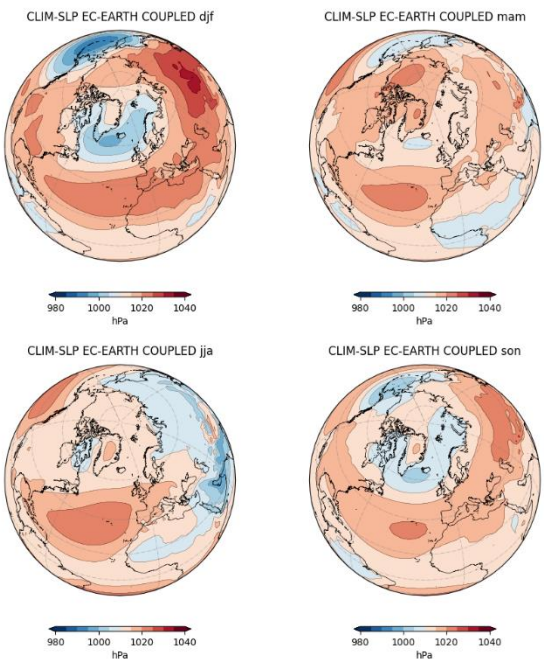

Standard Deviation

ERA 5 DATA

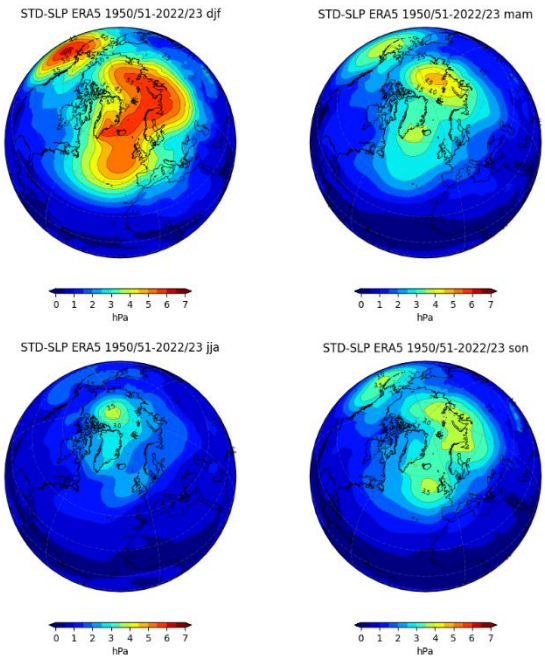

EC EARTH (a2am) – COUPLED

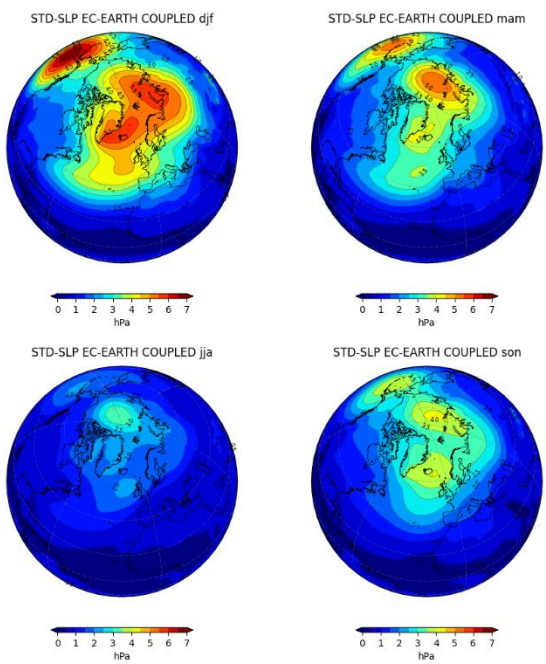

EC EARTH (a2al) – ATM

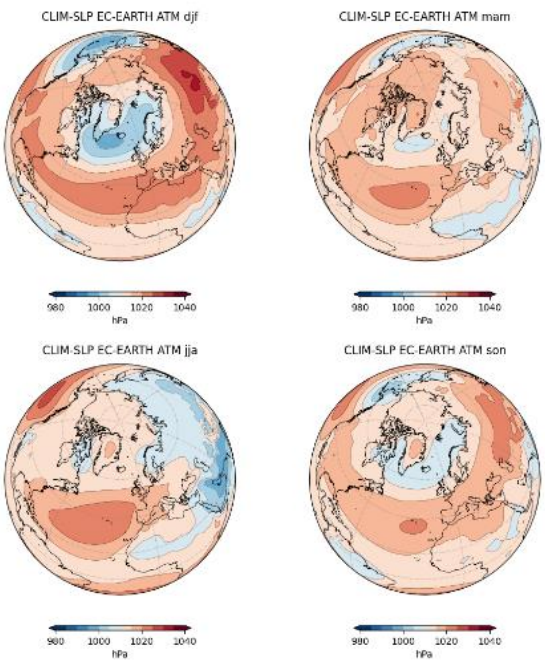

EC EARTH (a2al) – ATM

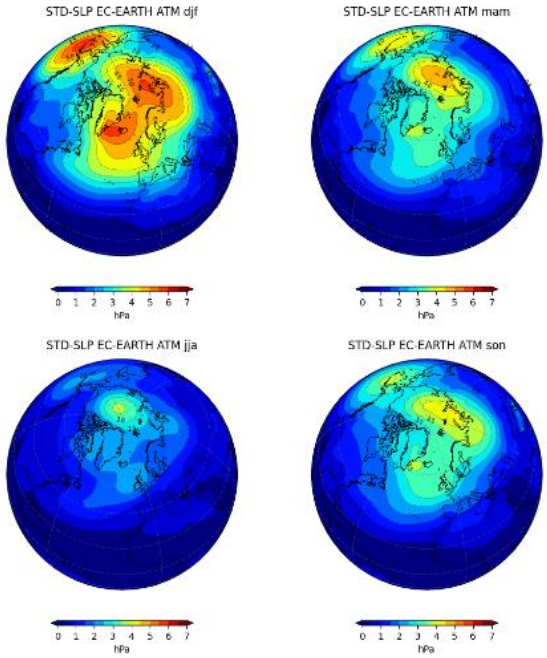

Figure 40 Climatology (left) and standard deviation (right) of SLP field (hPa) for DJF, MAM, JJA and SON seasons. ERA5 data from 1950 to 2023 on top. EC-EARTH coupled simulation data in the middle. EC-EARTH atmosphere-only simulation below.

1.2 t2m

Climatology

ERA 5 DATA

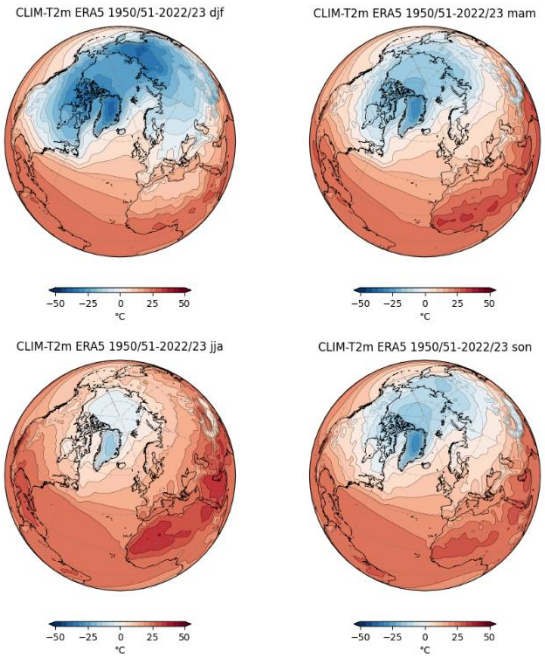

Standard Deviation

ERA 5 DATA

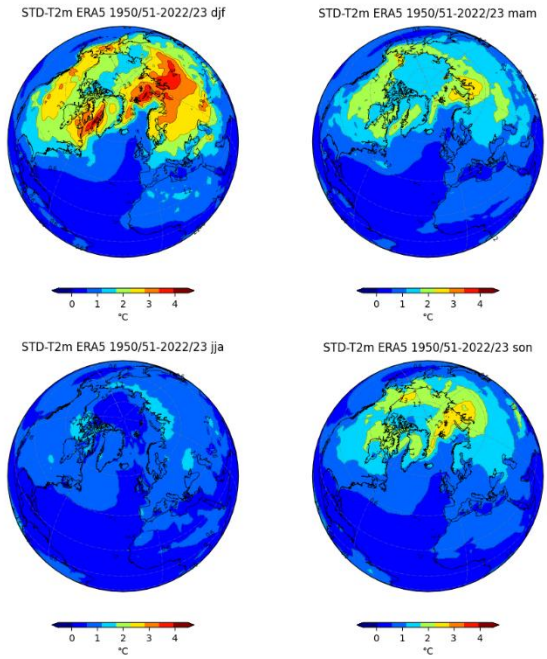

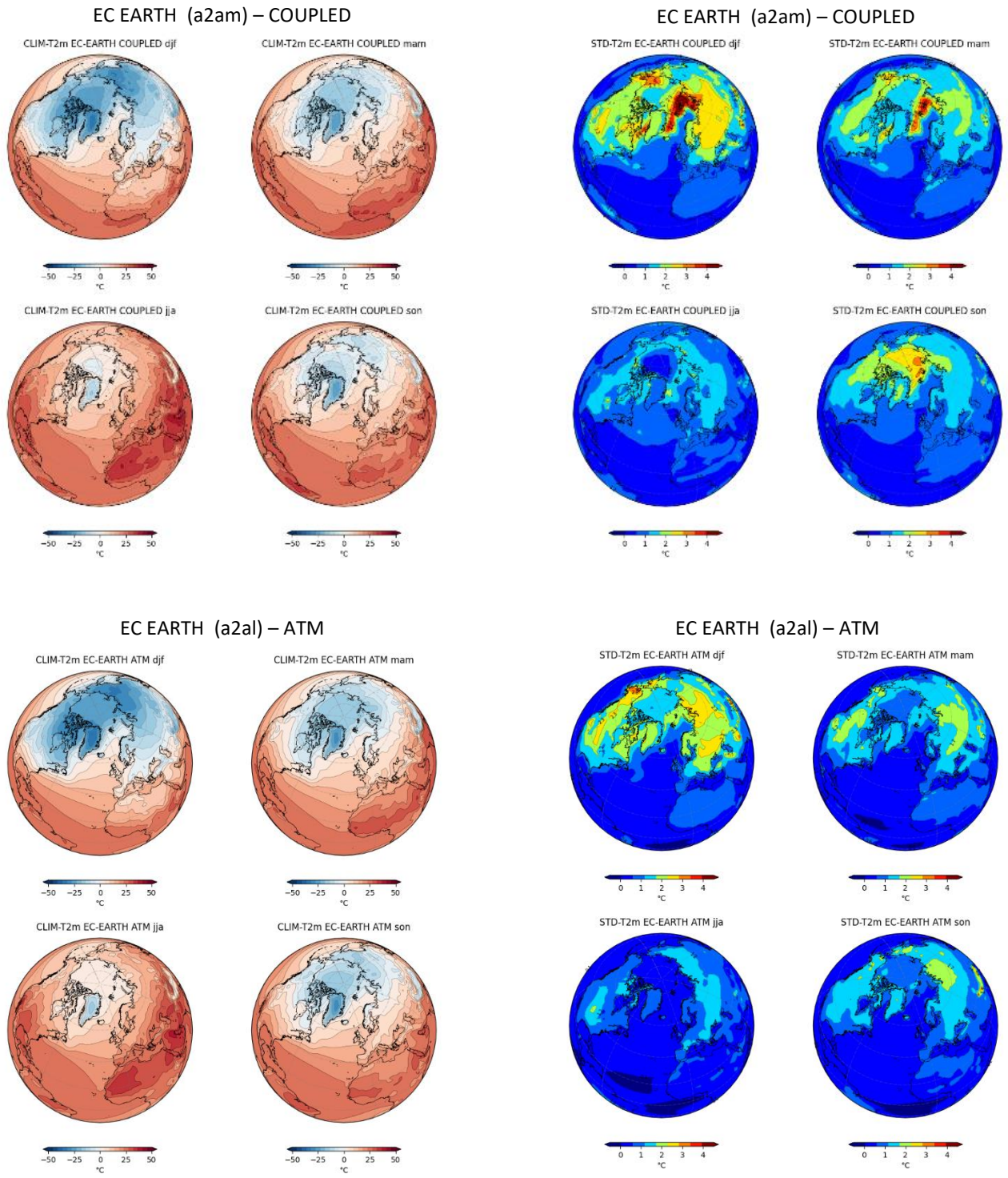

Figure 41 Climatology (left) and standard deviation (right) of t2m field (°C) for DJF, MAM, JJA and SON seasons. ERA5 data from 1950 to 2023 on top. EC-EARTH coupled simulation data in the middle. EC-EARTH atmosphere-only simulation below.

1.3 TP

Climatology

ERA 5 DATA

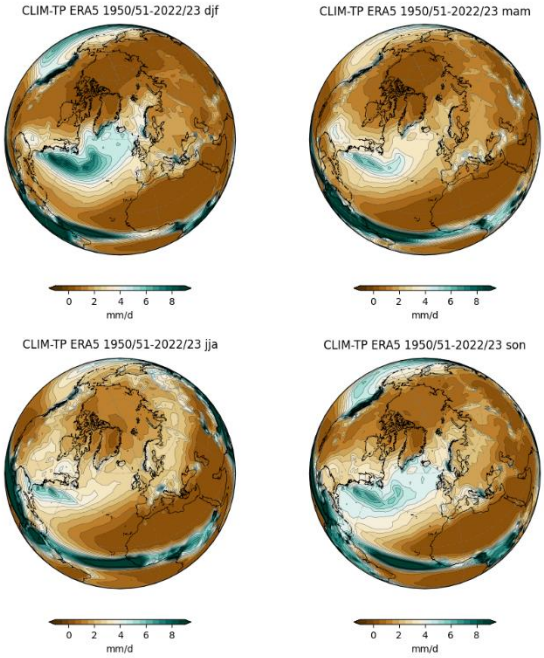

EC EARTH (a2am) – COUPLED

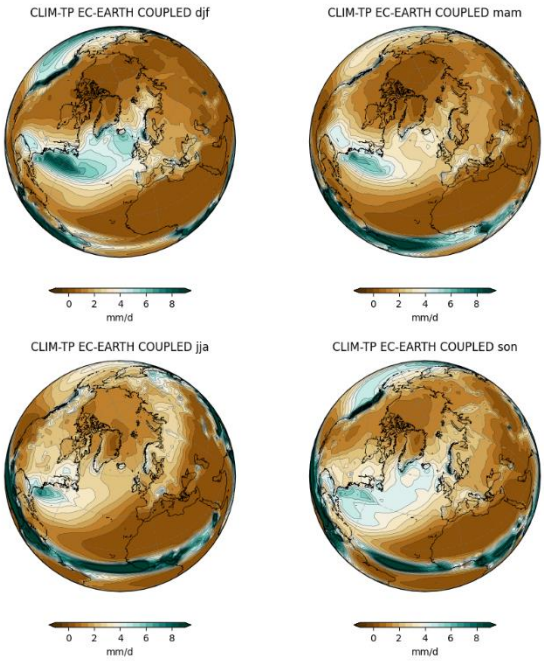

Standard Deviation

ERA 5 DATA

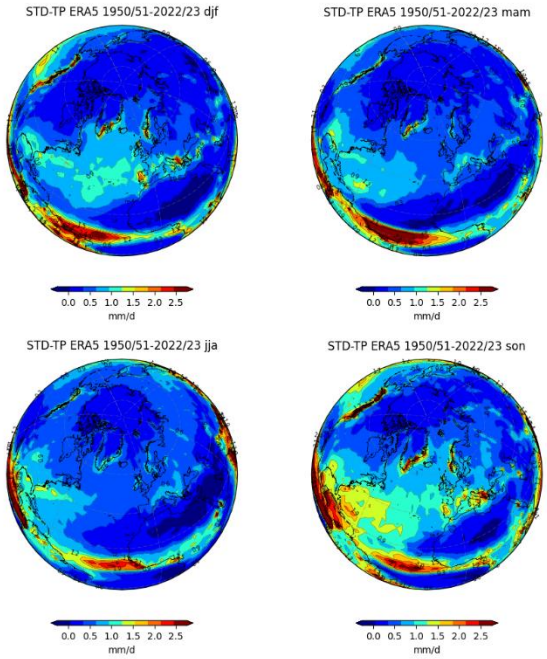

EC EARTH (a2am) – COUPLED

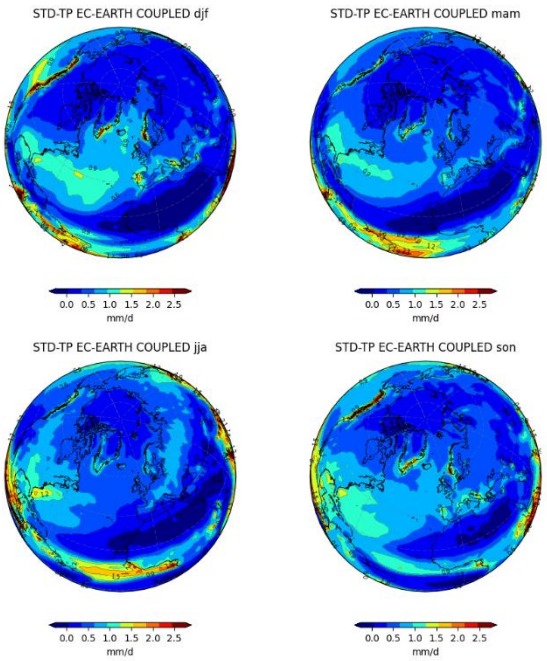

EC EARTH (a2al) – ATM

EC EARTH (a2al) – ATM

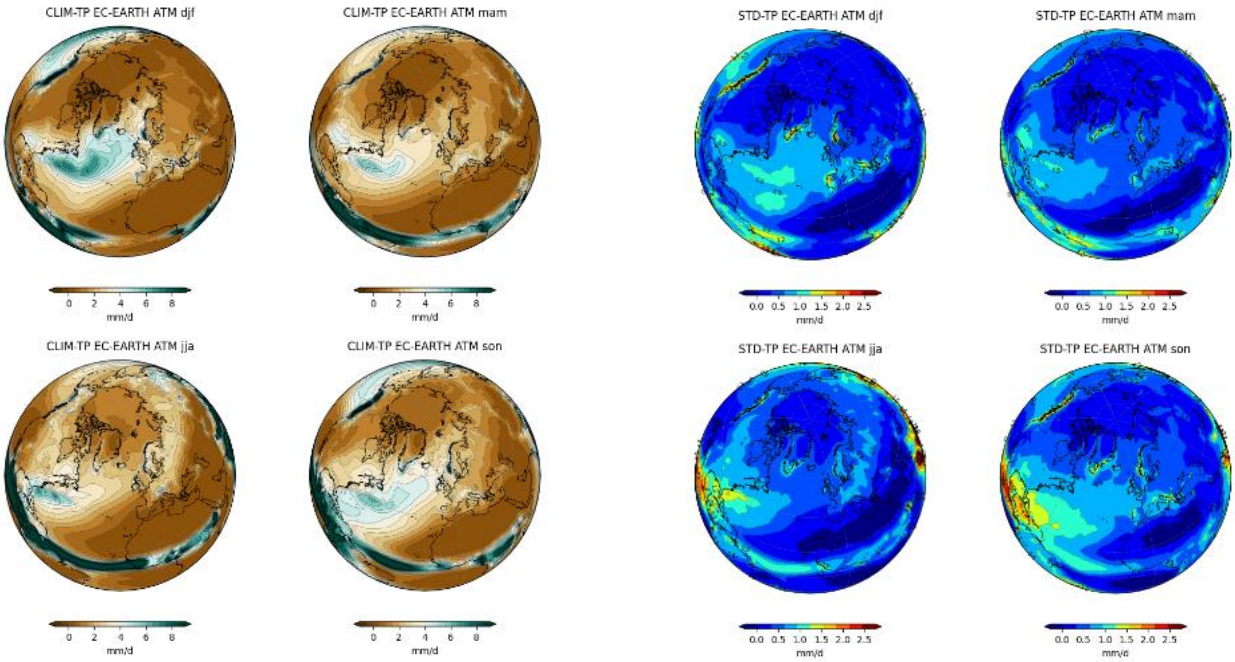

Figure 42 Climatology (left) and standard deviation (right) of TP field (mm/d) for DJF, MAM, JJA and SON seasons. ERA5 data from 1950 to 2023 on top. EC-EARTH coupled simulation data in the middle. EC-EARTH atmosphere-only simulation below.

2. The climatologies and standard deviations for EC-Earth coupled and atmosphere-only future simulation

2.1 SLP

Climatology **Standard Deviation**

EC EARTH COUPLED (a2ae) - FUT

EC EARTH COUPLED (a2ae) - FUT

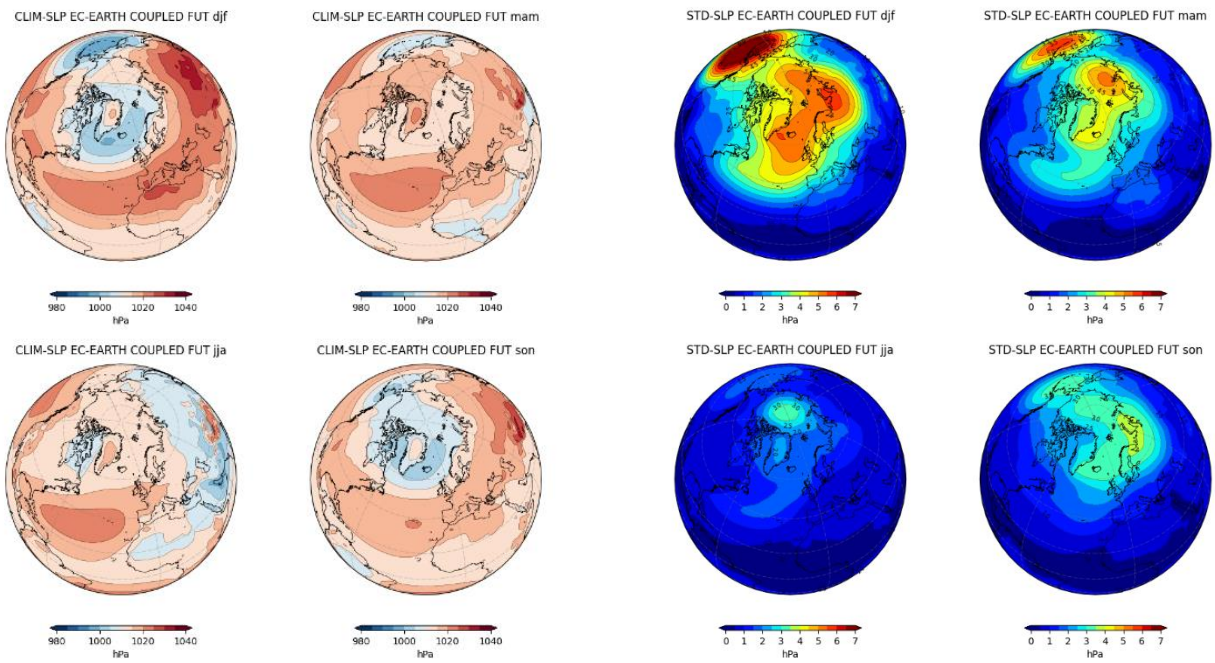

EC EARTH ATM-ONLY (a2ad) - FUT

EC EARTH ATM-ONLY (a2ad) - FUT

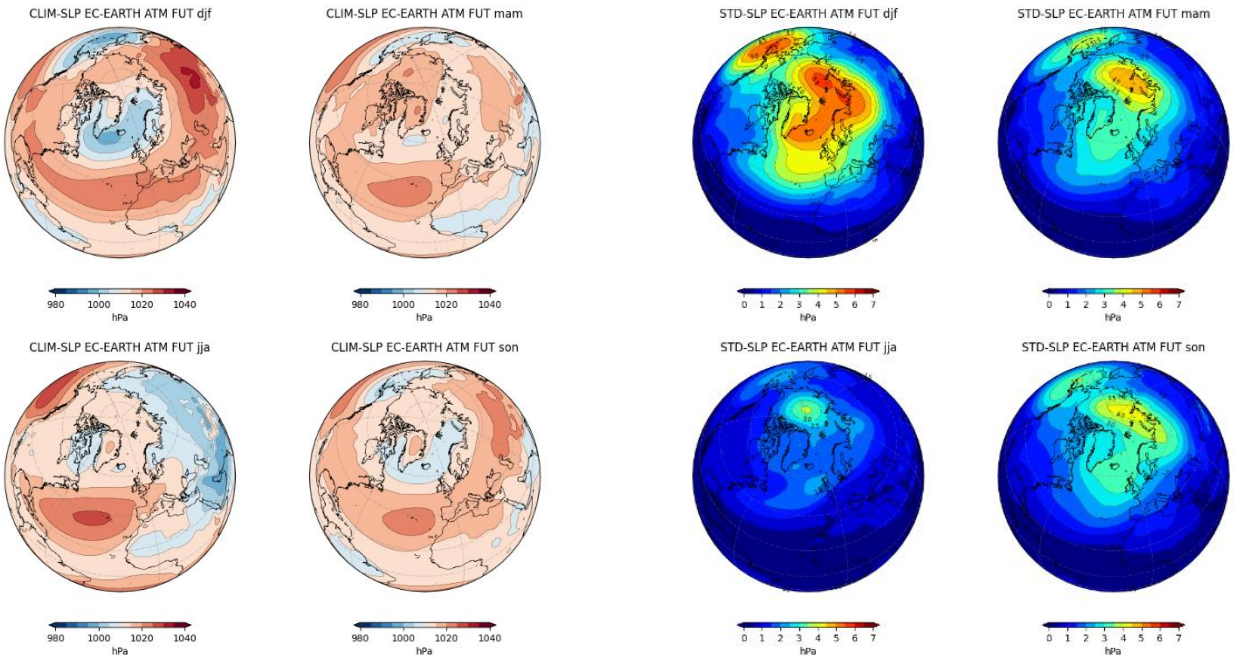

Figure 43 Climatology (left) and standard deviation (right) of SLP field (hPa) for DJF, MAM, JJA and SON seasons. EC-EARTH coupled future simulation data on top. EC-EARTH atmosphere-only future simulation below.

2.2 t2m

Climatology

Standard Deviation

EC EARTH COUPLED (a2ae) - FUT

EC EARTH COUPLED (a2ae) - FUT

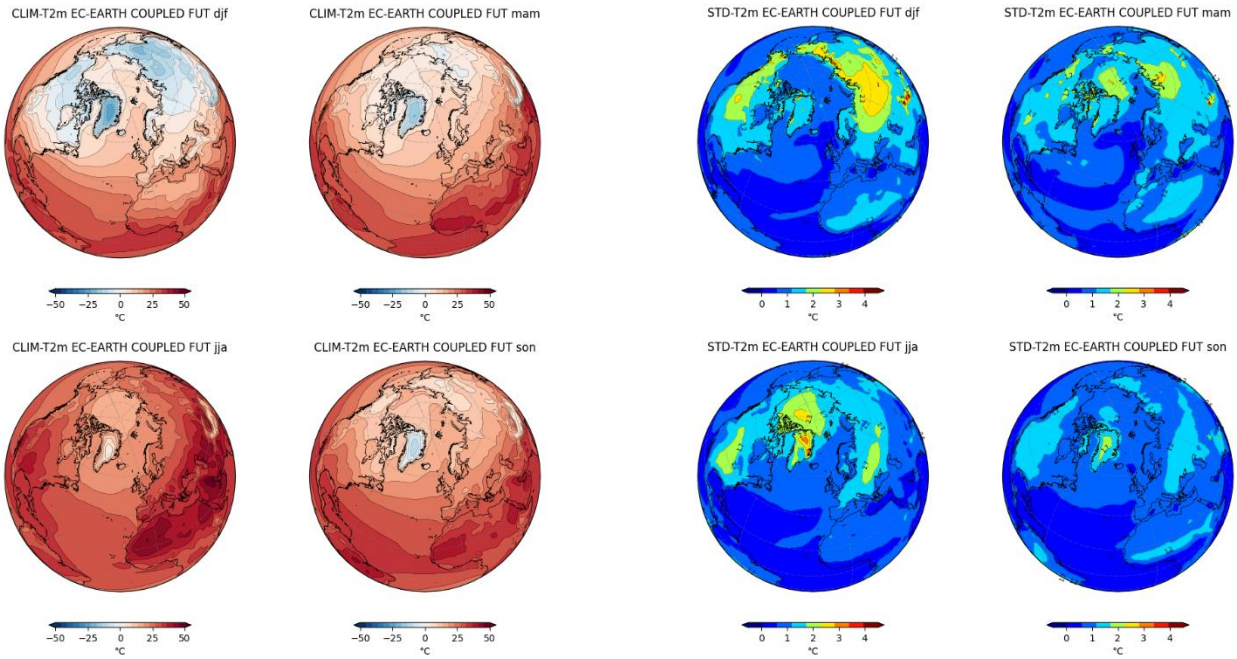

EC EARTH ATM-ONLY (a2ad) - FUT

EC EARTH ATM-ONLY (a2ad) - FUT

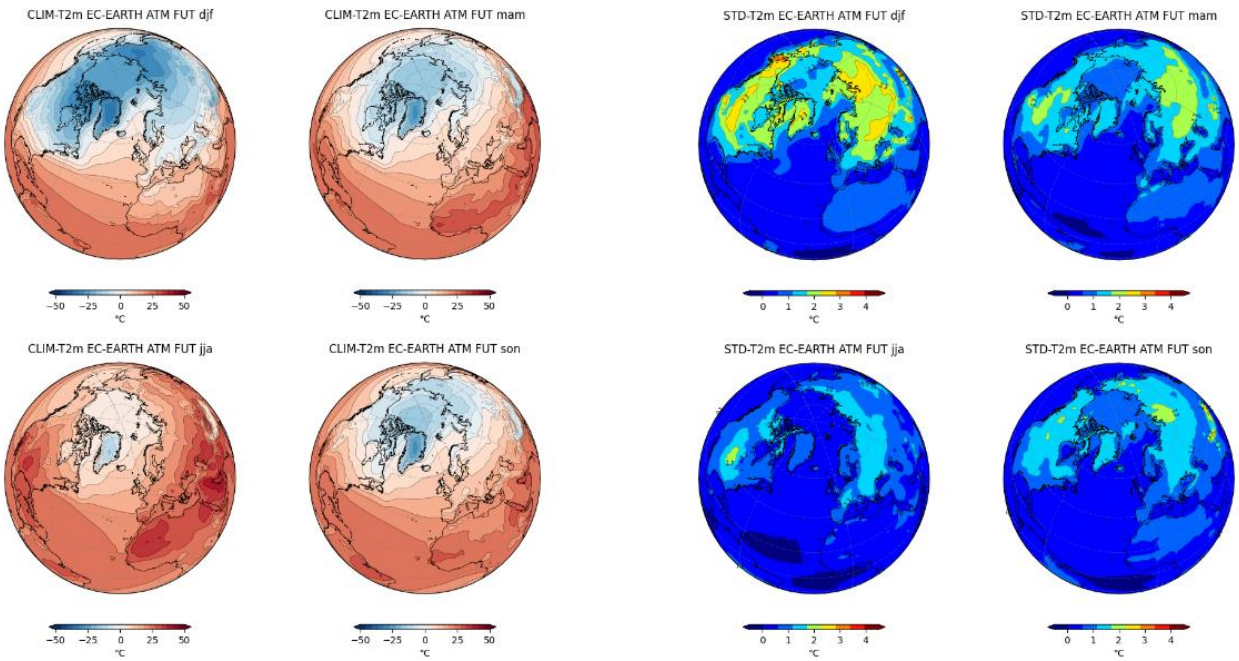

Figure 44 Climatology (left) and standard deviation (right) of t2m field (°C) for DJF, MAM, JJA and SON seasons. EC-EARTH coupled future simulation data on top. EC-EARTH atmosphere-only future simulation below.

2.3 TP

Climatology

Standard Deviation

EC EARTH COUPLED (a2ae) - FUT

EC EARTH COUPLED (a2ae) - FUT

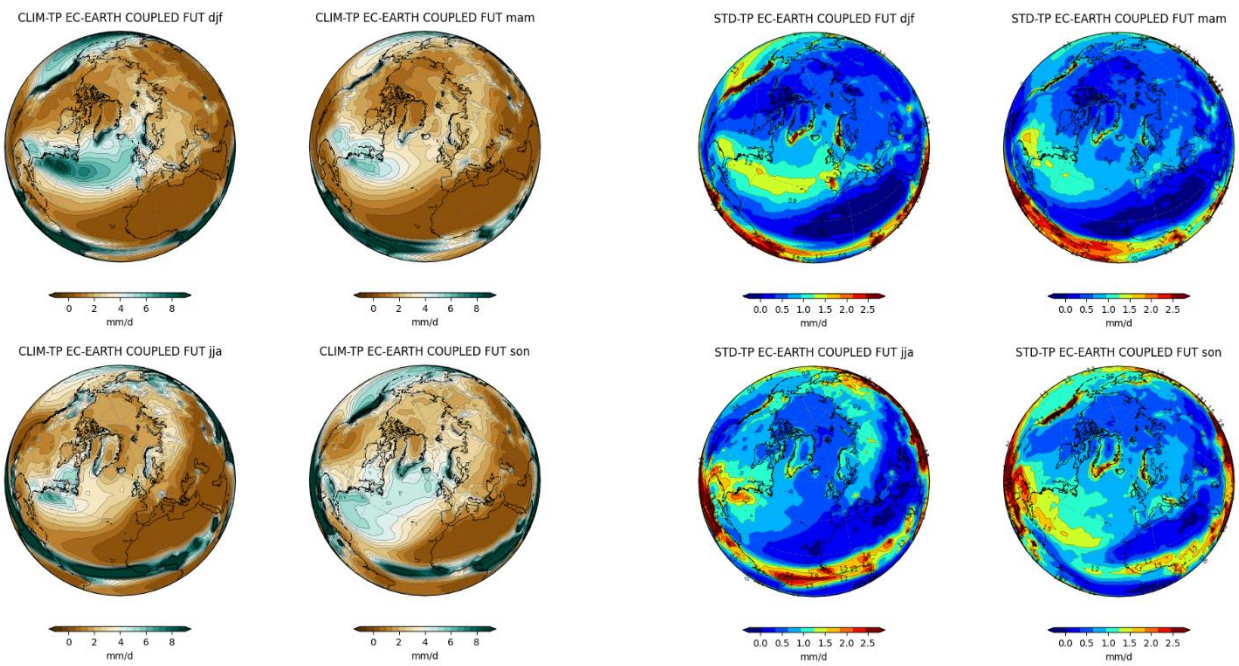

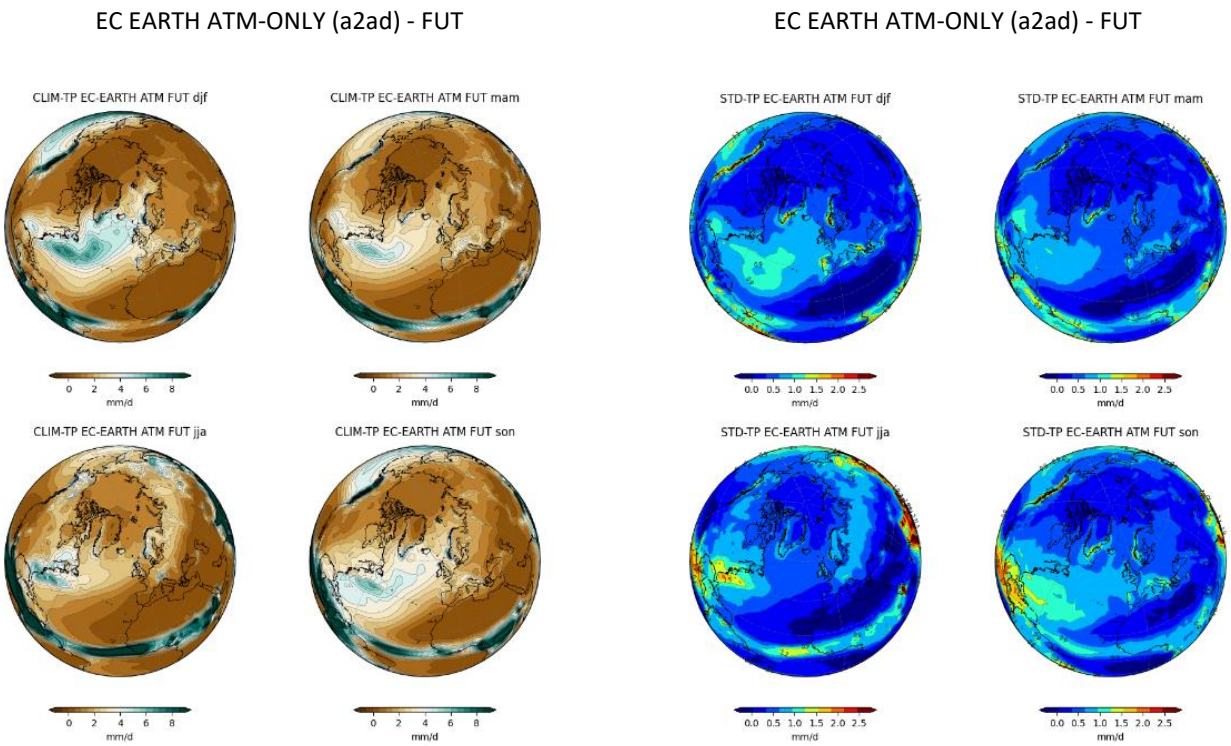

Figure 45 Climatology (left) and standard deviation (right) of TP field (mm/d) for DJF, MAM, JJA and SON seasons. EC-EARTH coupled future simulation data on top. EC-EARTH atmosphere-only future simulation below.